

**THERMAL ALTERATION OF COLLAGENOUS TISSUE
SUBJECTED TO BIAXIAL ISOMETRIC CONSTRAINTS**

A Dissertation

by

PAUL BRIAN WELLS

Submitted to the Office of Graduate Studies of
Texas A&M University
in partial fulfillment of the requirements for the degree of

DOCTOR OF PHILOSOPHY

May 2005

Major Subject: Biomedical Engineering

**THERMAL ALTERATION OF COLLAGENOUS TISSUE
SUBJECTED TO BIAXIAL ISOMETRIC CONSTRAINTS**

A Dissertation

by

PAUL BRIAN WELLS

Submitted to Texas A&M University
in partial fulfillment of the requirements
for the degree of

DOCTOR OF PHILOSOPHY

Approved as to style and content by:

Jay D. Humphrey
(Chair of Committee)

Lihong Wang
(Member)

Hsin-i Wu
(Member)

Harry A. Hogan
(Member)

Gerard L. Coté
(Head of Department)

May 2005

Major Subject: Biomedical Engineering

ABSTRACT

Thermal Alteration of Collagenous Tissue Subjected to
Biaxial Isometric Constraints. (May 2005)

Paul Brian Wells, B.S., Texas A&M University

Chair of Advisory Committee: Dr. Jay D. Humphrey

Clinical thermal therapies are widespread and gaining in appeal due to improved technology of heating devices and promising results. Outcomes of thermal treatment are often unpredictable and suboptimal, however, due in part to a lack of appreciation of the underlying biothermomechanics. There is a pressing need, therefore, to understand better the role of clinically-controllable parameters on the thermal damage processes of tissue. Heretofore, researchers have primarily sought to understand this process through various uniaxial experiments on tissues containing collagen as their primary constituent. Most biological tissues experience multiaxial loading, however, with complex boundary constraints inclusive of both isotonic and isometric conditions. The primary focus of this work is on the isothermal denaturation of fibrillar collagen subjected to a biaxial isometric constraint.

Results from our tests reveal a complicated process, the kinetics of which are not easily measured. Evolving isometric contraction forces during heating do not correlate with resultant mechanical behaviors, as thermal shrinkage does in biaxial isotonic tests. Furthermore, resultant mechanical behaviors at various

durations of heating reveal a two phase process with a rate dependent on the amount of isometric stretch. For tissues heated at 75°C for 15 minutes, at which point the first phase of mechanical alteration dominates for all constraints herein, resultant mechanical behaviors correlate well with the amount of isometric stretch. The correlation is similar to that between isotonic loads and resultant mechanical behaviors from previous studies. In light of the need for a better measure of thermal damage in isometric tests, we performed a histological analysis of tissues heated under varying constraints. Results show a good correlation between the level of isometric constraint and thermally-induced histological aberrations. Finally, we demonstrate that our seemingly limited and qualitative knowledge can be applied well to a specific clinical application: namely, the use of glycerol as a clearing agent for laser therapies. Our results suggest that glycerol is safe to use for such therapies because it increases the thermal stability of fibrillar collagen, and its hyperosmotic effects on mechanical behavior are fully reversed upon rehydration.

This work is dedicated to those who have made it possible:
namely, my parents Andy and Valerie Wells and my wife Valeska.

ACKNOWLEDGMENTS

This work is borne out of the faithfulness of my Lord and Savior Jesus Christ, who said, "...he who abides in Me and I in him, he bears much fruit..." Therefore, I thank God for the many ways in which He has provided for me. I have been especially blessed by the guidance and council of my advisor, Dr. Jay D. Humphrey. It goes without saying that his knowledge and experience have been indispensable. Equally influential has been his steadfast and well-balanced devotion to his Faith, his family and his students. I am also grateful for Dr. Lihong Wang, Dr. Hsin-i Wu, and Dr. Harry A. Hogan, who have sacrificed time and energy to serve on my committee, and for Dr. Jason L. Harris, who spent significant time showing me how to use the experimental device and interpret the data. I would also like to thank Dr. Seung-ik Baek, Dr. Luoyi Tao, Dr. Sharon Thomsen, Ms. Michelle Jones, and Ms. Jennifer James for meaningful talks and assistance with the histology. Financial support from the Texas A&M University Graduate School, the National Institute of Health, and the National Science Foundation is gratefully acknowledged.

I thank God most for giving me the perfect wife and help-mate in Valeska. Her sacrificial love, patience, and flexibility have kept me afloat through the rough times. Finally, I thank my parents Andy and Valerie and my siblings Jeff, Dave, and Glenda. Their love and encouragement have been unwavering throughout this process.

TABLE OF CONTENTS

		Page
ABSTRACT.....		iii
DEDICATION.....		v
ACKNOWLEDGMENTS.....		vi
TABLE OF CONTENTS.....		vii
LIST OF TABLES.....		ix
LIST OF FIGURES.....		x
CHAPTER		
I	INTRODUCTION.....	1
II	METHODS.....	10
	Specimen Preparation.....	10
	Description of Device.....	14
	Mechanical Testing.....	20
	Fluid Exchange Procedures.....	22
	Histological Processing.....	23
	Data Analysis.....	24
III	VALIDATION OF QUALITATIVE SALS DEVICE.....	30
	Introduction.....	30
	Methods.....	31
	Results.....	36
	Discussion.....	46
IV	KINETICS OF THERMAL CONTRACTION.....	50
	Introduction.....	50
	Methods.....	51
	Results.....	55
	Discussion.....	59

CHAPTER		Page
V	ALTERATION OF MECHANICS WITH HEATING.....	73
	Introduction.....	73
	Methods.....	74
	Results.....	75
	Discussion.....	79
VI	COMPARISON OF ISOMETRIC CONSTRAINTS.....	83
	Introduction.....	83
	Methods.....	84
	Results.....	84
	Discussion.....	87
VII	HISTOLOGY.....	94
	Introduction.....	94
	Methods.....	95
	Results.....	100
	Discussion.....	109
VIII	EFFECTS OF GLYCEROL.....	118
	Introduction.....	118
	Methods.....	119
	Results.....	122
	Discussion.....	130
IX	SUMMARY AND CONCLUSIONS.....	136
	REFERENCES.....	144
	APPENDIX A.....	152
	VITA.....	154

LIST OF TABLES

TABLE		Page
3.1	Comparison of orientation index and intensity threshold for the seven tissue specimens	38
4.1	Characteristic times for biaxial thermal contraction	58
6.1	Percent area changes for the four isometric test groups	87
7.1	Histological results for the free-shrinkage (i.e., mechanically unconstrained) group of tissues.....	104
7.2	Histological results for equibiaxial-stretch group of tissues.....	106
7.3	Histological results for equibiaxial-load group of tissues.	109
8.1	Average change in planar tissue area in the central region for the various configurations recorded in the experiment.....	127
8.2	Comparison of the characteristics times for the elbow-type isometric tests heated in glycerol and saline	129

LIST OF FIGURES

FIGURE	Page
2.1 Myocardium was carefully peeled from the epicardium, yielding a clean, undamaged sample	11
2.2 Small Angle Light Scattering (SALS) device used in our study	12
2.3 Top view diagram of the biaxial testing system	14
2.4 Illustration of the camera configuration for viewing the tracking markers	16
2.5 Marker numbering scheme, along with corresponding position coordinates	17
2.6 Parameterization of instantaneous marker positions	18
2.7 Fluid flow diagram	23
2.8 Representation of a biaxial stretch	28
3.1 Illustration of frame-mounted tissue	32
3.2 Top and side view illustrating the placement of the tissue between glass cover slips	34
3.3 Representative plot to show the intensity of transmitted light as a function of angle	35
3.4 Determination of Intensity profile for a single location	36
3.5 SALS scan of the native RV tissue	37
3.6 SALS scan of the native LV tissue	38
3.7 Digital photo and SALS image of LV heated at 75°C for 15 min while stretched approximately 20%.....	40
3.8 Digital photo and SALS image of RV heated at 75°C for 15 min while stretched approximately 20%.....	41

FIGURE	Page
3.9 Digital photo and SALS image of LV heated at 75°C for 15 min while stretched approximately 40%.....	43
3.10 Digital photo and SALS image of RV heated at 75°C for 15 min while stretched approx. 40%.....	44
3.11 SALS image of LV heated at 75°C for 15 min under zero constraint (i.e. free-shrinkage).....	45
4.1 Typical Cauchy membrane stress versus stretch response for native bovine epicardium in the stiffer direction	52
4.2 Schema of the isometric thermal damage protocol	54
4.3 Mean isometric contraction stresses for the ‘1.03’, ‘low stretch’, and ‘elbow’ tests.....	57
4.4 Schema of the three regimes of thermal contraction force...	57
4.5 Exponential relationship between characteristics times and the isometric constraint.....	59
4.6 Simplified representation of collagen fiber denaturation under mechanical stretch.....	66
4.7 Monotonic decay of stress during high stretch isometric heating.....	70
4.8 Monotonic decay of stress following rapid imposition of the high-stretch isometric constraint at room temperature.....	70
4.9 Mean isometric contraction stresses for the ‘1.03’, ‘low stretch’, and ‘elbow’ tests.....	71
5.1 Representative raw data from a ‘1.03’ test ($T = 75^{\circ}\text{C}$, $\tau = 900$ sec), which illustrates the altered biaxial mechanical behavior due to heating	76
5.2 Plot of the mean (equibiaxial) mechanical data following the ‘1.03’ isometric heating tests ($n = 5$).....	77

FIGURE	Page
5.3 Variation of mechanical behavior with duration of heating (at $T = 75^{\circ}\text{C}$) for tissues subjected to the '1.03' isometric constraint	78
5.4 Variation of mechanical behavior with duration of heating (at $T = 75^{\circ}\text{C}$) for tissues subjected to the 'Elbow' isometric constraint	79
5.5 Schema of the biphasic change in mechanical behavior with duration of heating.....	80
6.1 Plot of the mean equibiaxial data from the four test groups (n = 5 to 7 per group) and a representative mean 'native' curve (*).....	85
6.2 Nearly linear correlation between the relative extensibility of the damaged tissue at various levels of $ T $ (15, 25, 35, 45 and 55 N/m) and the relative amount of isometric stretch imposed during heating.....	86
6.3 Relation between resulting equibiaxial mechanical responses in isometric and isotonic tests	92
7.1 Representative cross-section of native epicardium	101
7.2 Progression of histological changes of bovine epicardium heated for various times at 75°C in the absence of mechanical constraints	103
7.3 Effect of equibiaxial isometric stretch on histological characteristics of thermal damage in epicardium heated <i>in vitro</i>	106
7.4 Effect of equibiaxial isometric load (at onset of heating) on histological characteristics of thermal damage in epicardium heated <i>in vitro</i>	108
7.5 Rupture (arrows) in the central region of heated epicardium subjected to the 100g-100g constraint prior to heating.....	116

FIGURE		Page
8.1	Profile and top views of the wire-frame (~15g) that was used to counter the increased buoyancy of the tissue when immersed in glycerol.....	121
8.2	Schema of the testing protocol for investigating the mechanical reversibility of glycerol	124
8.3	Reversibility of glycerol-induced changes in the mechanical behavior of a representative sample	125
8.4	Testing schema for investigating the effect of heated glycerol on the mechanical behavior	128
8.5	Data on the force (per length) generated by the tissue during heating as it tried to shrink against the fixed isometric constraint	128
8.6	Magnitude of the biaxial stress resultants versus normalized biaxial stretches	130
9.1	Biaxial device as configured for isotonic tests	139
9.2	Representative data showing a lack of shrinkage during a single test in which high isotonic loads are applied to the tissue during heating.....	140
9.3	Relation between resulting equibiaxial mechanical responses in isometric and isotonic tests	141

CHAPTER I

INTRODUCTION

Recent advances in heating technology have led to an unprecedented number of clinical procedures involving supraphysiologic temperatures (see Humphrey, 2003). For example, oncologists, gynecologists, cardiologists, dermatologists, and ophthalmologists use heat to treat cancer, endometriosis, atrial fibrillation, port-wine stains, and hyperopia, respectively. Outcomes of thermal treatment are often unpredictable and suboptimal, however, and there is a pressing need to understand better the thermal damage processes of tissue. Indeed, despite an extensive literature relating to this topic (see Humphrey, 2003; He and Bischof, 2003), we still lack a comprehensive understanding. This is due, in part, to a lack of appreciation of the underlying biothermomechanics. The effects of heat on tissue include cell death, expression of heat-shock proteins, protein denaturation (structural and functional), and altered hydration. Thus thermal damage has been studied by biologists, pathologists, biochemists, physicians, and of course, biomedical engineers.

The primary focus of this work is on the denaturation of fibrillar collagen (i.e. structural changes), which has been defined by Chen et al. (1997) as “a time-dependent irreversible transformation of the native (i.e. coiled) helical structure into a more random structure.” Collagen is the dominant structural

protein in the body, and forms the structural network to which many cells attach. There are at least 20 genetically distinct collagens, each with a unique set of three polypeptide chains that are bound together, at least in part, in a triple helix. Of the many types, five (Types I, II, III, V, and XI) are classified as fibrillar collagens and are typically found in bone, skin, tendon, arteries, and structural membranes such as the pericardium. Hence, fibrillar collagens are found in many tissues that are subjected to supraphysiologic temperatures during the course of clinical thermal therapies. Of the fibrillar collagens, type I is the most abundant, and therefore the most obvious choice for investigating thermal damage because the implications of the results would be far reaching. The specific aims of this study are (a) to examine the role of biaxial isometric constraints on the kinetics of collagen denaturation, (b) to determine the effects of isothermal, isometric heating on the resultant biaxial mechanical behavior of epicardium, of which type I collagen is the primary constituent (aside from water), (c) to seek a more reliable and universal metric of thermal damage, and (d) to determine the safety and efficacy of using glycerol as a clearing agent for thermal therapies.

Flory and Garrett (1958) suggested that collagen denaturation could be described as a first-order phase transition, therefore suggesting the existence of a characteristic melting (or denaturation) temperature. That idea gave birth to the use of differential scanning calorimetry (DSC) and hydrothermal isometric tension (HIT) tests to determine the so-called denaturation temperature of

collagen (Privalov, 1982; Le Lous et al., 1983; Lee et al., 1995). In the DSC tests, the temperature of the sample is increased at a constant rate (typically between 1 and 10 °C/min), and the power input required to maintain the linear rise in temperature is compared to that of a reference chamber, which is normally void of material. The temperature at which the peak of the resultant endotherm occurs is taken to be the so-called denaturation temperature. In HIT tests, a sample is uniaxially constrained at or near its natural length while submerged in solution (usually saline). The temperature of the solution is raised at a constant rate, and the force required to maintain the sample at the fixed length is monitored. The temperature at which the tissue begins to contract against its constraints (i.e. when the force becomes non-zero) is taken to be the denaturation temperature. (HIT tests were preferred over shrinkage tests due to the advent of electronic loads cells in the 1960's, which made it easier to measure force histories than to measure shrinkage histories with cathetometers; see Rasmussen et al., 1964; Allain et al., 1978). For both HIT and DSC tests it is well documented that the denaturation temperature is dependent on the rate of heating (slower rates yield lower denaturation temperatures; cf. Figure 5 in Miles et al., 1995). Therefore, while constant heating-rate tests have provided tremendous insight into differences in thermal stabilities for different types of collagen, and into the role of crosslinking in thermal stability, the notion of a characteristic denaturation temperature is clearly flawed.

Pioneering work by Henriques in the 1940's revealed a time-temperature coupling with regard to skin burns, which he believed suggested an underlying rate process. This led to the development of the Henriques Damage Integral,

$$\Omega(\tau) = \int_0^{\tau} A \exp\left(\frac{-E_a}{RT}\right) dt, \quad (1.1)$$

where $\Omega(\tau)$ is the accumulated damage parameter, A is the so-called frequency factor, E_a is the energy required for damage to occur (i.e. activation energy), R is the universal gas constant, and T is the absolute temperature (Henriques, 1947). The damage integral shows that for a chosen metric of thermal damage (i.e. tissue necrosis, cell death, birefringence loss, etc), equivalent levels of damage can be achieved using multiple combinations of temperature (T) and duration of heating (τ), assuming all other parameters remain unchanged. Evidently, this notion of a time-temperature equivalency is not unique to skin burns. On a microstructural level, Mixer (1963) studied thermally-induced cell death (cancer cells) and found that the Henriques damage integral fit well his data. Pearce et al. (1993) used the damage integral to describe the loss of collagen birefringence with heating in rat skin. Still others have modeled protein denaturation with the damage integral (Aksan and McGrath, 2003). Thus, the damage integral has found significant utility, yet it is not without limitations. Early research by Lennox (1949) and Weir (1949) demonstrated that the temperature at which thermal shrinkage initiates is modulated by mechanical load. Furthermore, isolated collagen molecules denature at a much lower

temperature than collagen fibrils ($\sim 39^{\circ}\text{C}$ vs. $\sim 56^{\circ}\text{C}$; Na, 1989), and so configurational entropic constraints may have an effect on the temperature of denaturation as well.

The majority of data suggest therefore that thermal damage of collagenous tissue is a rate process (Miles et al., 1995; Wright and Humphrey, 2002), wherein the rate likely depends on a host of factors, including temperature, loading, and prior thermal damage, but also local constituent to constituent interactions (Danielsen, 1981). Miles et al. (1995) showed that the temperature-dependence of the rate of thermal denaturation is best determined by a series of isothermal tests. Similarly, Chen et al. (1998a) used a series of uniaxial isotonic (constant load), isothermal tests to determine the effects of applied mechanical load on the kinetics of thermal shrinkage (a gross measure of denaturation). Specifically, they found that increasing uniaxial load delays thermal denaturation. The dependence on mechanical load is important because tissues are typically subjected to loads *in vivo*. The loads experienced by tissues are often complex and multi-dimensional, however, thus uniaxial experiments, though helpful for delineating general characteristics, are not sufficient. Harris and Humphrey (2004) performed a series of isothermal, biaxial isotonic tests on a collagenous membrane (bovine epicardium) to extend the results of Chen et al. to a multiaxial setting. They found a similar trend in the biaxial setting. Still, another possible constraint *in vivo* is one wherein the dimensions (i.e. the strain state) of the tissue are fixed (isometric).

Investigations into the effect of isometric constraints on the thermal damage of tissue are lacking. HIT tests, which have been the primary isometric test used for thermal damage studies, do not seek to determine the effect of varying the amount of isometric stretch. Lee et al. (1995) developed a variation of the HIT test that allowed for the application of pre-load (or pre-stretch), but they only report results on varying the amount of pre-load for gluteraldehyde-fixed tissue. Therefore, we have sought to determine the effect of a biaxial isometric constraint on the kinetics of isothermal denaturation of a collagenous membrane (bovine epicardium).

The kinetics are, however, merely one facet of the thermal damage process. Given our understanding of the process of mechanotransduction (i.e., the ability of a cell to sense local changes in the mechanical environment), knowledge of cell viability, loss of birefringence or protein denaturation is not sufficient to predict long-term clinical outcomes. Rather, we must consider also the changes to mechanical loading on viable cells as a result of the thermal intervention. Mechanical loading on cells can be altered by direct application (e.g. by inflating an angioplasty balloon), and/or by a change in the stress distribution within the tissue, which can be brought about by a change in structural properties. Mechanical loads applied during thermal treatments are transient in general (an exception could be the placement of a stent), and therefore not likely to incite a growth and remodeling response. With sufficient heating, however, damage to structural proteins (e.g. type I collagen) will

translate into a change of the structural properties (Chen et al., 1998b; Harris et al., 2003) and could thereby elicit such a response. Therefore, it is necessary to compare the mechanical behavior of the damaged tissue to that of the native. Significant changes to the mechanical behavior could suggest an aggressive, perhaps undesired, growth and remodeling response. Numerous studies have looked at the altered mechanical response due to heating under a uniaxial isotonic constraint (Lennox, 1949; Wiederhorn and Reardon, 1953; Consigny et al., 1989; Morgan et al., 1996; Wallace et al., 2001; and Chen and Humphrey, 1998), and Harris et al. (2003) were the first to perform similar tests in a biaxial setting. Still, we have found only one investigation that measured the mechanical response following an isometric (HIT) test (Hayashi et al., 2000). There is, therefore, a lack of data on mechanical changes resulting from heating under an isometric constraint. We have addressed this need by performing a series of isothermal biaxial isometric thermal damage tests wherein we compared the native and damaged tissue responses.

Having obtained a good qualitative understanding for the role of isotonic and isometric constraints in modulating thermal damage to tissue, it is important to recognize that tissues need not be subjected to only one kind of constraint. Rather, they are likely subjected to some complex combination of the two. Therefore, results from the two types of tests must somehow be compared, though their execution is fundamentally different. One such way to compare them is to identify a common (or universal) metric of thermal damage. We show

that by combining diffuse white light microscopy (LM) and transmission polarizing microscopy (TPM) one can assess the extent of prior thermal damage within tissues heated at a set temperature for various times and subject to either isotonic (zero load) or isometric mechanical constraints. It remains to be seen, however, if histological data can be quantified so as to allow for comparison between isometric and isotonic tests.

Finally, it makes sense to consider also clinical scenarios wherein chemical adjuncts may be applied to tissue to increase the efficacy. One such scenario under investigation is the use of glycerol as a clearing agent for laser therapies that require deeper penetration through turbid tissues. Tissues immersed in glycerol have reduced hydration due to its hyperosmotic effects. The role of hydration in governing the mechanics and thermal damage of soft tissue is significant. Tendons placed in a hypertonic solution exhibit altered viscoelastic behavior (Haut and Haut, 1997), that is, the strain-rate sensitivity is reduced. Therefore, water apparently endows tissue with at least part of its viscoelastic characteristics. Miles et al. (1995) showed that an increased water content (i.e., swelling) yields a lower endotherm peak temperature in DSC measurements, which they believe is due to an increase in the activation entropy. Ramachandran et al. (1973) hypothesized that 4-hydroxyproline stabilizes the collagen structure through incorporation of water bridges (i.e. excess hydrogen bonding) that form within and between molecules. Recent studies support their hypothesis (Burjanadze, 2000; Prockop and Kivirikko,

1995). Therefore, water affects soft tissue in a minimum of two ways: by changing the tissue volume and by directly interacting with the molecules. We investigate the effects of glycerol on the biaxial mechanical behavior and thermal damage kinetics of bovine epicardium.

CHAPTER II

METHODS

This chapter contains details of procedures that are used throughout most experiments. Therefore, it is intended to serve more as a reference when reading through the remaining chapters.

SPECIMEN PREPARATION

We tested bovine epicardium for we have considerable experience with this tissue (Humphrey et al., 1990; Kang et al., 1996; Harris et al., 2003), it is readily available, and it is a good model 2-D tissue. Like skin, the epicardium consists largely of type I collagen fibers that are arranged in a 2-D fashion; indeed, the gross mechanical behavior of these two tissues is very similar (Lanir, 1979; Harris et al., 2003). Bovine hearts were obtained from the slaughterhouse within 24 hours of death, and qualitatively assessed for size and for fat content. Those which were grossly oversized (generally greater than 3 kg, though the assessment was visual) or those with fat covering more than 75% of the right ventricular surface were discarded. From each remaining heart, a single rectangular block of tissue (~ 5 cm x 3 cm) was isolated from the right ventricular free wall. Each rectangular block was then pinned on a paraffin dissection tray with the epicardial surface down, and the myocardium was peeled away from the epicardium (see Figure 2.1). Finally, the pinned ends of the tissue were

removed, yielding an epicardial sample approximately 30 mm square (thickness $\sim 150 \mu\text{m}$).

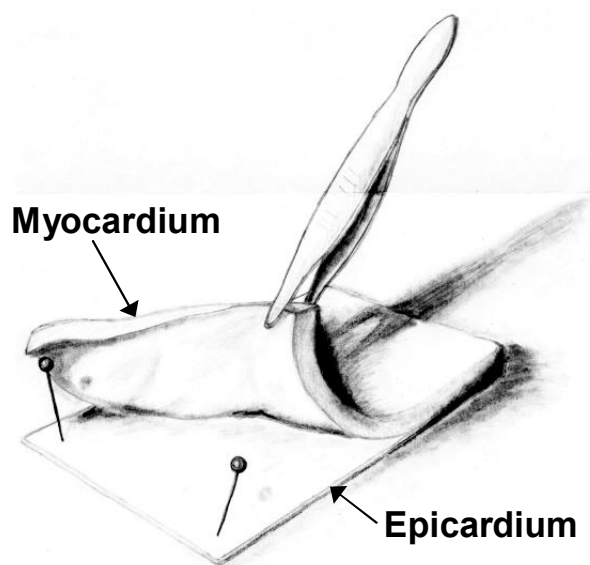


Figure 2.1 Myocardium was carefully peeled from the epicardium, yielding a clean, undamaged sample.

Next, the tissue was placed atop a circular piece of optical glass (~ 3.2 mm thick) and a thin layer of saline was injected between the tissue and the glass such that the tissue floated. This allowed the tissue to assume a near traction-free configuration. The saline was then withdrawn by absorption with a paper towel so that the tissue rested on the glass surface, thereby securing the traction-free configuration. Then, the glass was placed on the stage of a simplified, qualitative version of the Small Angle Light Scattering (SALS; see Figure 2.2) device, originally developed by Sacks et al. (1997). A circular laser beam (2 mm beam diameter, 6.5 mW HeNe) was directed perpendicular to the plane of the membrane via a mirror. The scattered, transmitted light projects

onto a piece of white paper situated approximately one centimeter below the tissue, and the projected image is captured by a CCD and output to a black and white monitor. The scattered light tends to take on a more elliptical shape, with the minor axis corresponding to the primary fiber direction in the tissue. Multiple areas of the tissue surface were imaged, and the 'average' preferred direction was determined qualitatively. Because of the importance of determining the preferred direction within reasonable error (discussed below), our qualitative SALS device was verified against the automated, quantitative SALS device in the lab of Dr. Michael Sacks at The University of Pittsburgh. Chapter III is dedicated to that study.

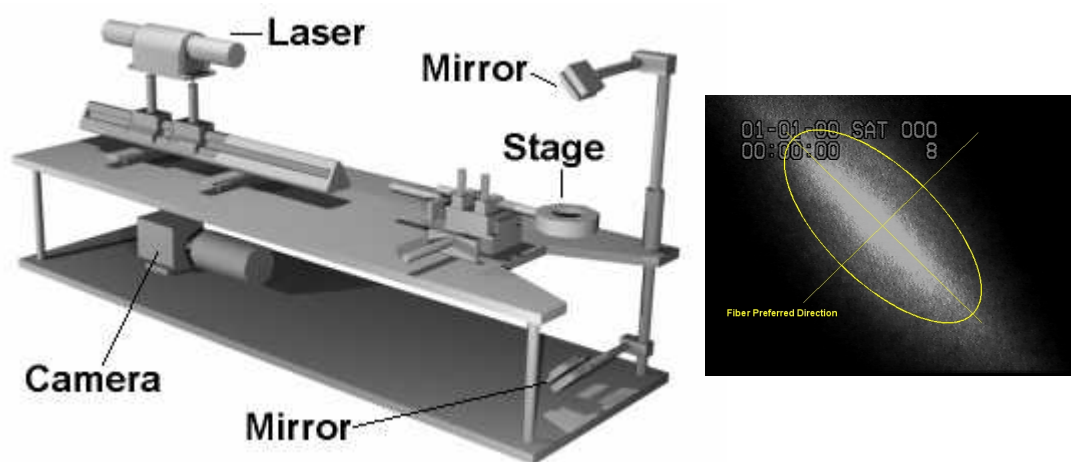


Figure 2.2 Small Angle Light Scattering (SALS) device used in our study. Laser light is directed perpendicular to the surface of the tissue, and the transmitted, scattered light is captured by a CCD to yield the image on the right. The minor axis of the ellipse corresponds to the preferred fiber direction. (Device was designed by Jason Campbell as part of an undergraduate project)

Next, the tissue was removed from the optical glass and placed atop a square grid such that the preferred fiber direction coincided with the demarcated side of the square (this allowed us to keep track of the preferred direction), and such that the myocardial surface was face down. Saline was again injected beneath the tissue and subsequently withdrawn to secure the tissue in a traction-free configuration. Dots of India ink were placed on the tissue to mark the suture locations (five dots per side), and small drops of glue were placed on the dots of India ink to prevent them from being inadvertently rinsed off or smeared during the suturing process. Next, working under a microscope, tracking markers (50 – 90 μm diameter, dyed microspheres) were placed in a four-by-four array in the central region ($\sim 1 \times 1 \text{ mm}^2$) of the tissue and glued to the surface, using a drawn pipette to dispense the glue. (During the marker placement and gluing, care was taken to prevent saline puddles from forming on the tissue surface.) After a minimum of five minutes was allowed for the glue to set, the tissue was transferred to the suturing apparatus, taking care to align the preferred direction with the y-axis. Next, a mounting rod was attached to each side of the tissue via a continuous loop of rayon thread. Finally, the tissue was placed in the specimen chamber of the device (Figure 2.3) such that the tracking markers were facing down, and the mounting rods were placed in the device load carriages.

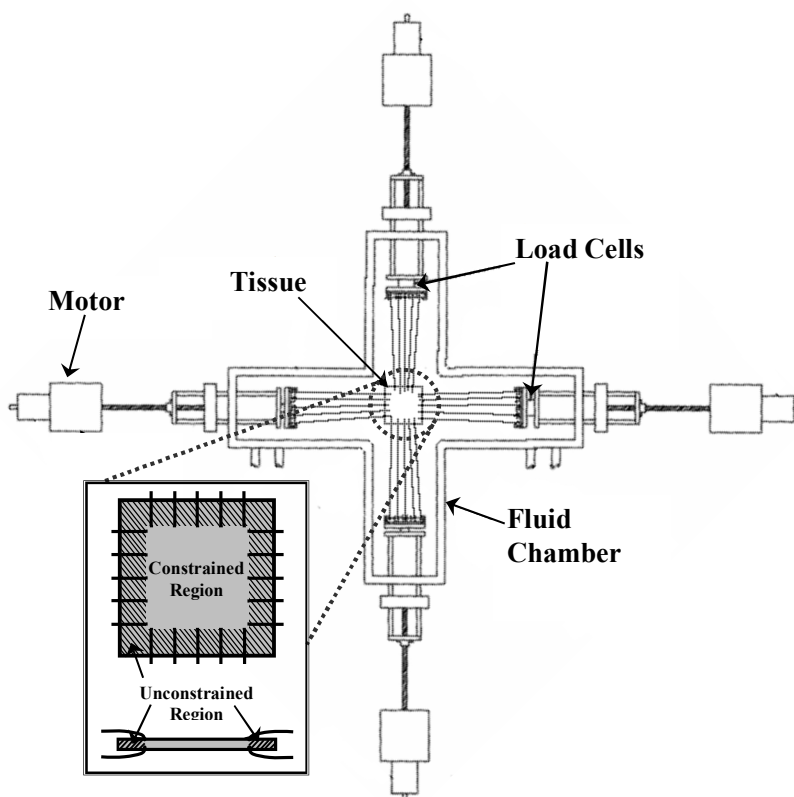


Figure 2.3 Top view diagram of the biaxial testing system. The chamber is constructed of 0.5 inch acrylic, insulated with 0.75 inch polystyrene, and covered from above. A quartz glass window under the specimen allows the tracking markers to be monitored by the CCD (not shown). Closed-loop feedback control is on force or stretch. The inset illustrates the regions of the tissue defined as outer (unconstrained) and central (constrained) in both a top view (above) and cross-section view (below).

DESCRIPTION OF DEVICE

The biaxial device was developed and constructed as part of the Ph.D. work of Dr. Jason Harris, under the instruction of Dr. Jay Humphrey. A concise overview of the device is given here, and explicit details can be found in Chapter II in Harris (2003). The device is capable of performing a wide array of load- or stretch-controlled mechanical tests on tissues immersed in a thermally-controlled, clear fluid. The water-tight specimen chamber (~2 L) is constructed

of one-half inch polycarbonate, in the shape of a cross. A circular optical window is centrally located in the floor of the chamber to allow for video capture of the tracking markers (discussed below). Within each arm of the cross is an aluminum loading carriage, into which an aluminum mounting rod fits. Two of the mountings carriages (one per axis) are attached to submersible, temperature-compensated load cells (Sensotec, 250g), which are rigidly attached to external computer-controlled stepper motors by means of stainless-steel rods that puncture the wall of the chamber. The other two loading carriages are similarly attached to stepper motors, minus the load cells. The holes through which the rods pass into the chamber are sealed with rulon bearings, which serve the dual purpose of reducing friction. The motors are controlled using custom-designed software via feedback from either the load cells (for load-controlled tests) or the positions of the tracking markers (for stretch-controlled tests; see 'Online Computation of Stretch Ratios' below). A CCD camera mounted beneath the specimen chamber "looks" at the underside of the tissue through the optical window, by way of a 45° mirror (see Figure 2.4). An image of the tracking markers is captured at 30Hz via the CCD camera and a video frame-grabber board, which digitizes the image to a 512 x 512 pixel array. (The image is also captured to video cassette in the event strains have to be calculated off-line.) For each capture (i.e. every 1/30 sec), a search algorithm based on pixel intensity values is used to locate the approximate pixel coordinates for the centroid of each marker. The software then computes the

stretch ratios by comparing the current marker positions, given by pixel coordinates, to the reference positions using bilinear isoparametric interpolation (Humphrey et al., 1987).

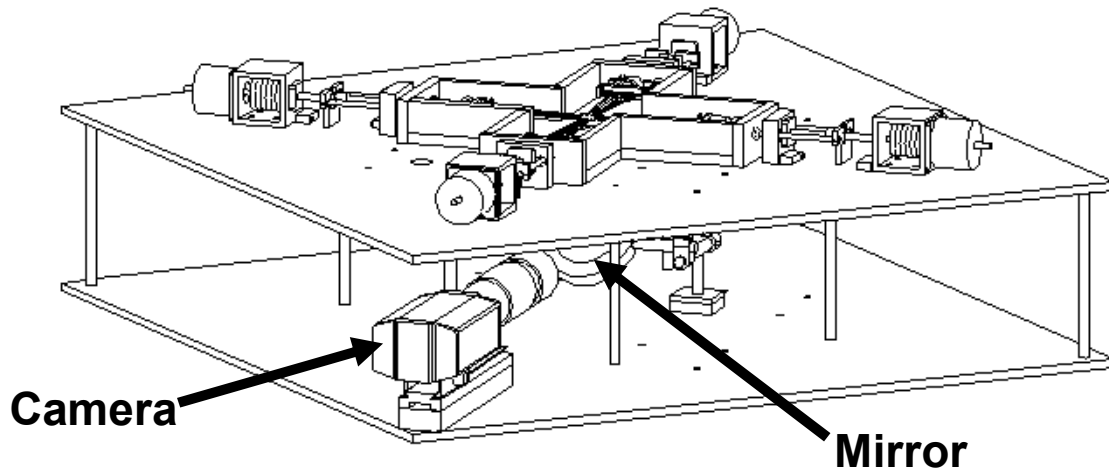


Figure 2.4 Illustration of the camera configuration for viewing the tracking markers. Markers are reflected off a mirror, through an optical window in the floor of the specimen chamber. (Figure taken from Harris, 2002)

We chose to use four markers in a quadrilateral configuration to compute the deformation. Though not required, the reference configuration was always chosen to be traction free (recall that traction free does not imply stress free). Let the marker locations be defined as shown in Figure 2.5.

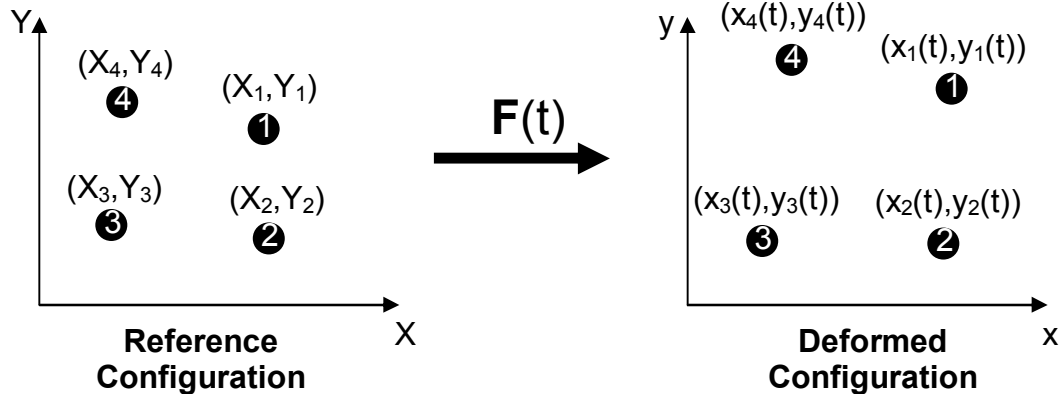


Figure 2.5 Marker numbering scheme, along with corresponding position coordinates.

$\mathbf{F}(t)$ is the deformation gradient, and the deformation field can be calculated at any time, t , as

$$\mathbf{F} = \begin{bmatrix} \frac{\partial x}{\partial X} & \frac{\partial x}{\partial Y} \\ \frac{\partial y}{\partial X} & \frac{\partial y}{\partial Y} \end{bmatrix} = \begin{bmatrix} \frac{\partial(X+u)}{\partial X} & \frac{\partial(X+u)}{\partial Y} \\ \frac{\partial(Y+v)}{\partial X} & \frac{\partial(Y+v)}{\partial Y} \end{bmatrix}, \quad (2.1)$$

where u and v are the instantaneous displacements relative to the reference position in the x and y directions, respectively. Note, too, that \mathbf{F} can be represented as the sum of two tensors, namely

$$\mathbf{F} = \begin{bmatrix} 1 + \frac{\partial u}{\partial X} & \frac{\partial u}{\partial Y} \\ \frac{\partial v}{\partial X} & 1 + \frac{\partial v}{\partial Y} \end{bmatrix} = \mathbf{I} + \begin{bmatrix} \frac{\partial u}{\partial X} & \frac{\partial u}{\partial Y} \\ \frac{\partial v}{\partial X} & \frac{\partial v}{\partial Y} \end{bmatrix} = \mathbf{I} + \mathbf{H}. \quad (2.2)$$

Therefore, to solve for \mathbf{F} , the gradient of the displacement field, \mathbf{H} , must be computed. To compute \mathbf{H} , the displacement of each marker must be calculated, which is easily done using the coordinates of each marker i :

$$u_i = x_i - X_i \quad , \quad v_i = y_i - Y_i \quad , \quad i = [1,2,3,4]. \quad (2.3)$$

Having calculated displacements at the four discrete locations, a bilinear interpolation function

$$f_i(r,s) = \frac{(1-r)r(1-s)s}{4} \quad , \quad r,s \in [-1,1] \quad (2.4)$$

is then used to formulate C^1 continuous functions for the approximate displacements over the domain of r and s , namely

$$\begin{aligned} u(r,s) &= \sum_{i=1}^4 f_i(r,s)u_i \quad , \\ v(r,s) &= \sum_{i=1}^4 f_i(r,s)v_i \quad . \end{aligned} \quad (2.5)$$

Effectively, the area defined by the marker locations is parameterized to a square (Figure 2.6), within which the displacements can be calculated at any point.

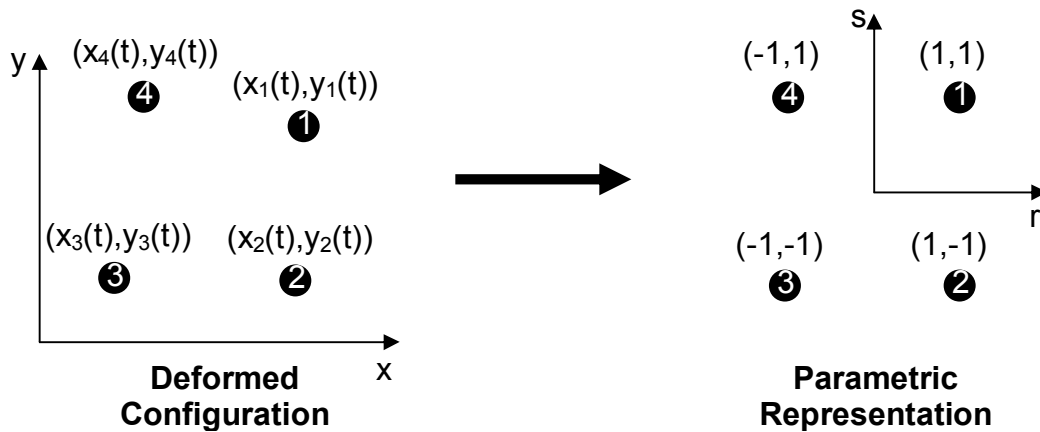


Figure 2.6 Parameterization of instantaneous marker positions.

Recognize now that the following relations hold for both u and v :

$$\frac{\partial}{\partial s} = \frac{\partial}{\partial X} \frac{\partial X}{\partial s} + \frac{\partial}{\partial Y} \frac{\partial Y}{\partial s} \quad \text{and} \quad \frac{\partial}{\partial r} = \frac{\partial}{\partial X} \frac{\partial X}{\partial r} + \frac{\partial}{\partial Y} \frac{\partial Y}{\partial r}, \quad (2.6)$$

or, in matrix form,

$$\begin{Bmatrix} \frac{\partial}{\partial s} \\ \frac{\partial}{\partial r} \end{Bmatrix} = \begin{bmatrix} \frac{\partial X}{\partial s} & \frac{\partial Y}{\partial s} \\ \frac{\partial X}{\partial r} & \frac{\partial Y}{\partial r} \end{bmatrix} \begin{Bmatrix} \frac{\partial}{\partial X} \\ \frac{\partial}{\partial Y} \end{Bmatrix}. \quad (2.7)$$

Therefore, \mathbf{H} is obtained by solving

$$\begin{Bmatrix} \frac{\partial}{\partial X} \\ \frac{\partial}{\partial Y} \end{Bmatrix} = \begin{bmatrix} \frac{\partial X}{\partial s} & \frac{\partial Y}{\partial s} \\ \frac{\partial X}{\partial r} & \frac{\partial Y}{\partial r} \end{bmatrix}^{-1} \begin{Bmatrix} \frac{\partial}{\partial s} \\ \frac{\partial}{\partial r} \end{Bmatrix} \quad (2.8)$$

for both u and v , from which it is evident we also need parametric representations for X and Y , which are assumed to be given isoparametrically as

$$\begin{aligned} X(r,s) &= \sum_{i=1}^4 f_i(r,s) X_i \\ Y(r,s) &= \sum_{i=1}^4 f_i(r,s) Y_i \end{aligned} \quad (2.9)$$

Finally, having solved for \mathbf{H} , and thus \mathbf{F} , the components of \mathbf{F} are

$$\mathbf{F}_{2D} = \begin{bmatrix} 1 + \frac{\partial u}{\partial X} & \frac{\partial u}{\partial Y} \\ \frac{\partial v}{\partial X} & 1 + \frac{\partial v}{\partial Y} \end{bmatrix} = \begin{bmatrix} \lambda_1 & \kappa_1 \\ \kappa_2 & \lambda_2 \end{bmatrix}. \quad (2.10)$$

It is worth noting that the true stretch ratios Λ_1 and Λ_2 for line segments originally along the primary stretching axes are given by equation (2.16). Those values were not used for the feedback control, primarily because the biaxial device in not

capable of compensating for excess shearing, but also because of the increased computational expense. It was for this reason that we were careful to align the preferred direction with one of the primary stretching axes. In doing so, the values of κ_1 and κ_2 are minimized, thus the error between λ and Λ is minimized. The values in equation (2.16) were used in all off-line data analysis.

The temperature of the fluid in the specimen chamber is controlled by means of fluid exchange with a six-liter, thermally-controlled reservoir. Fluid exchange is accomplished via two variable-speed analog roller pumps (Masterflex) operating in opposition, and all fluid conduits are insulated with foam to minimize heat dissipation. The reservoir contains two 500 watt immersion heaters, which are controlled by two digital temperature controllers (Cole-Parmer). One controller monitors the temperature in the specimen chamber using a T-type thermocouple placed very near the tissue, and the other controller monitors temperature within the reservoir using a thermistor (in general, the reservoir is maintained approximately 5°C above the chamber). This coupled control allows for the maintenance of a baseline temperature in the reservoir, while also allowing for additional heat input should the chamber temperature decrease below the set point.

MECHANICAL TESTING

For consistency, each specimen was subjected to nearly the same mechanical history. After mounting the tissue in the device, a nominal stretch

was applied so that the tissue had no folds. Because the tissue has a tendency to sink, and thus deviate from the focal plane of the camera, small pieces of polystyrene foam were placed on the underside of the tissue to render it nearly neutrally buoyant. Next, the tissue was preconditioned biaxially from 0.02 to 0.78 N for ten cycles (0.05 Hz), at which time the mechanical response remained consistent. The sutures were then slackened and the native traction-free reference configuration, β_N , recorded. Next, the native tissue was subjected to an equibiaxial stretching test, during which the tissue was cycled between zero and 0.88 N in the 'stiffer' direction at 0.03 Hz while the stretch ratios were maintained equal in each direction. It can be shown that the in-plane fiber orientations are maintained fixed in equibiaxial tests, thus allowing one to interrogate material symmetry (Appendix A). The next tests performed were 'constant-x' and 'constant-y' tests. In the 'constant-x' test, the x-direction is maintained at a chosen stretch while the y-direction is cycled between two prescribed values. For the tests herein, the bounds of stretch were 1.07 and λ_{\max} , where λ_{\max} is the maximum value of stretch obtained in the equibiaxial test. The 'constant-y' test is similar, merely reversing the directions. These tests are particularly useful in identifying functional forms of 2-D strain energy functions (see Humphrey et al., 1992). Finally, a proportional stretch ratio test was performed, during which the stretch in each direction was cycled between two prescribed values while maintaining the ratio of the two stretches equal to some constant other than one (which would coincide with an equibiaxial test). The

results of such tests are useful for parameter estimation and examining the predictive capability of any model that may be formulated. All tests were run for five cycles at 0.03 Hz.

FLUID EXCHANGE PROCEDURES

Exchanging room temperature fluid for heated, circulating fluid (saline or glycerol): Refer to the diagram in Figure 2.7. We attached tubes RT1 and RT2 to connectors PA1 and PA2, respectively, and then placed pump 'PA' in max-speed reverse flow until all room temperature fluid was evacuated from the specimen chamber. Next, we detached tubes RT1 and RT2, and then connected tubes HC1 and HC2 to connectors PA1 and PA2, respectively. Then, pump 'PA' was placed in forward flow at a moderate to low speed. Once the chamber had filled to the appropriate level (i.e. when all loading carriages were immersed), which took approximately 30 seconds, pump 'PB' was placed in reverse flow, and the speeds of both pumps were adjusted until a steady fluid level was achieved (i.e. inflow = outflow). Typically, the motor speeds were set near 60 percent of maximum, and they required fine, periodic adjustments if circulation was maintained in excess of 20 minutes.

Exchanging heated fluid for room temperature fluid: At the conclusion of heating, both pumps were placed in reverse flow at maximum speed until the specimen chamber was evacuated. Next, having turned the pumps off, we detached tubes HC1 and HC2 from, and connected tubes RT1 and RT2 to,

connectors PA1 and PA2, respectively. We then placed pump 'PA' in forward flow at a moderate to low speed until the specimen chamber was again filled to the appropriate level with the room temperature fluid. Note, approximately 60 seconds passed between the tissue losing contact with the heated fluid and making contact with the room temperature saline. Therefore, to quench the tissue more rapidly, we gently dripped room temperature saline on the tissue, using a 10 cc syringe, immediately after the tissue had lost contact with the heated fluid.

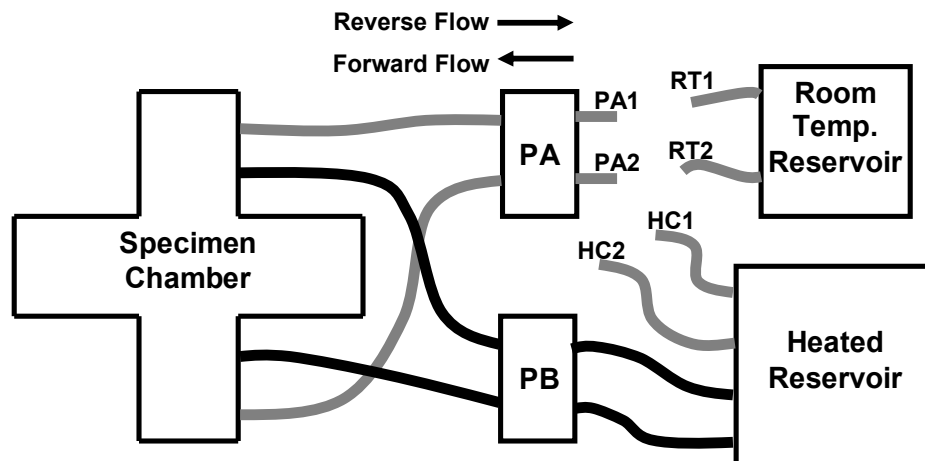


Figure 2.7 Fluid flow diagram. Note that pump PB was only used in reverse flow.

HISTOLOGICAL PROCESSING

At the conclusion of each experiment, the tissues were placed in a shallow pool of 10% neutral buffered formalin, covered, and then refrigerated for two to five days. This allowed us to “fix” the sample in a nearly flat, unloaded

configuration. The tissues and formalin were then transferred to clearly labeled specimen bags (100ml Whirl-Pak®) and refrigerated for no more than four weeks. For histological preparation, the samples were taken to the histology lab in the department of Veterinary Anatomy & Public Health at Texas A&M University. Samples were then sliced in half along the preferred fiber direction to maximize birefringence. Note that preferred directions were not determined for the free-shrinkage tissues herein, thus they were sliced in half along an arbitrary axis. Harris et al (2003) noted that free-shrinkage tissues were near isotropic, however, and therefore an arbitrary slicing axis is justified. Each half of the tissue was then embedded on-edge in separate paraffin blocks, with the sliced edge up. One block was stored for future use, and from the other block five sections (5 μm each) were taken. Sections 1, 3 and 5 were stained with hematoxylin and eosin (H&E) for analysis of morphology and birefringence, and sections 2 and 4 with Weigert van Gieson (WvG) stain for analysis of elastin distribution and morphology. Having sectioned the tissue in this way, we were able to look at both the periphery and the center of the specimen (away from stress concentrations due to the loading sutures in the biaxial tests; see inset of Figure 2.3).

DATA ANALYSIS

Marker positions (pixel coordinates) and load cell readings are output to a file, from which the deformation gradient is computed in the same fashion as

outlined above. From the deformation gradient, one can calculate the requisite stretch ratios along the axes of pull. Imagine a line segment in the reference configuration (i.e., prior to stretching) that lies in the direction of unit vector \mathbf{M} with magnitude dS . Following the deformation, the line segment will have an orientation in the direction of unit vector \mathbf{m} with magnitude ds . The stretch ratio Λ for that line segment is defined

$$\Lambda = \frac{ds}{dS}. \quad (2.11)$$

Recall, the deformation gradient relates line segments in the reference configuration to line segments in the current configuration, and therefore

$$d\mathbf{sm} = \mathbf{F} \cdot (d\mathbf{SM}). \quad (2.12)$$

Using the definition of vector magnitude to our advantage, the stretch ratio can be determined as follows:

$$\begin{aligned} ds &= \sqrt{[\mathbf{F} \cdot (d\mathbf{SM})] \cdot [\mathbf{F} \cdot (d\mathbf{SM})]} \\ ds &= dS \sqrt{(\mathbf{M} \cdot \mathbf{F}^T)(\mathbf{F} \cdot \mathbf{M})} \\ \frac{ds}{dS} &= \sqrt{\mathbf{M} \cdot \mathbf{C} \cdot \mathbf{M}}, \end{aligned} \quad (2.13)$$

where $\mathbf{C} = \mathbf{F}^T \cdot \mathbf{F}$ is the right Cauchy-Green tensor. Note that by the polar decomposition theorem,

$$\mathbf{F} = \mathbf{R} \cdot \mathbf{U} \quad (2.14)$$

$$\mathbf{R} \in Orth^+ \quad \mathbf{U} \in Psym$$

where \mathbf{R} contains all of the rigid body motion. Therefore,

$$\mathbf{C} = \mathbf{U}^T \cdot \mathbf{R}^T \cdot \mathbf{R} \cdot \mathbf{U} = \mathbf{U}^2, \quad (2.15)$$

which reveals that \mathbf{C} , and thus the stretch ratios, are insensitive to rigid body motion. The stretch ratios along the primary axes of pull are easily found by solving equation (2.14):

$$\text{for } \mathbf{M} = \begin{bmatrix} 1 & 0 \end{bmatrix} \Rightarrow \Lambda_1 = \sqrt{F_{11}^2 + F_{21}^2}. \quad (2.16)$$

$$\text{for } \mathbf{M} = \begin{bmatrix} 0 & 1 \end{bmatrix} \Rightarrow \Lambda_2 = \sqrt{F_{22}^2 + F_{12}^2}$$

Stresses may also be calculated from the data file. Cauchy stress \mathbf{t} is defined as the current force acting over the current area, and can be found through the deformation gradient and measurable quantities using

$$\mathbf{t} = \frac{1}{J} \mathbf{F} \cdot \mathbf{P}, \quad (2.17)$$

where J is the determinant of \mathbf{F} , and \mathbf{P} is the first Piola-Kirchhoff tensor, defined as force per unit undeformed area, and the components of \mathbf{t} are

$$t_{ij} = \frac{1}{J} F_{iA} P_{Aj}. \quad (2.18)$$

For the biaxial stretching of a membrane, \mathbf{F} and \mathbf{P} are given as

$$\mathbf{F} = \begin{bmatrix} \lambda_1 & \kappa_1 & 0 \\ \kappa_2 & \lambda_2 & 0 \\ 0 & 0 & \lambda_3 \end{bmatrix}, \quad \mathbf{P} = \begin{bmatrix} \frac{f_1}{L_2 H} & 0 & 0 \\ 0 & \frac{f_2}{L_1 H} & 0 \\ 0 & 0 & 0 \end{bmatrix}, \quad (2.19)$$

where f_1 and f_2 are the forces along the primary stretching axes, L_1 and L_2 are the undeformed planar dimension of the tissue, and H is the undeformed thickness (see Figure 2.8). Therefore the components of \mathbf{t} are

$$t_{11} = \frac{f_1 \lambda_1}{J L_2 H} \quad , \quad t_{22} = \frac{f_2 \lambda_2}{J L_1 H} \quad , \quad t_{12} = \frac{\kappa_1 f_2}{J L_1 H} \quad , \quad t_{21} = \frac{\kappa_2 f_1}{J L_1 H} \quad , \quad (2.20)$$

where $t_{12} = t_{21}$ by symmetry. Because thickness measurements are difficult, we exploit the membrane theory, which is valid for any problem wherein the thickness is small relative to the planar dimensions, the out-of-plane stresses are negligible, and the in-plane stresses do not vary significantly through the thickness of the membrane. Therefore, we can compute the components of the in-plane Cauchy stress resultant \mathbf{T}

$$T_{ij} = \int_{-h/2}^{h/2} t_{ij} dx_3 = t_{ij} h \quad , \quad (2.21)$$

where h is the deformed thickness. Now, recalling that $h/H = \lambda_3$, the stress resultants are given as

$$T_{11} = \frac{f_1 \lambda_1}{(\lambda_1 \lambda_2 - \kappa_1 \kappa_2) L_2} \quad , \quad T_{22} = \frac{f_2 \lambda_2}{(\lambda_1 \lambda_2 - \kappa_1 \kappa_2) L_1} \quad , \quad T_{12} = T_{21} = \frac{\kappa_1 f_2}{(\lambda_1 \lambda_2 - \kappa_1 \kappa_2) L_1} \quad . \quad (2.22)$$

Note that when the values of κ_1 and κ_2 are small, T_{12} and T_{21} are approximately zero, and therefore the κ values give us an indirect indication of shear within the tissue.

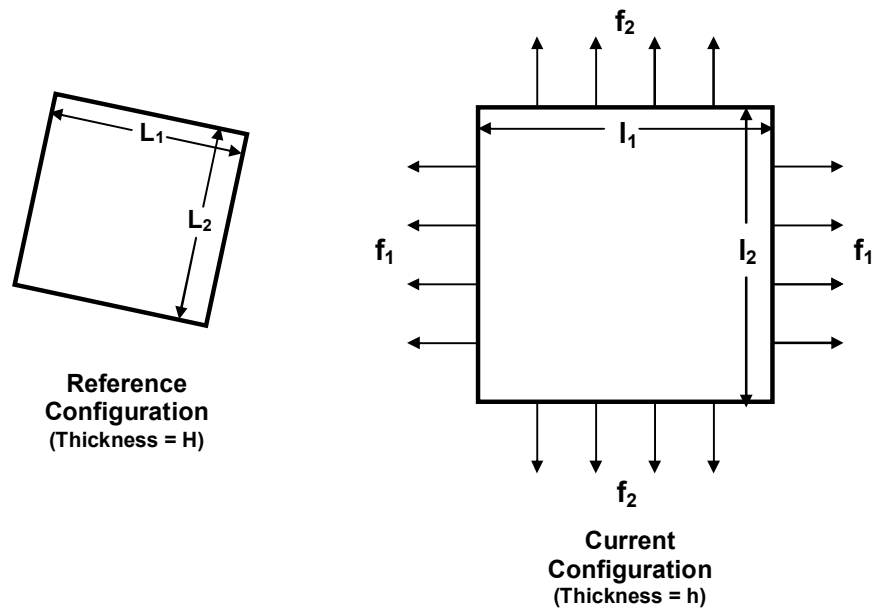


Figure 2.8 Representation of a biaxial stretch. The membrane is shown also to rotate with the applied load, which illustrates that rigid body motions are present. The measure of strain chosen, however, is insensitive to rigid body motion.

The epicardium is mechanically anisotropic, in general, and after several experiments were performed it became evident that the anisotropy was inconsistent from tissue to tissue, and that changes induced by thermal damage also varied. Therefore, it proved convenient to analyze data in terms of a single scalar measure of the tensorial membrane stress, namely the magnitude of \mathbf{T} , which is defined as

$$|\mathbf{T}| = \sqrt{\text{tr}(\mathbf{T} \cdot \mathbf{T}^T)}. \quad (2.23)$$

In doing so, we had to choose also a single scalar measure for the stretch. \mathbf{T} is a one-point tensor that exists in the current configuration. Similarly, the left

“stretch” tensor $\mathbf{V} = \sqrt{\mathbf{F} \cdot \mathbf{F}^T}$ exists in the current configuration, and was therefore a logical choice. The magnitude of \mathbf{V} is found in the same way as that for \mathbf{T} .

CHAPTER III

VALIDATION OF QUALITATIVE SALS DEVICE

INTRODUCTION

Recall from Chapter II that feedback for stretch-controlled tests is based on that $\lambda_1 \equiv F_{11}$ and that $\lambda_2 \equiv F_{22}$, whereas the actual stretch ratios along the axes of stretch are $\Lambda_1 = \sqrt{F_{11}^2 + F_{21}^2}$ and $\Lambda_2 = \sqrt{F_{22}^2 + F_{12}^2}$ (see equation (2.16)). Therefore, as the off-diagonal components of \mathbf{F} (which reflect shear strain and rigid body rotation) become larger, the error in the calculation for the stretch ratios λ_1 and λ_2 becomes greater. Shearing is minimized when the preferred fiber direction is aligned with a primary stretching axis, and therefore it is important that our qualitative SALS device be reasonably accurate. Also, because we cannot re-suture the tissue after heating, it is desirable that the preferred fiber direction not change, that it remains along a primary stretching axis. Finally, in comparing our results on right ventricular tissue to isotonic tests on left ventricular tissue (Harris et al., 2003), it is important to recognize that differences (or similarities) in mechanical behavior may reflect differences in fiber architecture. In this chapter we report results on the mapping of fiber architecture of left ventricular (LV) and right ventricular (RV) tissues, before and after heating under different biaxial isometric constraints. For contrast, we also report results for one tissue that was heated with no constraints (i.e. free-

shrinkage). The mapping was performed using the automated, quantitative SALS device of Sacks et al. (1997), from which we took the inspiration for our simplified qualitative SALS.

METHODS

Specimen Preparation

Eight tissues were dissected from four hearts according to the method in Chapter II, with the exception that four of the tissues were taken from the left ventricle (LV) and four were taken the right ventricle (RV). Next, the preferred fiber direction was determined using the simplified SALS technique described in Chapter II under “specimen preparation”. The preferred fiber direction was marked by placing two dots of India ink near the border of the tissue, opposite one another. Small drops of glue were then placed on the India ink to prevent it from being rinsed off. Next, two of the RV tissues were stretched, one by 20% and one by 40%, in both the preferred and non-preferred directions, and affixed to plastic frames via staples (Figure 3.1). The same was done for two of the LV tissues. The percentage of stretch was approximated visually, with the help of a scale. A third LV tissue was designated for a free-shrinkage test, and two tissues, one from the LV and one from the RV, were set aside to be used as native controls. The fourth RV tissue was not used. Care was taken to couple the tissues such that both native tissues came from the same heart, both tissues subjected to 20% stretch came from the same heart, and likewise for the 40%

stretch tissues. This at least facilitated direct comparison between the LV and RV for each test constraint (i.e. native, 20% stretch, and 40% stretch), while comparisons between the different constraints would be mildly blurred by specimen variability.

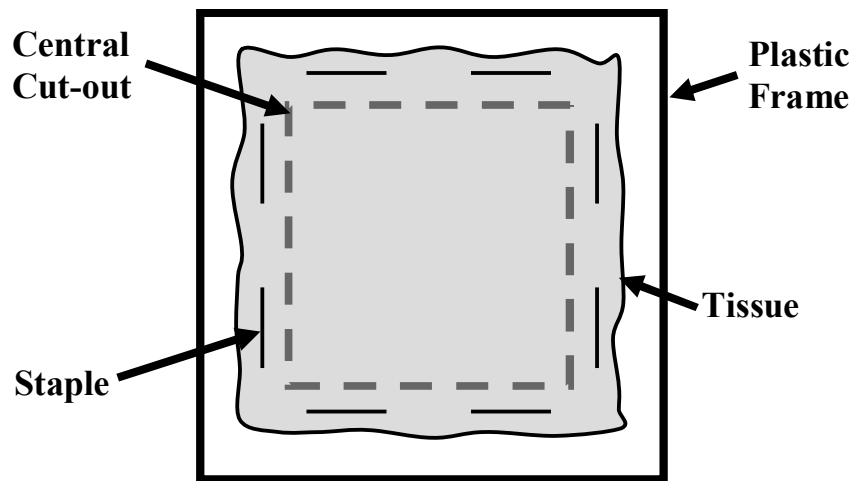


Figure 3.1 Illustration of frame-mounted tissue. The cut-out in the center of the frame allows for heated saline to contact both sides of the tissue.

Thermal Treatment

A 200 ml beaker filled with normal saline was placed atop a hotplate (Cole-Parmer model # 4803-00) and heated to equilibrium at 75°C, which took approximately 15 minutes, during which the beaker was covered to prevent evaporation and thus a change in solute concentration. The cover was then removed, and the frame-mounted tissues, as well as the free-shrinkage tissue, were placed in the beaker. The cover was replaced and the tissues remained in the heated saline for 900 seconds. At the conclusion of heating, the samples

were rapidly transferred to a 1000 ml beaker filled with room temperature saline. Next, the tissues were removed from the mounting frames, and all tissues were transferred to clearly labeled, individual specimen bags (100ml Whirl-Pak®) filled with 10M glycerol and refrigerated for 16 hours.

Automated Quantitative SALS

SALS experiments were performed in Dr. Michael Sacks' lab, at the University of Pittsburgh, with the help of David Merryman, a Ph.D. candidate. Details of the automated SALS device and its operation can be found in Sacks et al. (1997). Briefly, one tissue was removed from its specimen bag and placed between two large glass cover slips (~ 8 x 5 cm) that had been sealed on three sides (tissue mounting rig; Figure 3.2). The space between the cover slips was slightly larger than the thickness of the tissue, and so the tissue was not 'pressed'. The empty volume between the cover slips was then filled with 10M glycerol, because glycerol renders the tissue more optically transparent. Next, the contraption was mounted in the automated SALS device and the surface was scanned. Briefly, a circular laser beam is directed perpendicular to the surface of the tissue, and the transmitted, scattered light is projected onto a thin, white plastic screen. The projected image is captured by a CCD and fed into a computer, which measures and stores the transmitted light intensity at every point (i.e. pixel) in the image. A biaxial motorized carriage then moves the tissue a small amount, and the intensity is again measured. The scanning continues

until the entire area of interest has been measured, and the data output to a text file. Finally, the tissue mounting rig was removed from the SALS device, a digital photo was taken of the tissue, and the tissue was removed and discarded. This procedure was repeated for all seven tissues.

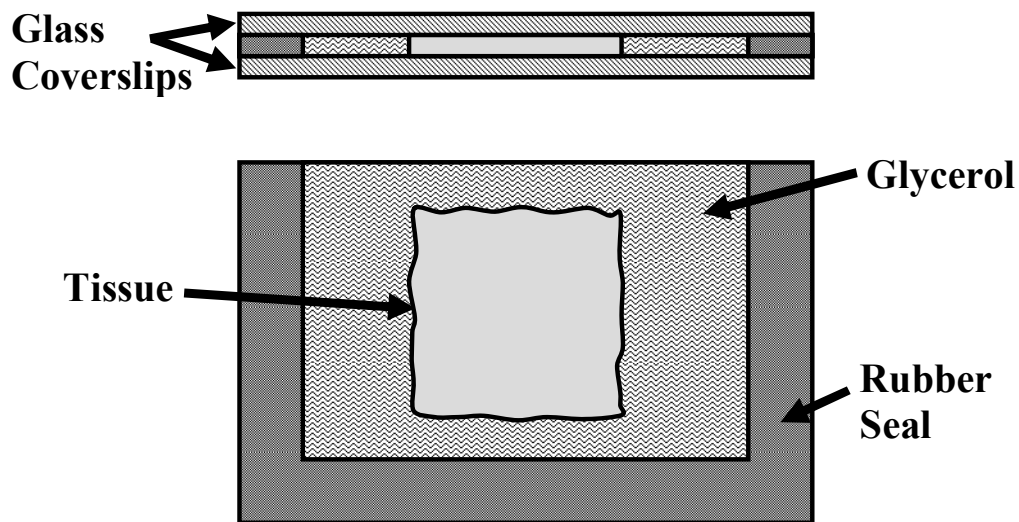


Figure 3.2 Top and side view illustrating the placement of the tissue between glass cover slips. This mounting rig was then placed into the automated SALS device (Sacks et al., 1997).

Post-Processing of Data

The data files were analyzed using the Small Angle Light Scattering Analysis (SALSA) software provided by Dr. Michael Sacks. From each data file, the software computes three parameters – *intensity distribution*, *orientation index* (OI), and *preferred fiber angle*. The intensity distribution is determined by summing the light intensities of the elliptical scattering pattern along radial lines in one-degree increments. The net result is a graph similar to Figure 3.3.

Because the intensities at angle θ and $\theta + \pi/2$ lie along the same axis, the average of the two is taken as the intensity profile for $\theta = [0, \pi/2]$ (Figure 3.4). The 'preferred' fiber direction is the angle at which the area under the solid curve is divided in half. The OI is then taken to be the span about the preferred fiber direction, wherein the area under the curve is equal to 50% of the total area. Therefore, a very narrow peak will yield a small OI, which represents a high degree of orientation. Finally, as a means to qualitatively compare the magnitude of the intensities for each tissue, we adjusted the intensity threshold in the SALSA program until approximately 50% of the total tissue surface was visible. A higher intensity threshold signifies a larger transmitted light intensity, and therefore an increased optical transparency. For this reason, we refer henceforth to the intensity threshold as the transparency.

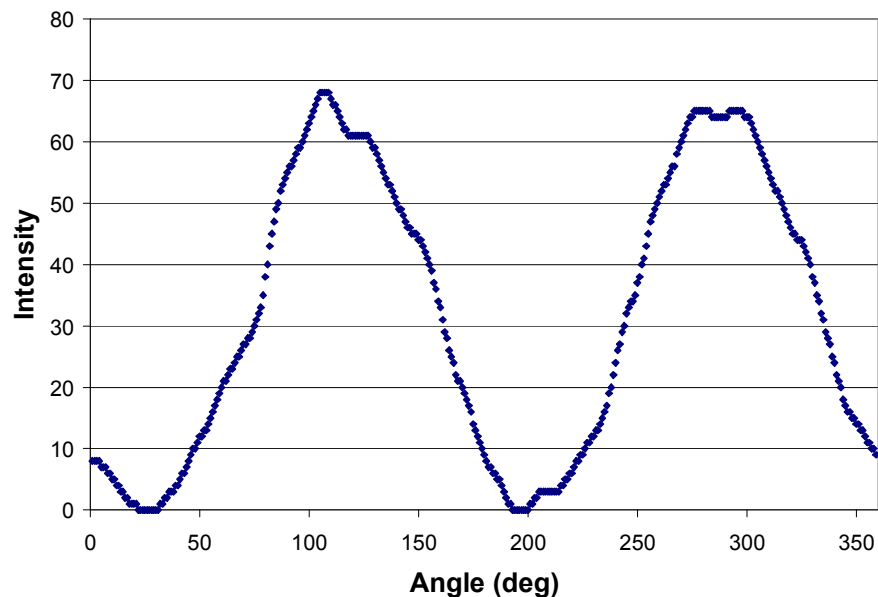


Figure 3.3 Representative plot to show the intensity of transmitted light as a function of angle. Note, the curve has been smoothed to eliminate 'noise', and values have been shifted vertically such that the minimum value is forced to be zero.

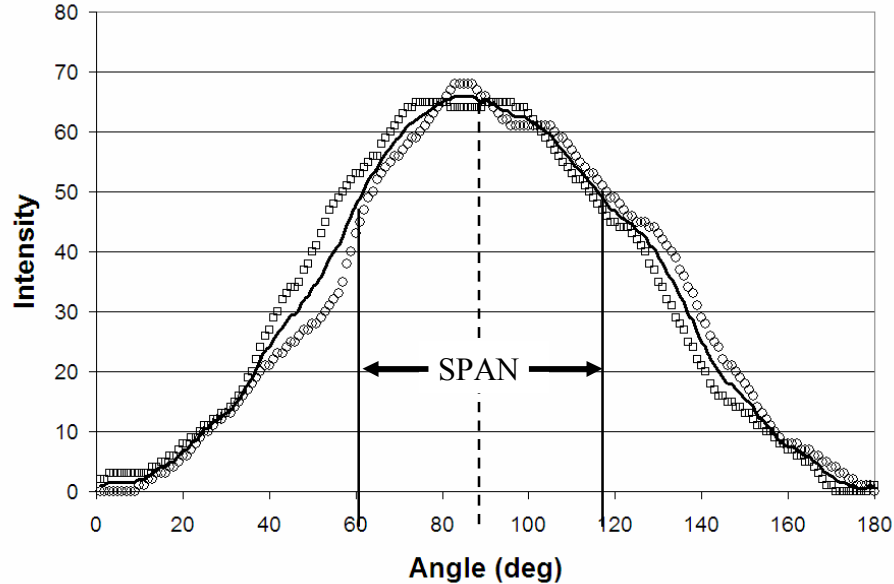


Figure 3.4 Determination of intensity profile for a single location. The solid curve represents the average of the intensities at θ and $\theta + \pi/2$ for the analyzed region. The vertical dashed line is located at the preferred fiber direction. The two vertical solid lines represent the boundaries that define the orientation index (OI), which is equal to the difference in the angles.

RESULTS

Native Tissues

As mentioned previously, fiber orientation as determined in our lab at Texas A&M was marked with India ink on the tissue surface. Scans performed with the automated SALS device confirmed that our gross measure of overall fiber orientation in the native tissues is valid for both the RV and the LV (See Figure 3.5 and Figure 3.6, respectively). Furthermore, values for the average OI (averaged over a 0.5-inch square region) were indistinguishable between the RV and LV, meaning they both had the same degree of orientation. The

transparency was slightly lower for RV than for LV, which could be due to a difference in tissue thickness, hydration, or even composition (see Table 3.1).

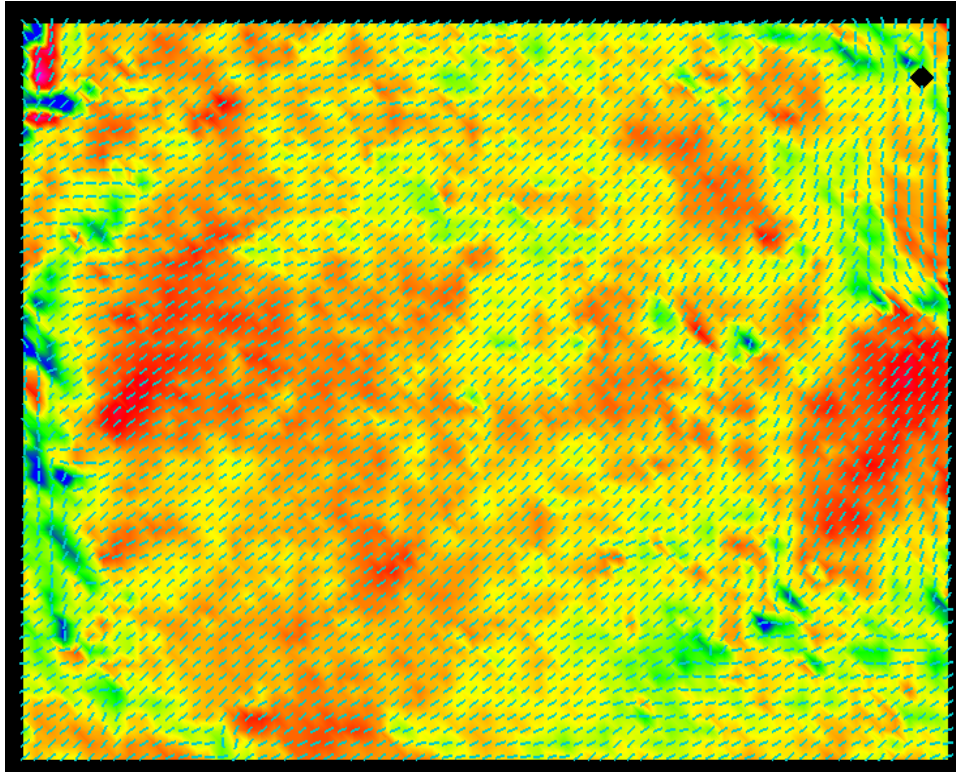


Figure 3.5 SALS scan of the native RV tissue. The colors represent the orientation index (see scale on left), and therefore pink is highly oriented whereas blue is mildly oriented. The short lines throughout the picture represent the local preferred fiber directions within the tissue. Note how fiber orientations are fairly consistent, especially through the central region.

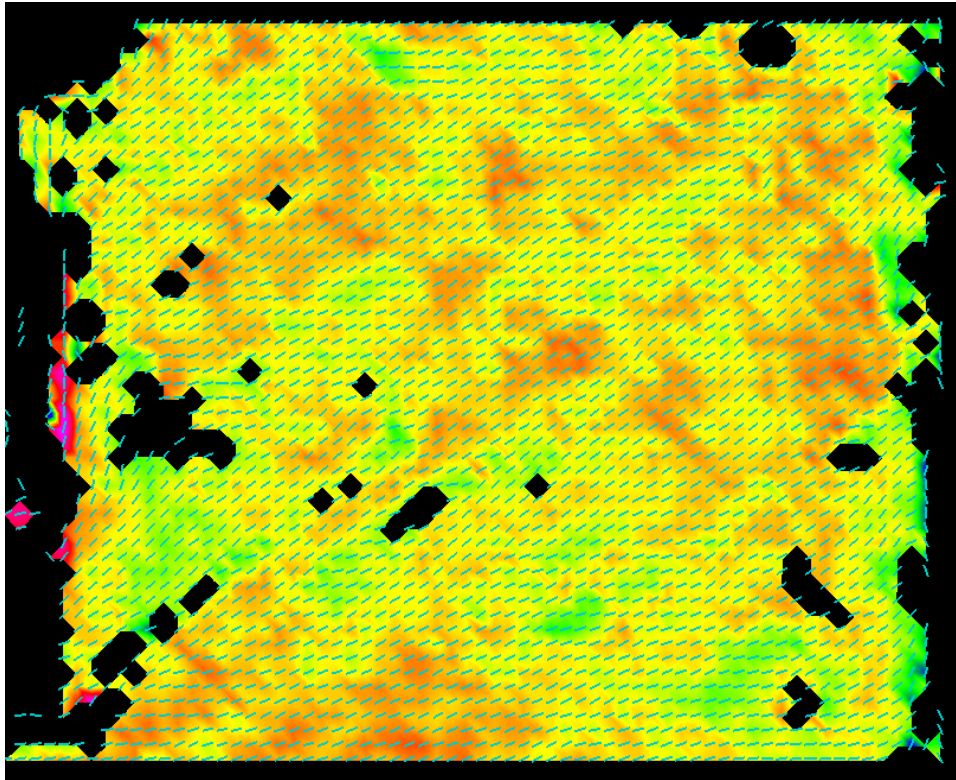


Figure 3.6 SALS scan of the native LV tissue. The colors represent the orientation index (see scale on left), and therefore pink is highly oriented whereas blue is mildly oriented. The short lines throughout the picture represent the local preferred fiber directions within the tissue. Note how fiber orientations are fairly consistent, especially through the central region.

Table 3.1 Comparison of orientation index and intensity threshold for the seven tissue specimens

	LV				RV		
	Native Control	Heated Free ξ	Heated 20% Stretch	Heated 40% Stretch	Native Control	Heated 20% Stretch	Heated 40% Stretch
Average OI	44	48	41	39	43	43	43
Intensity Threshold	77	63	77	91	72	67	81

LV, 20% Stretch, 15 Minutes of Heating

A digital photo along with the SALS image of the tissue is shown in Figure 3.7. As with the native tissues, the preferred fiber direction corresponded well to the India ink marks, and the orientation was consistent throughout the tissue.

The OI, however, was generally lower than that of the native tissues (as seen by increased amount of red), which suggests that the imposed stretch during heating increased the ‘strength’ of orientation within the tissue. Tissue transparency (as marked by intensity threshold) was unchanged from that of the native tissue (Table 3.1).

RV, 20% Stretch, 15 Minutes of Heating

Again, fiber direction corresponded well with India ink marks (Figure 3.8). Unlike the LV, however, the OI was unchanged from that of the native tissue (Table 1). The image in Figure 3.8 illustrates well the effect of the staples (points of applied constraint) on fiber directions. In particular, fibers in the immediate vicinity of the staple points have very low OI values (pink color on image), which reflects a high degree of orientation. Finally, tissue transparency was only slightly lower than that of native tissues.

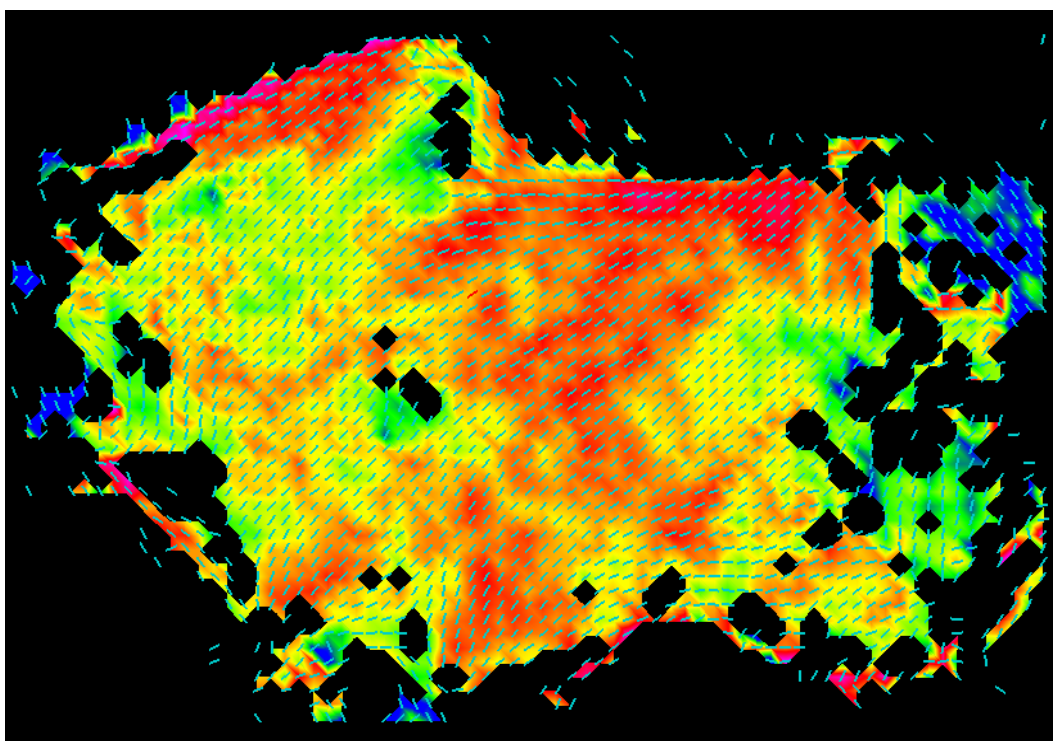
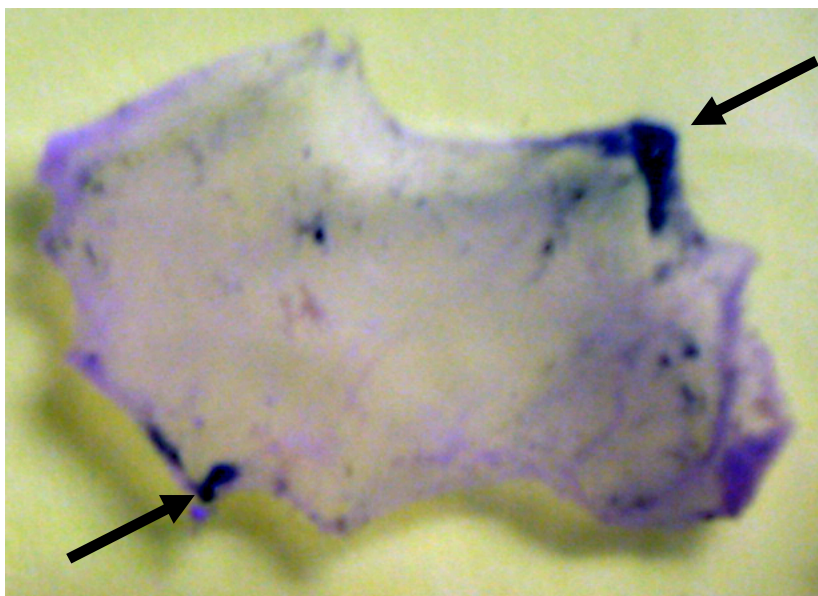


Figure 3.7 Digital photo and SALS image of LV heated at 75°C for 15 min while stretched approximately 20%. Arrows on the photo point to India ink, which marks the preferred fiber direction as determined by our lab. Note how the small lines on the SALS image point in the same direction as the India ink marks.

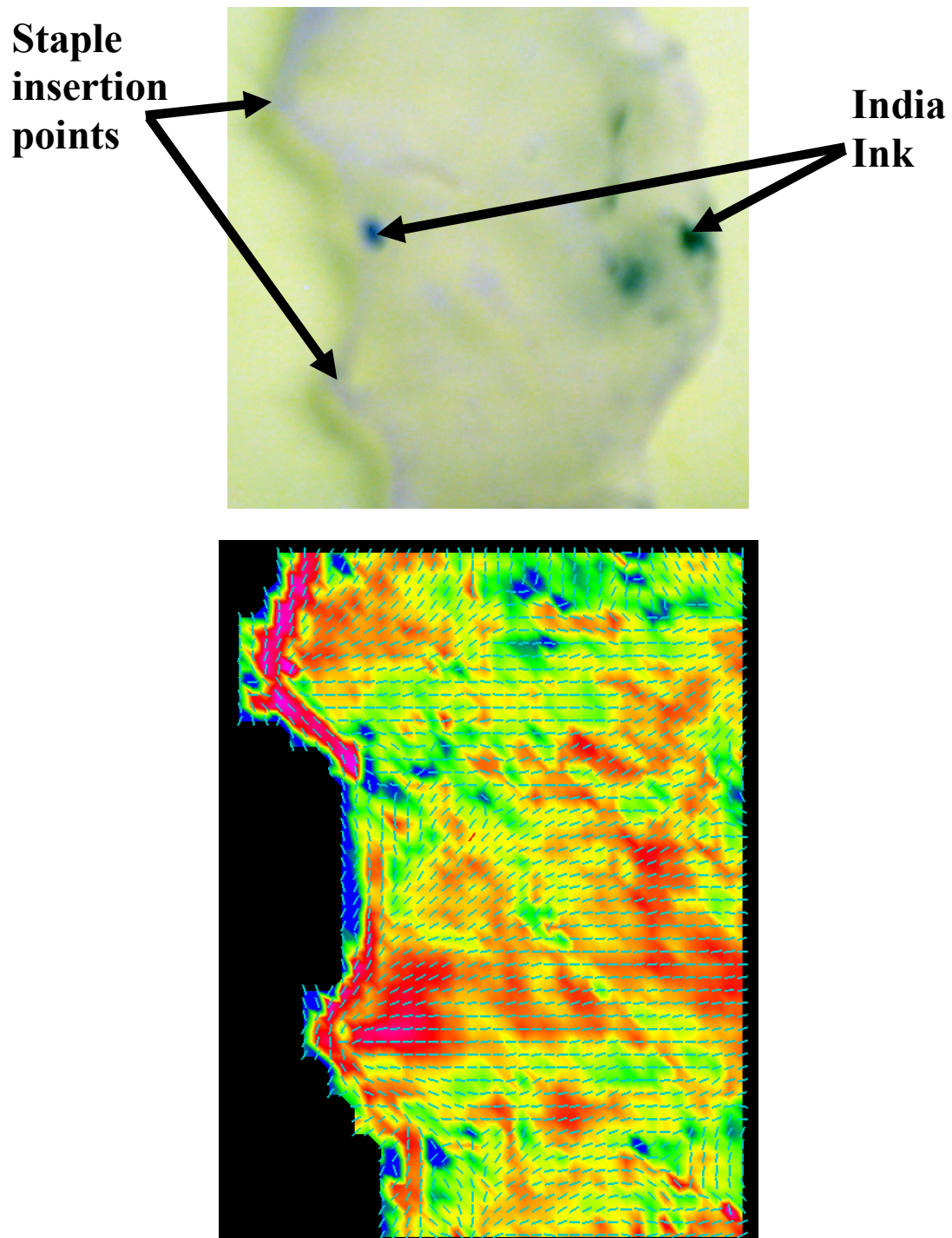


Figure 3.8 Digital photo and SALS image of RV heated at 75°C for 15 min while stretched approximately 20%. The India ink marks the preferred fiber direction as determined by our lab. Note the correlation between the staple insertion points, and regions of highly aligned (pink) fibers in the SALS image.

LV, 40% Stretch, 15 Minutes Heating

Fiber orientation is the most dramatic in this sample (Figure 3.9). Orientations are very consistent within the tissue, and more than 60% of the area is shown as highly oriented (red color). The average OI is approximately 11% lower than that for the native tissue (Table 3.1). Furthermore, tissue transparency is approximately 18% greater than for native tissue. Overall, it appears that the high imposed stretch had a significant affect on the LV tissue.

RV, 40% Stretch, 15 Minutes Heating

This tissue was not affected as dramatically as the LV (Figure 3.10). The SALS image appears to reveal a decrease in the overall OI, because of the increased amount of red. The increased red, however, is offset by an increase in the brilliant green color (increased OI), thereby yielding no net change in the average OI value (Table 3.1). Furthermore, we see only a modest increase in tissue transparency (approximately 11% versus the 18% seen in the LV).

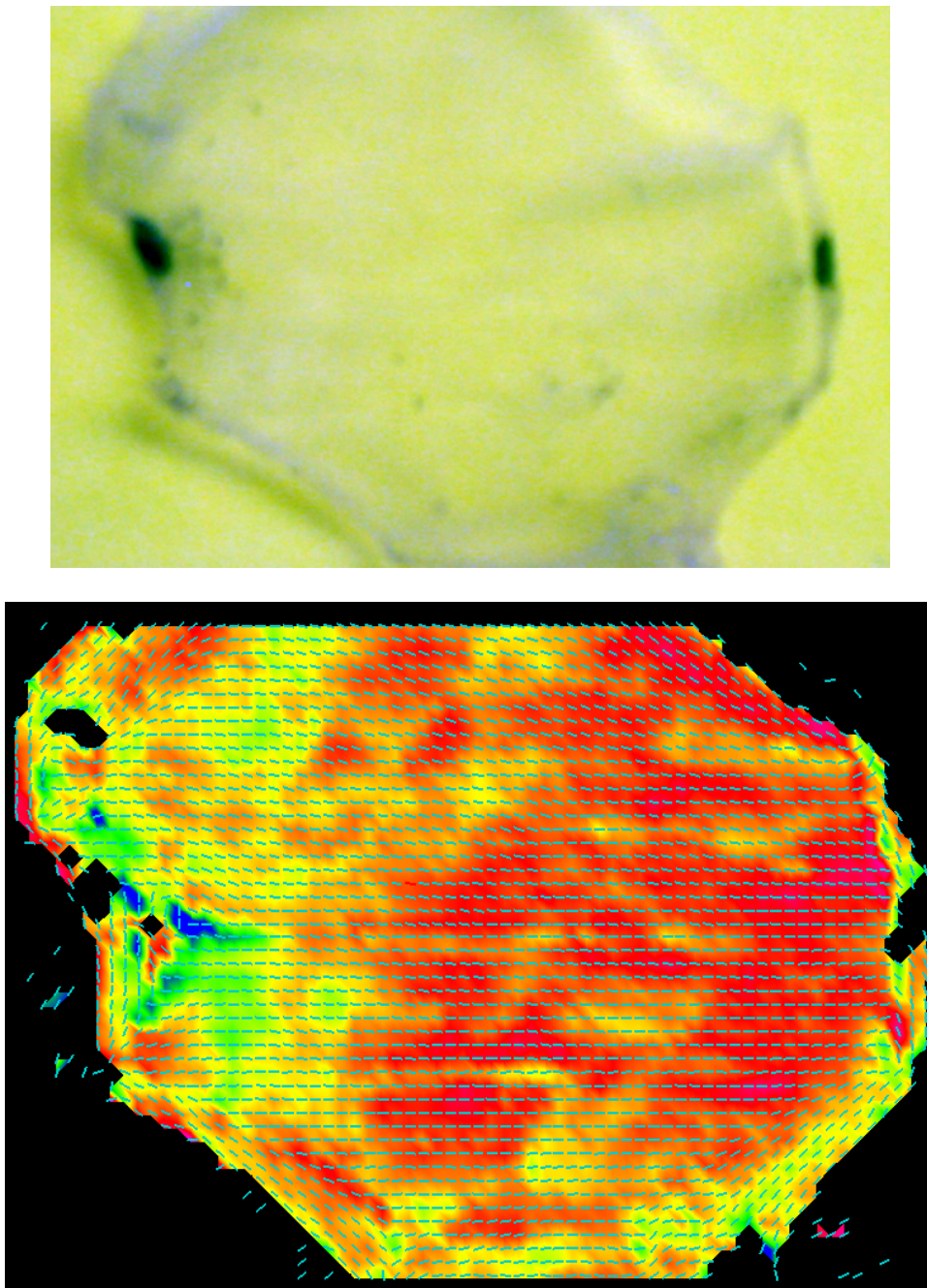


Figure 3.9 Digital photo and SALS image of LV heated at 75°C for 15 min while stretched approximately 40%. The tissue has significantly more aligned than the native LV, which is well-illustrated by the abundance of red in the SALS image. Again, the fibers are aligned in the direction of the India ink marks in the photo.

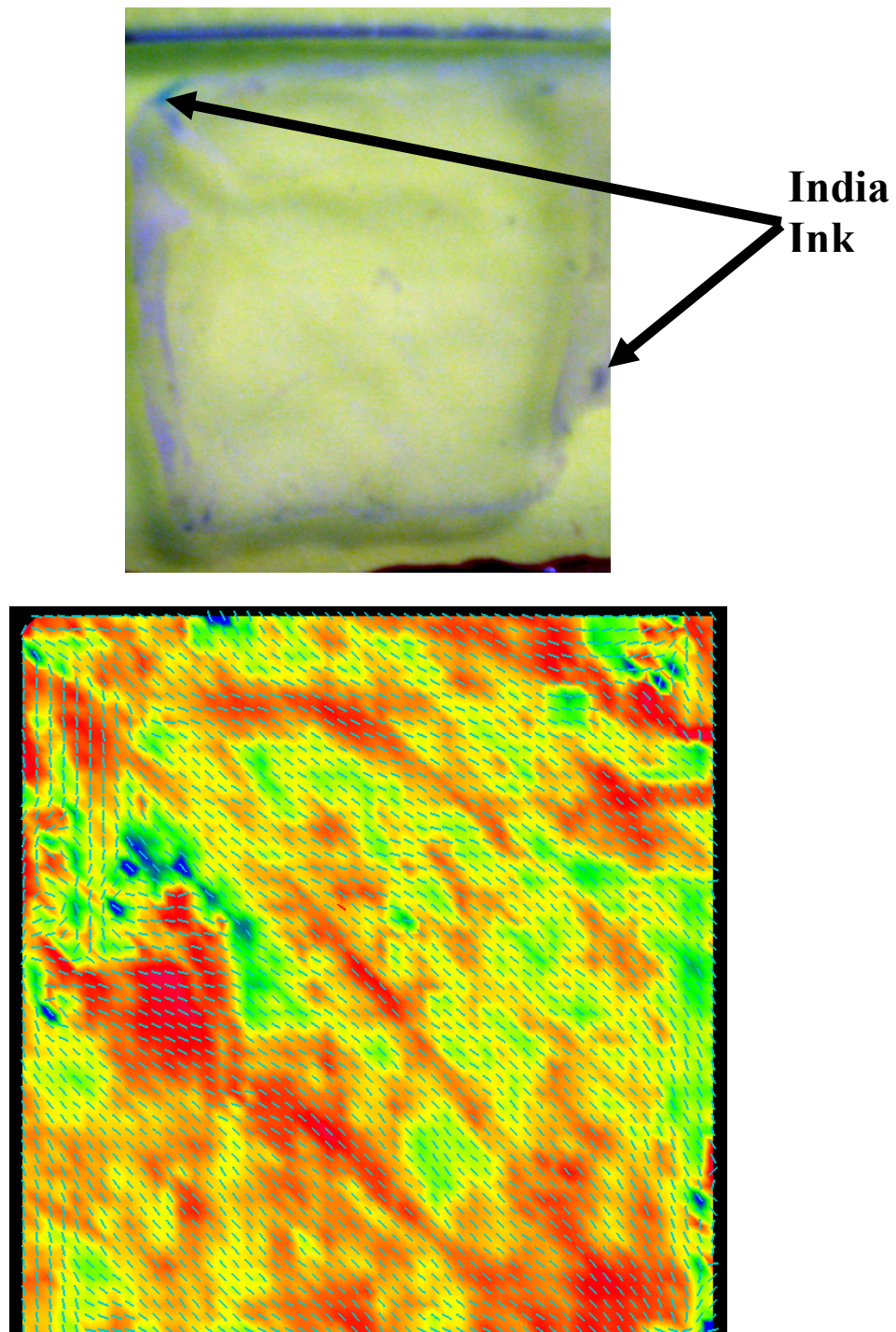


Figure 3.10 Digital photo and SALS image of RV heated at 75°C for 15 min while stretched approximately 40%. The tissue has a larger number of highly aligned (red) regions than the native tissue, however they are offset by an increased number of poorly aligned (green) regions, and therefore the overall ‘strength’ of alignment is unchanged. Again, the fibers are aligned in the direction of the India ink marks in the photo.

Free Shrinkage

Unlike the stretched samples, the free-shrinkage sample had a higher average OI than the native tissue (approximately nine percent increase), which suggests the fibers were less oriented. This is graphically depicted as an abundance of green in Figure 3.11. Though the strength of orientation was decreased, the direction of orientation remained fairly consistent throughout the tissue. Also in contrast to the stretched tissues, the transparency decreased by approximately 18 percent (see Table 3.1)

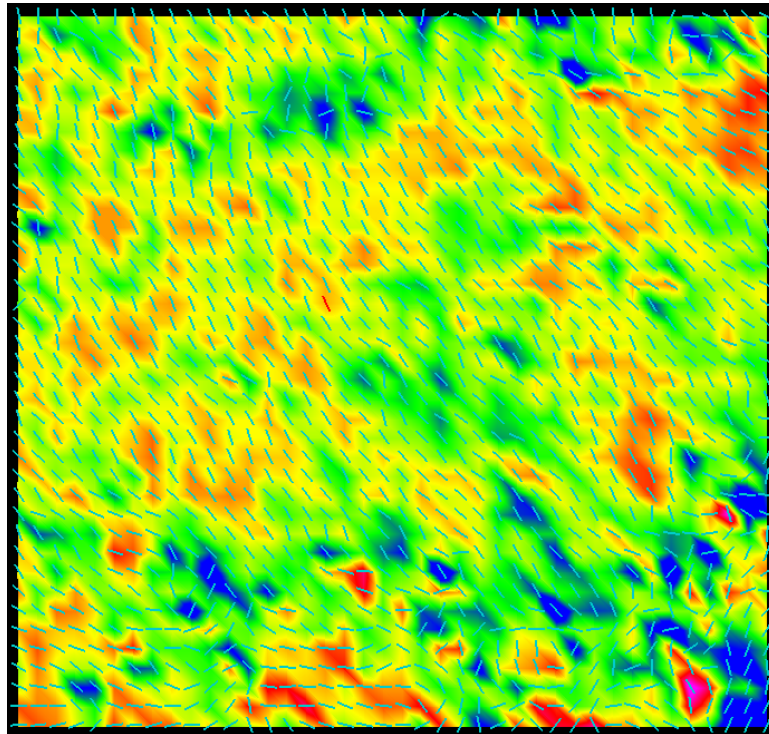


Figure 3.11 SALS image of LV heated at 75°C for 15 min under zero constraint (i.e. free-shrinkage). Note the lack of highly aligned (red) regions, in stark contrast to the highly aligned fibers in Figure 3.9. This image reinforces the point that mechanical constraint influences fiber alignment. Though the India ink marks are not apparent in the photo (not shown), the fibers are more or less aligned in the direction of the marks .

DISCUSSION

SALS is a proven method for quantifying the fiber architectures of tissue up to 500 μ m thick (Sacks and Chuong, 1992; Sacks et al., 1994; Sacks et al., 1997; Sacks and Gloeckner, 1999). Herein we have used this method to validate our simplified, qualitative SALS, and to explore the effects of various mechanical constraints on the fiber architecture and tissue transparency. Using our qualitative SALS device, the primary fiber direction is generally more difficult to determine in the RV than in the LV. We were surprised, therefore, to see that the two tissues were very similar when analyzed with the automated, quantitative SALS device. We had expected the RV to have a much larger OI (less orientation), but that was not the case. Interestingly, however, the transparency of the native RV was slightly less than the native LV, which could account for the increased difficulty in estimating the primary fiber direction of the RV with our simplified SALS device. The observation that our gross determination of the preferred fiber direction was in agreement with local fiber directions as determined by the quantitative SALS is very encouraging. Indeed, it lends credibility to our device and our methods. Furthermore, the 'near-homogeneity' of fiber orientation in the native tissues is important because it indicates that tissue samples are not sensitive to the location from which we cut them. In other words, if one sample is located nearer the base of the heart, and another nearer the apex, the two will likely be very similar.

We have shown repeatedly that imposed constraints during heating of the bovine epicardium have an affect on resultant mechanical properties (see Harris et al., 2003). The results herein are the first to show effects of imposed isometric constraints, during heating, on the resultant fiber orientations (and tissue transparency). Consistent for all stretch tests is that the primary fiber direction is unchanged by the isometric heating. Heated fibers remained in-line with India ink marks placed according to native fiber alignment. If one were to make an argument for a change in the fiber orientation, it could only be that more fibers were aligned in the primary direction following heating. Of particular interest is the apparent difference between the effects of constraint on the LV and RV tissues. The data in Table 3.1 reveal a consistent decrease in the OI of the LV with increased isometric stretch, yet no change in the OI of the RV with increased stretch. In essence, this suggests that LV tissue becomes more highly aligned when isometric constraints are imposed during heating, while RV tissue alignment is unchanged (on average). Mechanically speaking, this would perhaps translate into an increased anisotropy for LV tissues after heating. We have examined our data for isometric tests on LV tissue (data not shown), however, and do not see any tendency towards increased anisotropy, though the constraints imposed were comparable to the 20% and 40% stretches used for this SALS study. Therefore, it seems that the decreased OI in the present study is either a result of tissue-to-tissue variability or that a change in the OI is not indicative of a change in mechanical properties. Finally, the observation that

the areas immediately surrounding the staple points (stress concentrations) have extremely low OI values was not surprising. Indeed, it was expected.

With regards to the change in tissue transparency (as measured by the intensity threshold), the LV showed the largest change with imposed isometric constraint (18 percent change with 40 percent stretch, versus 12.5 percent change for RV). Again, it is difficult to determine if the difference is due to tissue variability or if the LV is more sensitive to mechanical environment during heating. Tissue variability is not as likely because the tissues were taken from the same heart. It may be that the OI and intensity threshold are highly coupled values, therefore it would make sense that the LV changes more drastically than the RV in both quantities.

Finally, a few comments on the free-shrinkage sample. It is well-known that a planar collagenous tissue that is sufficiently heated under zero constraint will shrink in the planar dimensions and become thicker in the out-of-plane dimension. Indeed, the free-shrinkage tissue herein became smaller and more opaque. Therefore, as one might expect, the optical transparency decreased (approximately 18 percent, see Table 3.1). Perhaps more interesting was the apparent increase in the average OI, which suggests that the tissue became more isotropic (less oriented) upon heating under zero constraint. Hence, we again see the effect of a constraint (or lack thereof). Still, the observation that the overall preferred fiber direction was unchanged from the native state would seem to suggest that shrinkage occurs equally in all directions. We know,

however, that shrinkage is not equal in all directions (Harris and Humphrey, 2004).

We recognize that this study is not comprehensive, and there are shortcomings. The most obvious shortcoming is the relative lack of samples. Specimen variability is a well-known challenge in tissue studies, and this study is no different. It could be that the changes evident in Table 3.1 are due only to differences between the hearts, or it could be that the differences are real. More data are needed answer that question. Furthermore, the isometric stretches were only visually estimated with a ruler, and therefore are not precise. That said, we have firmly established that our qualitative SALS device is sufficient for determining the preferred fiber direction in our samples. Furthermore, we have shown convincingly that the preferred fiber direction is unaffected by imposing an isometric constraint on the tissue during heat treatment. Thus, the primary objectives of the study have been fulfilled.

CHAPTER IV

KINETICS OF THERMAL CONTRACTION

INTRODUCTION

Although the literature on thermal damage of collagen has been dominated by studies that employ the concept of equilibrium thermodynamics, collagen denaturation is clearly a rate process (Miles et al., 1995; Wright and Humphrey, 2002). It is difficult, however, to determine the reaction rate because it depends on multiple experimentally-controllable parameters, some of which may be coupled. Furthermore, the variation in one of the parameters is often used as a means of measuring the thermal damage. For example, Harris and Humphrey (2004) performed biaxial thermal damage tests wherein they held the temperature and the load constant, and measured shrinkage. Yet shrinkage is likely associated with a change in configurational entropy, which has been implicated as a determinant of the rate of thermal damage (Miles and Burjanadze, 2001). The complexities notwithstanding, we can still delineate general characteristics for the role of various parameters on the rate of thermal denaturation. The purpose of this chapter is to investigate the role of a biaxial isometric constraint on the isothermal kinetics of thermal denaturation, as measured by the evolution of so-called contraction forces. Indeed, this is the first study to do so biaxially. Tissues are held at a constant deformation and temperature while a change in isometric contraction force is measured. It is

shown that the characteristic times of isometric contraction ($\tau_{1/2}$ and τ_2 , defined herein) depend exponentially on the amount of stretch imposed on the tissue during heating. Furthermore, the ultimate values of contraction force along both axes are independent of the isometric stretch. Results are discussed in light of previous studies on the kinetics of thermal damage to collagenous tissue.

METHODS

Specimens were prepared and placed in the device as described in *Specimen Preparation* in Chapter II and subjected to the mechanical testing protocol, also outlined in Chapter II. Following mechanical testing in the native state, specimens were subjected to one of four isometric conditions (see Figure 4.1): (a) '1.03', with $\lambda_1 \approx \lambda_2 = 1.03$, where $\lambda_1 = F_{11}$, $\lambda_2 = F_{22}$ and \mathbf{F} is the deformation gradient relative to the native reference configuration, β_N , (b) 'low-stretch', with $\lambda_1 \approx \lambda_2 = 1 + 0.4(\lambda_{MAX} - 1)$, where λ_{MAX} was the maximum stretch ratio attained during the equibiaxial loading test to 0.88N, (c) 'elbow', with $\lambda_1 \approx \lambda_2 = 1 + 0.7(\lambda_{MAX} - 1)$, and (d) 'high-stretch', with $\lambda_1 \approx \lambda_2$ chosen such that the pre-load was equal to 0.49 N in the stiffer direction. Specimens were first taken to the prescribed equibiaxial stretch ratio (e.g., $\lambda_1 \approx \lambda_2 = 1.03$), and the loading carriages were moved inward (toward the specimen) a set distance of 10 mm such that the sutures became slack. The specimen was placed within a polystyrene insulating cell filled with room temperature saline, and the room temperature solution in the chamber was then replaced with a high temperature,

normal saline solution maintained at 75°C, following the procedure described in Chapter II. Adequate time was allowed for all chamber components to reach thermal equilibrium; although the load cells are thermally compensated, small heat-induced offsets were observed and recorded. The specimen was then removed from its insulating cell and suspended above the heated chamber (for no more than 15 seconds to avoid premature thermal damage). Each loading carriage was then rapidly (and simultaneously) moved outward (10 mm) so that the prescribed equibiaxial stretch was regained, and the specimen quickly submerged (it took approximately one second to get the specimen back to this configuration).

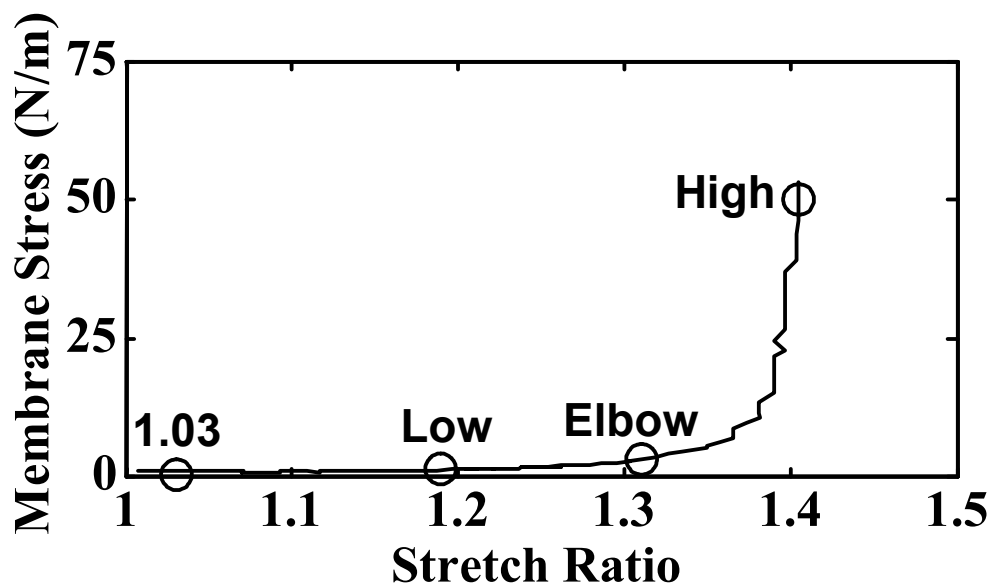


Figure 4.1 Typical Cauchy membrane stress versus stretch response for native bovine epicardium in the stiffer direction. Shown, too, are the approximate isometric constraints, relative to the native tissue equibiaxial response, imposed during heating. These constraints are called ‘1.03’, ‘Low’, ‘Elbow’, and ‘High’; see text for specific definitions. Note that the High constraint is the only one that imposes a significant pre-stress prior to heating.

The specimen was kept in the high temperature bath for 900 seconds, during which the forces required to maintain the tissue at its fixed length were recorded. The high temperature saline was then replaced with room temperature normal saline, using the procedure described in Chapter II, and the specimen was allowed to 'recover' for 60 minutes while maintaining the isometric constraint. Immediately following recovery, the configuration β_p was recorded. The motors were then moved inward once again until the sutures became slack and the unloaded configuration, β_R , was recorded. For consistency, the specimen was again preconditioned from 0.02 to 0.78 N for ten cycles, and the new unloaded configuration, β_C , recorded for use in subsequent stretch-controlled mechanical testing. Mechanical tests were then carried out in the same manner as for the native tissue (see Chapter II). Figure 4.2 is a schema of the overall experimental protocol.

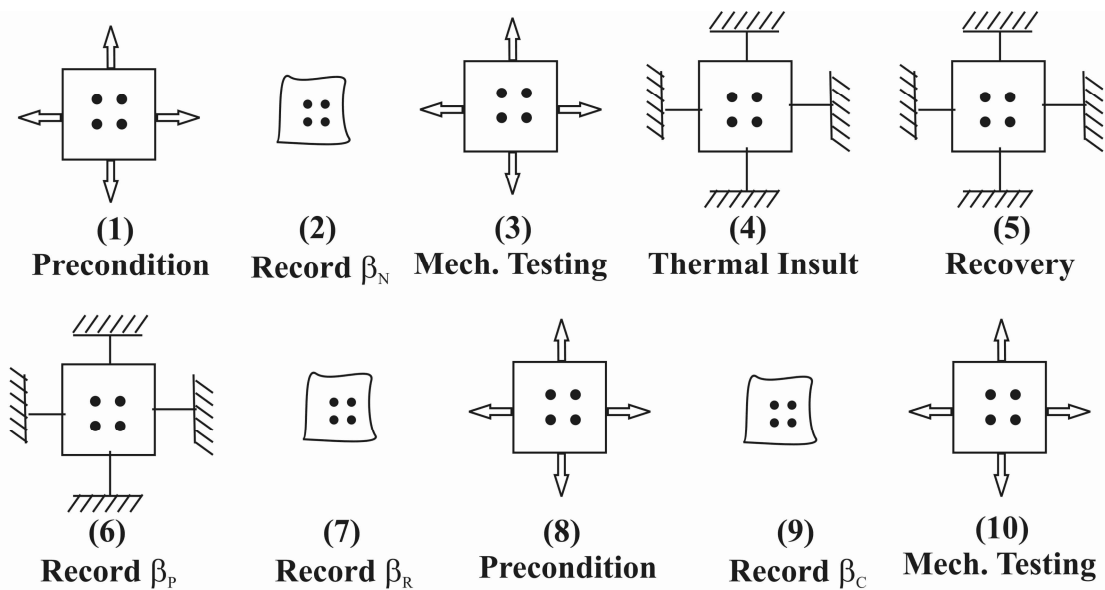


Figure 4.2 Schema of the isometric thermal damage protocol. The specimen is shown with four central tracking markers. β_x denotes various traction-free reference configurations. Arrows denote load-induced stretching, and hatched ends denote an isometric biaxial constraint.

Data Analysis

Load cell outputs were written to a data file at 30Hz for the duration of heating, and subsequently used to calculate the evolving Cauchy membrane stress. To do so required an assumption that the deformation applied to the tissue during heating was homogenous, which allowed us to estimate the gross dimensions of the tissue during heating, knowing only the motion of the markers. For example, assuming the isometric constraint was defined as $\lambda_1 = \lambda_2 = 1.4$, then we assumed the gross dimensions of the tissue were increased by 40% in both directions. We recognize this assumption has some uncertainty, yet we submit that the uncertainty was no greater than with other available options. Direct measurement of the gross tissue dimensions with a scale would have

relied significantly on “eyeballing”. Furthermore, the point of zero stretch is difficult to define due to the high compliance of the tissue at low strains, and therefore the use of an LVDT to measure load carriage displacement was precluded. After estimating the gross tissue dimensions, the Cauchy membrane stress was found by simply dividing the evolving force along each axis by the length over which it acted, which was constant. Because there was a high variability amongst the tissues, average values of the evolving force were calculated for each test group ($n \geq 4$). Data were plotted as the group mean stress along each side of the tissue, versus the time. Note that in order to capture the entire heating profile, data recording began just prior to submersing the tissue in the heated saline. The point in time in which the tissue broke the surface tension of the water (upon immersion) was clearly evident on all heating plots, and all data up to and including the instant of immersion were considered noise, and thus eliminated.

RESULTS

Tissues subjected to the ‘high stretch’ constraint exhibited a monotonic decay of stress during heating that was not present for the other three constraints. For the benefit of comparison, and because the mechanisms responsible for the relaxation are not obvious, we chose to base our analysis on the other three constraints, which exhibited similar trends to one another. The high stretch tests are discussed briefly near the end of this chapter.

Forces generated during our isothermal, biaxial isometric heating were similar to cases reported in the HIT literature (e.g., Rasmussen et al., 1964; Andreassen et al., 1981; Le Lous et al., 1983)). That is, there were three distinct regimes characterized by (i) an initial period of very little change in force, followed by (ii) an abrupt and rapid increase, and finally (iii) a slow phase wherein the rise in force was only detectable if time was plotted logarithmically (Figure 4.3). Although some HIT studies show that the force eventually decreases after it reaches some maximal value (e.g., Allain et al., 1978; Andreassen et al., 1981; Horgan et al., 1990; Brinkmann et al., 2000)), we did not observe such a trend in our tests. The times at which the transitions occurred between the first and second regime (τ_1), and the second and third regime (τ_2) were determined by performing linear regressions on the three regimes, and finding the points of intersection. $\tau_{1/2}$ was defined at the inflection point (see Figure 4.4 and Table 4.1).

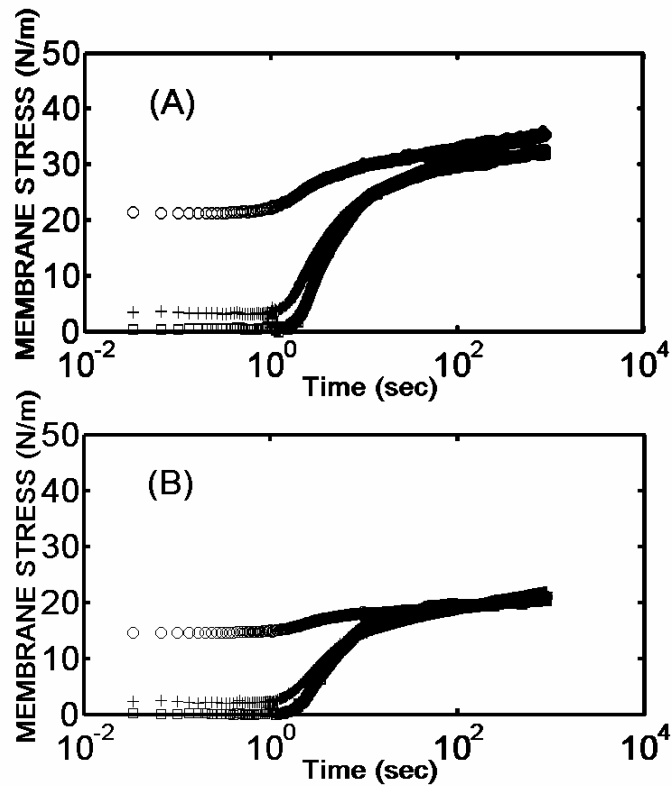


Figure 4.3 Mean isometric contraction stresses ($n \geq 4$) for the '1.03' (squares), 'low stretch' (pluses), and 'elbow' (circles) tests. Panels (A) and (B) are the preferred and non-preferred directions, respectively. The ultimate values of stress are independent of the constraint, and the difference between the two axes is indicative of the material anisotropy.

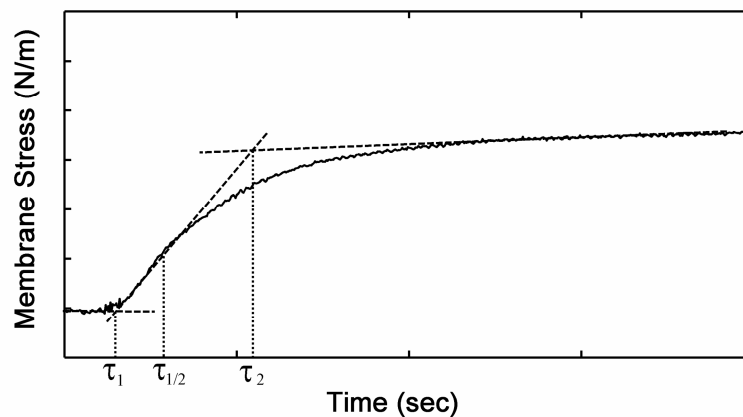


Figure 4.4 Schema of the three regimes of thermal contraction force. The first regime, wherein there is little or no rise in force, is followed by an abrupt and rapid rise in force, which then slowly transitions into the slow rise (third) regime. The characteristic times are defined as shown. $\tau_{1/2}$ occurs at the inflection point in the force curve.

Table 4.1 Characteristic times for biaxial thermal contraction. The times do not vary much with differing isometric constraint, and the times appear independent of the fiber orientation (i.e. axis). Preferred and non-preferred refer to the stretching directions.

	1.03			Low Stretch			Elbow		
	τ_1	$\tau_{1/2}$	τ_2	τ_1	$\tau_{1/2}$	τ_2	τ_1	$\tau_{1/2}$	τ_2
Preferred	1.65	2.40	6.48	1.10	2.10	6.21	0.72	1.80	5.55
Non-preferred	1.71	2.60	6.97	1.08	2.00	6.59	0.87	2.10	5.67
Average	1.68	2.50	6.73	1.09	2.05	6.40	0.79	1.95	5.61

The values for τ_1 are within the time-frame required for the tissue to reach thermal equilibrium with the heated saline ($\tau_{eq} \approx 1.8$ sec.; see Harris, 2002). Due to the uncertainty introduced by the transient temperature of the tissue, we focus our attention on $\tau_{1/2}$ and τ_2 . A greater amount of stretch during heating resulted in shorter characteristic times, that is, quicker force generation (Table 4.1). Furthermore, the characteristic times for the preferred and non-preferred fiber axes were practically the same for any one test. Because the characteristic times for biaxial shrinkage of epicardium have been shown to depend exponentially on both temperature and load (Harris and Humphrey, 2004). we investigated the possibility of an exponential dependence of $\tau_{1/2}$ and τ_2 on the isometric constraint. To do so, we plotted $\ln(\tau_{1/2})$ and $\ln(\tau_2)$ versus a measure of the isometric constraint we define as $\Phi = |\mathbf{V}|_C / |\mathbf{V}|_N$, where $|\mathbf{V}|_C$ is the magnitude of the left stretch tensor for the constraint, calculated relative to β_N , and $|\mathbf{V}|_N$ is the magnitude of the left stretch tensor for the native equibiaxial test at $|\mathbf{T}| = 60$ N/m. The relationship is near linear for both characteristic times (Figure 4.5), suggesting that the characteristic times for isometric contraction depend

exponentially on the level of stretch. Of note is that the slopes are almost identical. Finally, there was a marked difference in the ultimate magnitude of the stress along both axes, with the mechanically preferred direction achieving the greater stress, in general. This difference was independent of the isometric constraint, however. Note that an equilibrium value of stress was not achieved in any case.

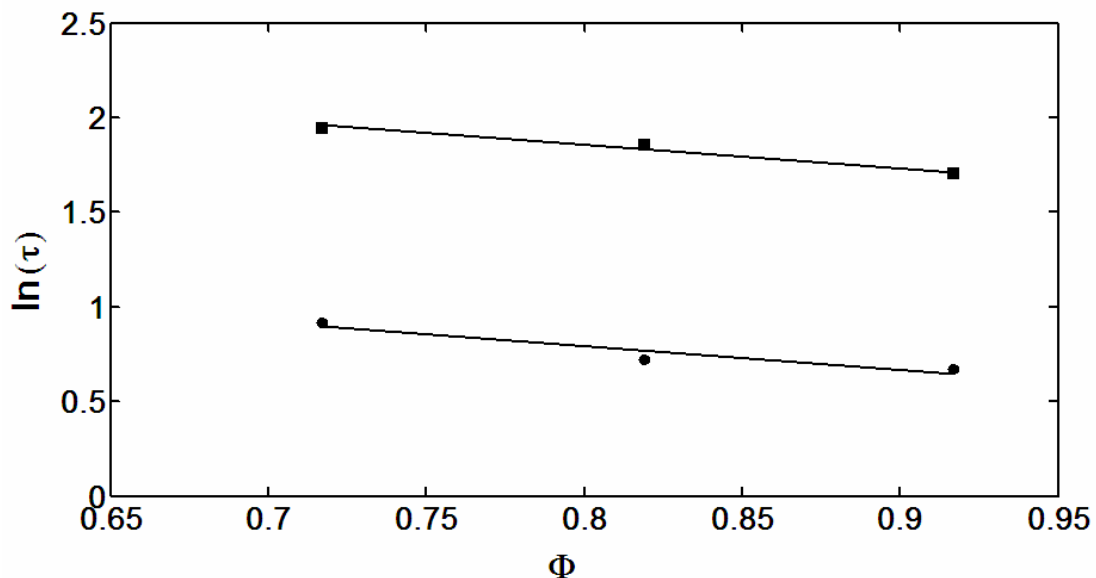


Figure 4.5 Exponential relationship between characteristics times and the isometric constraint. The slope for the lines of τ_2 (squares) and $\tau_{1/2}$ (circles) are nearly the same. $\Phi = |V_c|/|V_w|$

DISCUSSION

Prior to P.J Flory's suggestion in 1958 that collagen denaturation is a first order phase change, and thus that collagen has a melting (denaturation) temperature, Henriques (1947) had demonstrated that equivalent levels of thermal damage to skin (a primarily collagenous tissue) could be achieved with

different combinations of time and temperature. He suggested, therefore, that collagen denaturation is a rate process, wherein the rate depends on temperature. Furthermore, Lennox (1949) and Weir (1949) had shown that the rate of thermal denaturation could be modified by applied load, thus precluding the existence of a unique denaturation temperature. Surprisingly, those observations were largely ignored until recently, as most scientists pursued constant heating rate DSC and HIT tests to find the so-called denaturation temperature of different types of collagen with varying amounts and types of crosslinks. While those tests have provided tremendous insight into the role of crosslinks within tissue, and into the differences in thermal stabilities of different types of collagen, they are not adequate for determining parameters pertinent to the modeling of thermal denaturation.

For a simple, 2-state (native and damaged) reaction, collagen denaturation has been modeled as a first-order rate process,

$$\frac{dN}{dt} = -k(\dots)N(t), \quad (4.1)$$

where N is the instantaneous number of native molecules at time t and $k(\dots)$ is the rate of denaturation, which is likely a function of multiple independent parameters. Supposing we could perform a thermal damage experiment wherein all independent parameters are maintained constant during heating, the solution to equation (3.1) would be

$$N(t) = N_i \exp^{-k(\dots)t}. \quad (4.2)$$

Thus we can compute the corresponding rate, k , at specified values of the independent parameters, assuming we could measure the number of native molecules remaining at time t , which is not generally convenient. One way to do so is to place a sample with a known number of native molecules, N_i , into a DSC and heat the tissue isothermally (note that, realistically, the heating rate in DSC can be very near zero, but not equal to zero). The number of native molecules remaining at time t can then be inferred from the power input to the DSC to maintain the isothermal condition (see Miles et al., 1995). Of course, the tacit assumption is made that no independent parameters were varying during the DSC measurements. Realistically, we cannot maintain all parameters constant for the duration of a test, and therefore the solution to equation (4.1) becomes non-trivial. The primary challenge is in identifying the independent parameters, and then finding the functional form for $k(\dots)$.

Studies have shown the rate of thermal denaturation to depend on temperature (Wier, 1949; Miles et al., 1995; Wall, 1999), load (Lennox, 1949; Chen et al., 1998a; Harris and Humphrey, 2004), and configurational entropy (Miles and Ghelshvili, 1999; Miles and Burjanadze, 2001). However, the studies that showed dependence on temperature and load did not specify constant configurational entropy, and the dependence on configurational entropy was found by using non-isothermal experiments. If load, temperature, and configurational entropy are independent, then the dependencies of the rate found in the aforementioned studies are not what they seem. On the other

hand, if two or more of the parameters are coupled, then the dependencies may be legitimate. In other words, assuming the reaction depends only on temperature, load, and configurational entropy, which act independently, we have

$$k = k(T, f, \eta), \quad (4.3)$$

and the functional form is found best by experiments in which all three are maintained constant. If, for instance, load and configurational entropy are coupled (i.e. dependent), then we have

$$k = k(T, \eta(f)), \quad (4.4)$$

and we need only specify a constant temperature and load to find the functional form of k . These tacit assumptions on the coupled nature of the experimentally-controllable parameters are prevalent in literature.

Harris and Humphrey (2004) imposed biaxial isotonic (constant load) constraints on a tissues that were heated isothermally (constant T), and measured the shrinkage (change in \mathbf{F}) during heating. Their results suggest that the rate of thermal denaturation, as measured by a characteristic time of shrinkage (τ_2), depends exponentially on both temperature and applied load,

$$\tau_2 \approx A e^{\beta I_P} e^{\frac{m}{T}}, \quad (4.5)$$

where I_P is the first invariant of the first Piola-Kirchhoff membrane stress (\mathbf{P}), and A , β , and m are material parameters. \mathbf{P} is defined as the force per unit length of the traction-free (i.e. undeformed) configuration, and is traditionally coupled with

a measure of the deformation (\mathbf{F}), such that a change in stress necessitates a change in length. In isotonic thermal damage tests, the underlying traction-free configuration evolves due to thermal shrinkage. If defined relative to the evolving configuration, \mathbf{P} evolves with thermal shrinkage and \mathbf{F} may remain nearly constant (i.e. the unloaded configuration may change at the same rate as the loaded configuration). However, if \mathbf{P} is defined relative to the original, unheated traction-free configuration, then \mathbf{F} must be referenced to the same configuration. In doing so, we see that \mathbf{P} remains constant throughout the experiment, yet \mathbf{F} evolves with shrinkage. Clearly, this is a special case wherein the stress and deformation appear to vary independently, most likely due to evolving physical properties of the tissue (e.g. in linear elasticity, this would be analogous to an evolving modulus). Much work remains for determining the evolution equations for properties of the tissue. The complexities notwithstanding, the results of their study are provocative and motivate further investigation. Hence, we performed isothermal biaxial isometric tests, during which the temperature and deformation (relative to β_N) were held constant while the change in force was measured. Unlike the aforementioned isotonic experiments, the traction-free reference length of our isometric tissues changed little with heating (cf. Table 6.1; note that we assume an affine deformation). Therefore, the evolution of \mathbf{P} is dependent only on the evolution of the isometric contraction force; yet again \mathbf{P} changes independent of the deformation and temperature. Although we do not understand fully the coupling between the

various clinically-controllable parameters, we can potentially delineate general characteristics for the role of various parameters on the rate of thermal denaturation using the tests described herein. For the purpose of discussion, we will henceforth treat temperature, stretch, and isometric contraction force as though they are independent.

Recall that the rate of biaxial isothermal, isotonic shrinkage varies exponentially with load and temperature (equation (4.5)). Similarly, it appears that the rate of isometric contraction depends exponentially, albeit mildly, on the level of isometric stretch (see Figure 4.5). In contrast to the direct relation between load and τ_2 revealed in equation (4.5), the stretch dependence herein is of an inverse nature. We submit that this inverse relationship may be due to the amount of collagen fiber crimp present prior to heating. Thermal contraction of collagen is caused by the breakage of intrahelical hydrogen bonds, particularly in the thermally labile domain (Miles and Bailey, 2001), which causes an irreversible transition of the triple helix to a shortened, entropically-favored random coil. For an isometrically constrained tissue, the constituent molecules will attempt to contract at the instant that a sufficient number of consecutive hydrogen bonds are broken, and thus exert a force on the constraints. Because the activation energy of the hydrogen bonds is independent of the applied mechanical constraint, one may expect the characteristic time for the onset of contraction (τ_1) to be independent of the isometric stretch. However, excised tissues contain fibers that are undulated in their native, unloaded state (i.e.

stretch ratio equal to unity). For illustrative purposes, one may think of a fiber as a simple collection of collagen molecules connected in series (see Figure 4.6). When the fiber is slack, a certain number of molecules must denature (and therefore shorten) before the length of the fiber becomes equal to the fixed end-to-end distance (defined by the constraint). Any subsequent helix-to-coil transitions will then be hindered and thus registered by the load cells. Larger isometric stretches imposed prior to heating would reduce the initial undulation, and thereby reduce the number of molecules required to denature before a contraction force is registered by the load cells. We believe this difference in the number of molecules required to shorten prior to registration of force is the cause of the increased characteristic times for the lower isometric constraints. In contrast, the delayed onset of shrinkage with increased load in isotonic tests is likely due a larger number of bonds having to break before the cumulative contraction force is greater than the applied load.

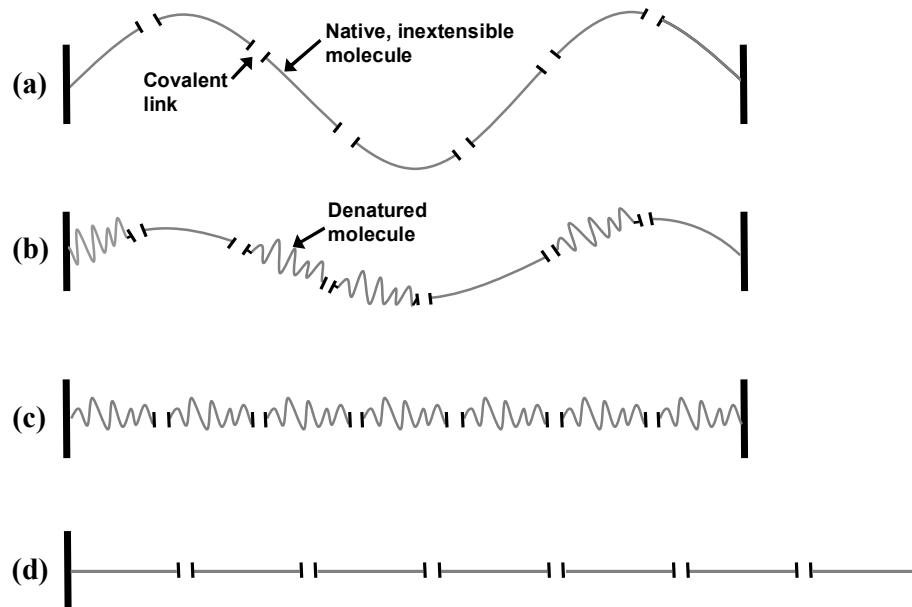


Figure 4.6 Simplified representation of collagen fiber denaturation under mechanical stretch. Panel (a) represents a native, undulated fiber constrained less than a physiologic length (e.g. '1.03' constraint). Panels (b) and (c) illustrate the progressive denaturation at a constant temperature, with local shrinkage. Notice as the molecules denature, the fiber length decreases and undulation is eventually eliminated (Panel (c)), at which point subsequent shrinkage will exert a force on the constraints. If the undulation is removed prior to heating (d), contraction force will be registered immediately upon denaturation because the fiber length is already equal to the end-to-end distance.

Following the same line of thought, the stress generated during isometric heating can be viewed as the tendency for the tissue to contract, whereas the shrinkage during isotonic heating is the actual manifestation of that tendency. In essence, the shrinkage tendency is a measure of the stored entropic energy that would be released upon heating if the tissue were allowed to contract. It makes sense, then, that the ultimate stress achieved during heating (along either axis) in the isometric tests was independent of the imposed stretch (see Figure 4.3), for the same tendency (i.e. stored energy) would exist. In contrast, the

equilibrium shrinkage in the biaxial isotonic tests is more muted for heavier isotonic loads (Harris and Humphrey, 2004), because the total stored energy is only capable of doing a certain amount of work. Indeed, isotonic tests with the load maintained at zero (i.e. free-shrinkage tests) exhibit the most rapid and significant thermal shrinkage because only internal forces resist the shrinkage. In essence, thermal shrinkage is manifested at the same instant as the onset of the 'tendency' in free-shrinkage tests. This notion is supported by the observation that biaxial free-shrinkage data, when extrapolated to 75°C, yields characteristic times in line with those seen for the onset of contraction force in our biaxial isometric tests (c.f. Figure 7 in Harris and Humphrey, 2004). Finally, that the tendency to contract was dependent on the orientation (as seen by the different values of stress along the two axes) is in agreement with an earlier report by Rasmussen (1964) that the amount of thermal shrinkage is dependent on orientation. Harris and Humphrey (2004) also showed that thermal shrinkage along the preferred fiber direction was greater than for the non-preferred direction.

It is not clear why the load in the initial regime of the heating curves was greater for larger isometric stretches, particularly the elbow constraint. Recall that to avoid premature thermal damage, tissues were subjected to the isometric constraints rapidly. To investigate the possibility of a strain-rate effect, a mock 'elbow' test was run with room temperature saline in place of the heated saline. The load remained zero upon rapidly taking the tissue to the isometric

constraint, thus the increased force does not appear to be a strain-rate effect. We have considered the possibility of a different viscoelastic response at the elevated temperature. Quantifying the viscoelastic behavior at an elevated temperature, however, is complicated by the evolving thermal denaturation. To investigate the possibility of premature thermal damage, a second mock test was run wherein the native tissue was suspended over the heated, steaming saline for two seconds, as is done in the actual tests, but then placed back in the room-temperature insulated capsule. We then interrogated the room temperature mechanical behavior of the tissue, and it was found to be unchanged by the short steam treatment. Therefore, the increased load does not appear to be due to pre-mature denaturation by steam.

Finally, recall that we have excluded the high stretch isometric tests from the analysis thus far because the thermal contraction forces were distinct in character. Specifically, the force increased abruptly and significantly at the onset of heating and then 'relaxed' monotonically for the duration (Figure 4.7). There was no sign of thermal contraction. Recall that for the high stretch tests, a much larger value of stress was imposed initially than for the other constraints (cf. Figure 4.1). Baek et al. (2005) demonstrated stress relaxation at room temperature in bovine epicardium using the same biaxial device as used herein. Therefore, a thermoviscoelastic response is likely the cause of the stress relaxation seen here, and thus we investigated the possibility. Like the mock elbow test mentioned previously, we performed a tests wherein a tissue was

taken to the high stretch isometric constraint in room temperature saline. The room-temperature tissue stress-relaxed monotonically, just as the heated tissue had done (Figure 4.8).

We submit that the biaxial viscoelastic response of bovine epicardium at room temperature is comparable to the viscoelastic response at elevated temperature because the degree of intermolecular covalent bonding is likely very similar and because thermal damage is minimized. Covalent crosslinks endow the tissue with most of its structural integrity, while limiting the mobility of molecules relative to one another. Therefore, without decreased covalent bonding, stress-relaxation is likely to occur at much the same rate. Stress relaxation could occur more rapidly and to a larger extent as heating progresses, due to thermal damage (Baek et al., 2005). However, the high stretch constraint limits the amount of thermal damage (see Chapter VII), thus an alteration in stress relaxation behavior due to evolving material characteristics is unlikely. Thus, if these arguments hold true, and assuming the viscoelastic response and the thermal response are additive, then it is prudent to subtract the response in Figure 4.8 from that in Figure 4.7 to reveal the thermal response. Indeed, after doing so the thermal contraction became evident (Figure 4.9). In fact, the curves correspond well to the trend for the other three constraints with respect to the initial stress level and the time at onset of contraction (note that characteristic times could not be determined well for the high stretch tests). However, within the time scale of τ_2 for the constraints, the force achieves a

maximum and then begins to decay. The decay is possibly due mechanical damage resulting from excessive thermoelastic loading. In Chapter VII, we give evidence for such mechanical damage (see page 116), and discuss how it may also be the cause of increased collagen hyalinization as viewed with light microscopy.

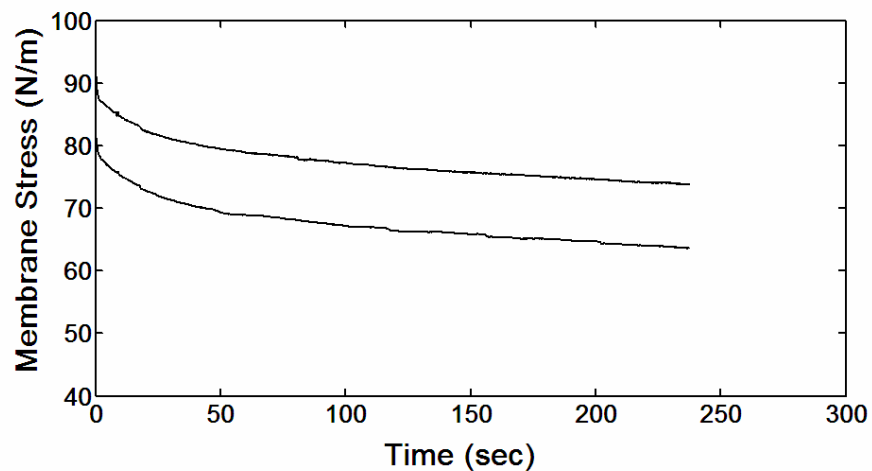


Figure 4.7 Monotonic decay of stress during high-stretch isometric heating. The two curves correspond to the two directions of interest.

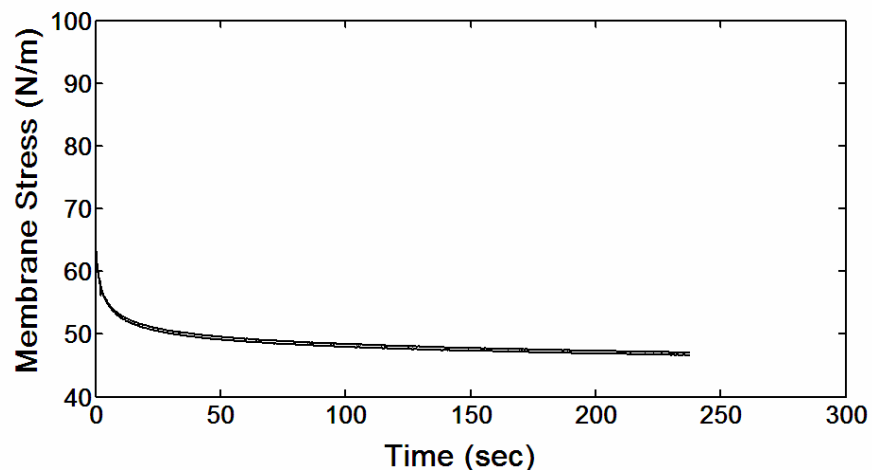


Figure 4.8 Monotonic decay of stress following rapid imposition of the high-stretch isometric constraint at room temperature. The two directions of interest are difficult to differentiate because they are nearly identical.

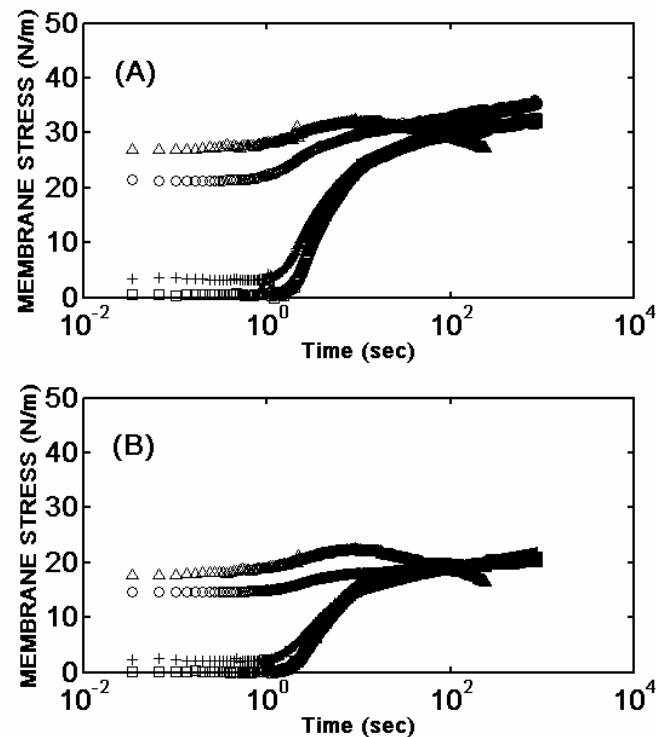


Figure 4.9 Mean isometric contraction stresses ($n \geq 4$) for the '1.03' (squares), 'low stretch' (pluses), and 'elbow' (circles) tests. Shown also are the mean stresses for the 'high stretch' tests (triangles, $n = 4$), which have been corrected for the viscoelastic response (i.e. curves in Figure 4.8 were subtracted from those in Figure 4.7). Panels (A) and (B) are the preferred and non-preferred directions, respectively.

Much remains unclear with regard to the role of mechanical constraints on the kinetics of thermal denaturation to a collagenous tissue. Obviously, there are significant qualitative correlations between biaxial isotonic shrinkage and biaxial isometric contraction. This begs the question of whether or not the essential characteristics of isotonic and isometric kinetics can be captured within a single model. To formulate such a model, we need to identify a metric of thermal damage that is common to the two tests. In the following chapters, we begin to address this issue by using post-heating mechanical behavior as an

indicator of prior thermal damage. We also evaluate the feasibility of using histology as a tool to accurately assess prior thermal damage.

CHAPTER V

ALTERATION OF MECHANICS WITH HEATING

INTRODUCTION

Clearly, the kinetics of the thermal damage process are not completely understood. It may be, however, that the result of the thermal intervention is more important than the path by which the result is achieved. Knowledge of post-heating stresses are key to understanding the resultant mechanobiology and thus healing process. Therefore, let us consider now the changes in mechanical behaviors with heating. Previous research has shown a correlation between thermal damage (shrinkage) and tissue mechanical behavior (Chen and Humphrey, 1998; Harris et al., 2003). The same studies have shown that the rate at which the mechanical changes occur is altered by mechanical constraint. In this chapter, we have selected two of the isometric constraints studied in the previous chapter (namely the 1.03 and elbow constraints), and performed additional sets of tests wherein we used different durations of heating. The alteration in mechanical behavior becomes greater (relative to native behavior) with increased durations of heating for both constraints, but then becomes progressively smaller as the duration is increased further still. This rate at which the material behavior progresses through these “two phases” of alteration is dependent on the level of isometric stretch.

METHODS

Specimens were prepared and mechanically tested as per the procedures detailed in Chapter II. Following mechanical testing in the native state, specimens were subjected to one of two isometric conditions (cf. Figure 4.1): (a) '1.03', with $\lambda_1 \approx \lambda_2 = 1.03$, where $\lambda_1 = F_{11}$, $\lambda_2 = F_{22}$ and \mathbf{F} is the deformation gradient relative to the native reference configuration, β_N , and (b) 'elbow', with $\lambda_1 \approx \lambda_2 = 1+0.7(\lambda_{MAX}-1)$, where λ_{max} was the maximum stretch ratio obtained during the native equibiaxial test. Specimens were first taken to the prescribed equibiaxial stretch ratio (e.g., $\Lambda_1 \approx \Lambda_2 = 1.03$), and the loading carriages were moved inward (toward the specimen) a set distance of 10 mm such that the sutures became slack. The specimen was placed within a polystyrene insulating cell filled with room temperature saline, and the room temperature solution in the chamber was then replaced with a high temperature, normal saline solution maintained at 75°C, following the procedure described in Chapter II. Adequate time was allowed for all chamber components to reach thermal equilibrium; although the load cells are thermally compensated, small heat-induced offsets were observed and recorded. The specimen was then removed from its insulating cell and suspended above the heated chamber (for no more than 15 seconds to avoid premature thermal damage). Each loading carriage was then rapidly (and simultaneously) moved outward (10 mm) so that the prescribed equibiaxial stretch was regained, and the specimen quickly submerged (it took approximately one second to get the specimen back to this configuration).

The '1.03' specimens were kept in the high temperature bath for 1, 900, 1800, or 3000 seconds, and the 'Elbow' specimens for 900, 1800, 3000, or 10,800 seconds. The forces required to maintain the tissue at its fixed length were recorded during heating. The high temperature solution was then replaced with room temperature normal saline, following the procedure detailed in Chapter II, and the specimen was allowed to 'recover' for 60 minutes while maintaining the isometric constraint. Immediately following recovery, the configuration β_p was recorded. The motors were then moved inward until the sutures became slack and the unloaded configuration, β_R , was recorded. For consistency, the specimen was again preconditioned from 0.02 to 0.78 N for ten cycles, and the new unloaded configuration, β_C , recorded for use in subsequent stretch-controlled mechanical testing. Mechanical tests were then carried out in the same manner as for the native tissue. Figure 4.2 is a schema of the overall experimental protocol. Data were analyzed as outlined in Chapter II.

RESULTS

A representative stress-stretch plot from the raw data of an equibiaxial test is shown in Figure 5.1 to familiarize the reader. The two sets of curves (native and damaged) correspond to the two primary stretching axes. Note that the mechanical characteristics of native epicardium are similar to those of skin, and are dominated by collagen. The tissue is easily stretched to a certain point (i.e. when all undulations have been removed), it then goes through a small

transition (elbow) region wherein the slope begins to increase slowly, and finally becomes very stiff and anisotropic. Recall from Chapter II, however, that to simplify the analysis for these complex specimens with differing anisotropies, it is convenient to plot $|T|$ versus $|V|$. Figure 5.2 shows data from Figure 5.1 plotted in this way.

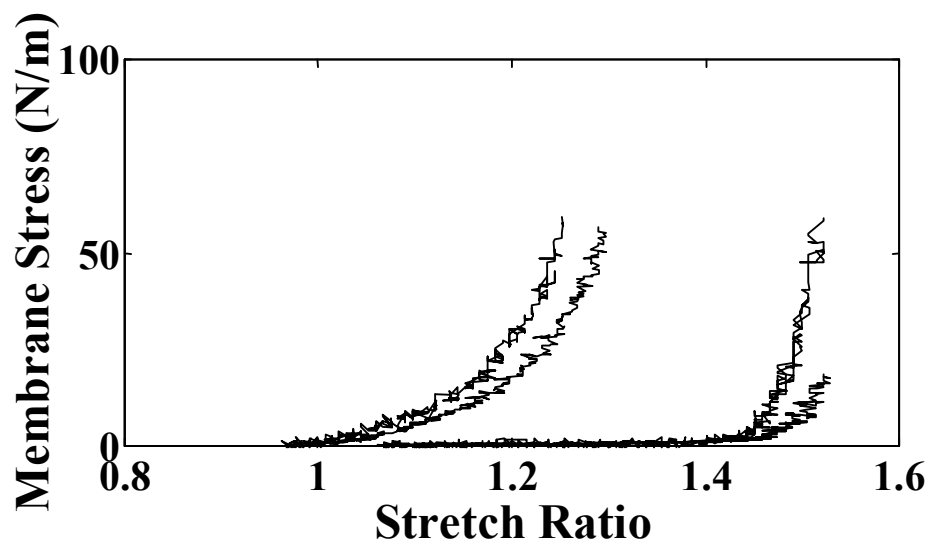


Figure 5.1 Representative raw data from a single '1.03' test ($T = 75^{\circ}\text{C}$, $\tau = 900$ sec), which illustrates the altered biaxial mechanical behavior due to heating. The two curves represent the primary stretching axes. Note the non-zero initial slope for the damaged specimen, the loss of extensibility, and in this case a tendency towards decreased anisotropy. All data are plotted relative to β_N (cf. Figure 4.2).

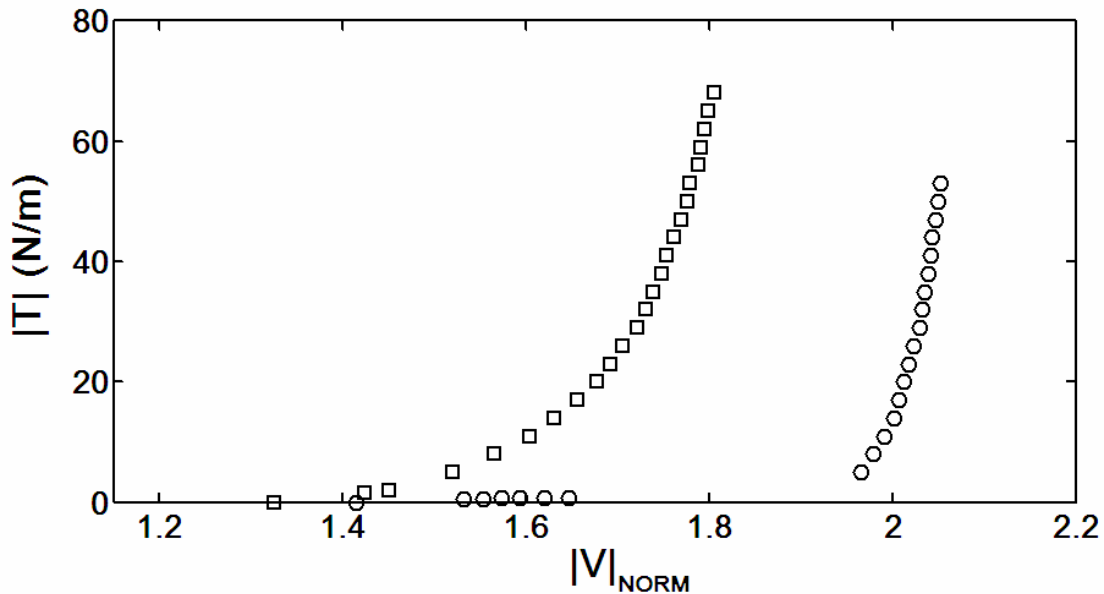


Figure 5.2 Plot of the mean (equibiaxial) mechanical data following the '1.03' isometric heating tests ($n = 5$). Circles represent the 'native' tissue mechanical response, whereas the squares represent that of the heated tissue. The stretch magnitudes are calculated relative to the 'native' undeformed configuration, β_N . Note that $|v| = \sqrt{2}$ in the reference configuration.

Mechanical behaviors for both the 1.03 and elbow isometric groups exhibit a two-phase transition over the durations of heating we tested. That is, the mechanical behaviors progressively become less extensible than that of the native tissue until a 'critical' duration of heating has been achieved, after which the tissue returns progressively towards native tissue behavior. Though the critical duration could not be determined precisely from the experiments herein, the severity of the isometric constraint imposed during heating clearly has an effect. Recall, the durations of heating for the '1.03' tests were 1, 900, 1800, and 3000 seconds, and for the 'elbow' tests were 900, 1800, 3000, and 10800 seconds. A marked reduction in extensibility for the '1.03' tests is evident after only 1 second of heating, with the largest reduction occurring after 900 seconds

(Figure 5.3). The 1800 and 3000-second heatings for the '1.03' tests trend back toward native tissue extensibility. For the elbow tests, the reduction in extensibility after 900 seconds of heating was not as pronounced as for 1 second of heating under the 1.03 constraint. Furthermore, the maximum reduction in extensibility was not achieved until 3000 seconds of heating (Figure 5.4).

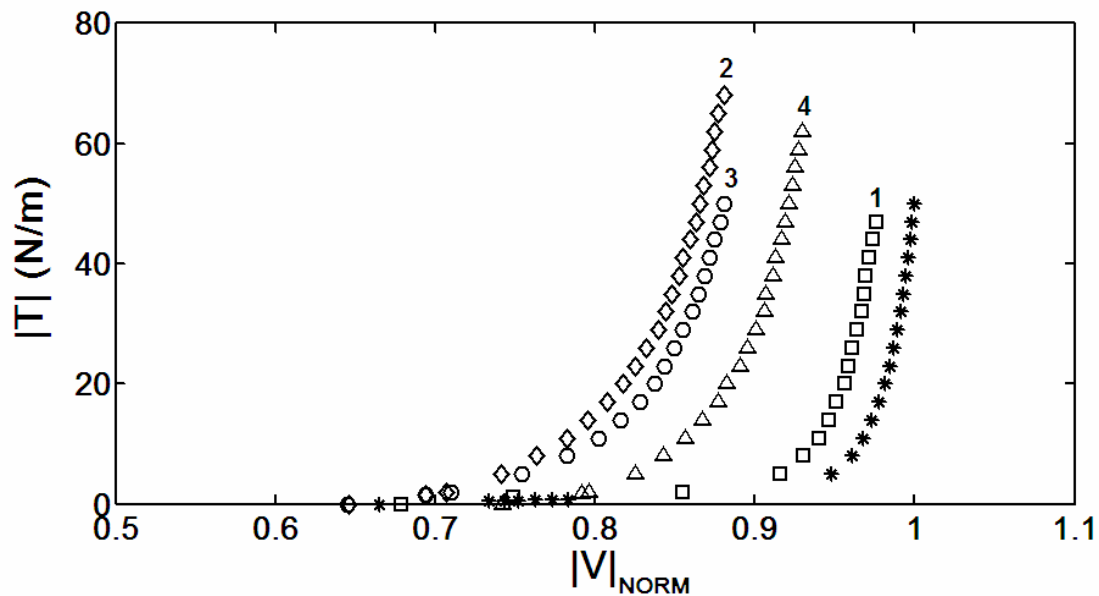


Figure 5.3 Variation of mechanical behavior with duration of heating (at $T = 75^{\circ}\text{C}$; $n \geq 4$) for tissues subjected to the '1.03' isometric constraint. The durations (in seconds) are 1 (squares), 900 (diamonds), 1800 (circles), and 3000 (triangles). The asterisks represent the native behavior. The lines are numbered consecutively, according to duration, to assist in illustrating the biphasic trend.

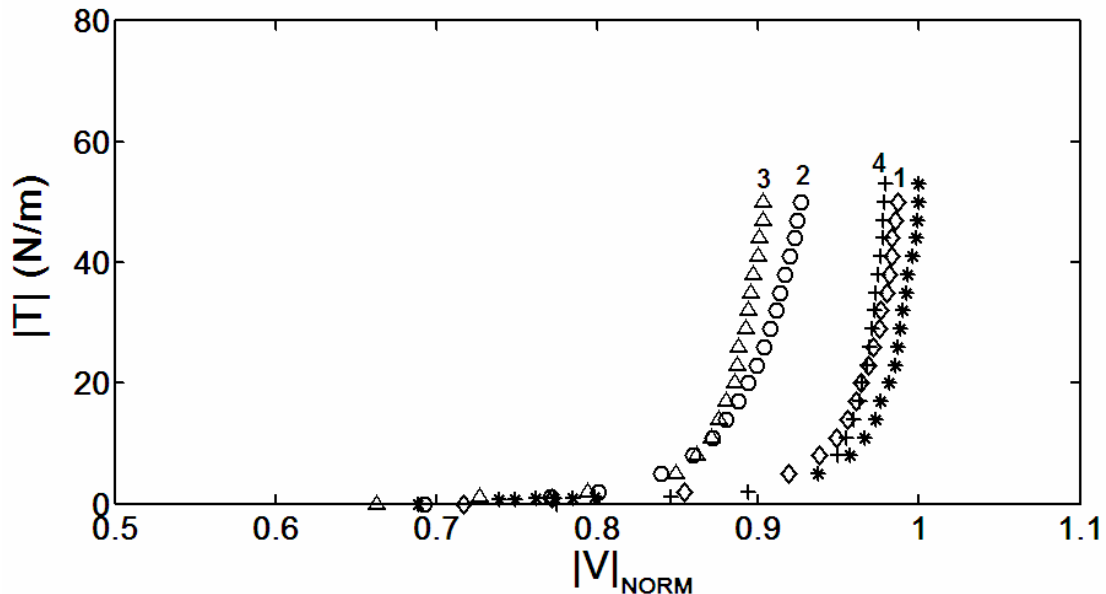


Figure 5.4 Variation of mechanical behavior with duration of heating (at $T = 75^{\circ}\text{C}$; $n \geq 4$) for tissues subjected to the ‘Elbow’ isometric constraint. The durations (in seconds) are 900 (diamonds), 1800 (circles), 3000 (triangles), and 10800 (pluses). The asterisks represent the native behavior. The lines are numbered consecutively, according to duration, to assist in illustrating the biphasic trend.

DISCUSSION

Chen and Humphrey (1998) showed that, for uniaxial isotonic tests on bovine chordae tendinae, similar mechanical behaviors resulted from heating a native tissue if equivalent combinations of time, temperature, and load were used. In particular, for an increased temperature, a decrease in the duration of heating was required to achieve the same resultant mechanical behavior (assuming the load was unchanged). A similar relationship exists for biaxial isotonic tests on bovine epicardium (cf. Figure 9 in Harris et al., 2003). Clearly, the time-temperature coupling for the results herein is more complex. For example, tissues constrained near the elbow (cf. Figure 4.1) and heated at 75°C

for 900 seconds and 10,800 seconds, exhibit nearly the same mechanical behavior (Figure 5.4). This is problematic from a modeling perspective, because the dependence of the resultant mechanical behavior on the duration of heating (holding all other parameters constant) is not unique (see Figure 5.5).

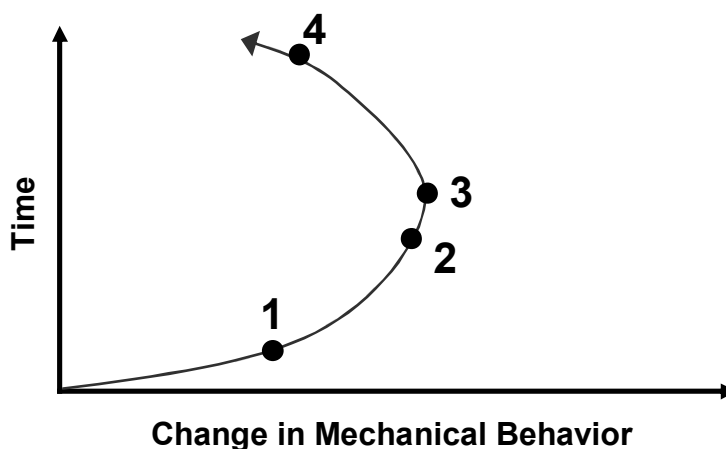


Figure 5.5 Schema of the biphasic change in mechanical behavior with duration of heating. Compared the numbers to those in Figure 5.4. Clearly, the solution is non-unique in time.

Perhaps even more problematic is that the cause of this biphasic behavior is not clear. One possibility would be that the second phase represents a partial reversal of the thermal damage that has occurred during the first phase, which is illustrated by



where N and D are the number of native and damaged molecules, and k_1 and k_2 are the rate constants for phase one and phase two, respectively. This is highly unlikely, however, because reversibility of a thermally (energetically) activated

reaction always occurs upon cessation of the energy application. All of the experiments were subjected to the same cool-down and recovery procedure, and therefore reversibility should have had an equal chance to ‘play out’ for all durations. Furthermore, reversibility generally (if not always) becomes less likely as the reaction proceeds (i.e. as heating duration is increased). Finally, Miles et al. (1995) demonstrated clearly that thermal denaturation of unrestrained (i.e. free-shrinkage) fibrillar collagen is irreversible. A more likely possibility for the biphasic behavior is simply two mechanisms of thermal damage that dominate on different time scales. In other words, phase one would represent the transition to some intermediate damage state D^* , such that



From a thermodynamics perspective, this is the more reasonable scenario. We can only speculate, however, on the mechanisms of each phase. Regardless, if we assume a model similar to the one in equation (5.2), then we can think of the second phase as a continuation of damage. In other words, thermal damage would strictly be an increasing function of time for all durations tested herein, which aides in our comparison of the two constraints. Recall that the tissues constrained near the elbow were heated in excess of 3000 seconds before the second phase of mechanical alteration dominates, versus only 900 seconds for the 1.03 tissues. At 3000 seconds of heating, the 1.03 tissues had already regained much of their native extensibility. It appears, therefore, that tissues subjected to greater isometric constraints progress through both phases of

thermal damage at a much slower rate. These results agree in principle with previous isotonic tests that show thermal damage (i.e. shrinkage) is slowed by mechanical constraint (Lennox (1949); Weir (1949); Chen et al. (1998a); Harris and Humphrey (2004)).

The two isometric constraints used herein have proven sufficient for delineating qualitative characteristics of altered mechanical behavior for various durations of heating. To understand better the effect of isometric constraints on the resultant mechanical behavior, comparisons must be made for more than two constraints and for equal durations of heating. Indeed, that is the focus of the next chapter.

CHAPTER VI [†]

COMPARISON OF ISOMETRIC CONSTRAINTS

INTRODUCTION

Numerous studies have looked at the altered mechanical response due to heating under various isotonic constraints (Wiederhorn and Reardon, 1953; Consigny et al., 1989, Morgan et al., 1996; Wallace et al., 2001; Chen and Humphrey, 1998; Harris et al., 2003), but we have found only one investigation that measured the mechanical response following an isometric test (HIT; Hayashi et al., 2000). There is, therefore, a complete lack of multiaxial data on the altered mechanical response due to heating under various isometric constraints. Herein, we explore this issue for the first time by performing a series of multiaxial thermal damage tests on bovine epicardium at a set temperature and for a set duration, but for four different isometric stretches (Figure 4.1). We saw in the previous chapter that the alteration of mechanical behavior is biphasic in time. Given the uncertainty of the mechanisms responsible for the biphasic alteration with duration of heating, it was prudent to choose a duration wherein the first phase dominates for all constraints. Assuming the 1.03 constraint progresses through the phases more rapidly than the other constraints, and that the first phase still dominates after 900 seconds

[†] Reprinted with permission from “Altered mechanical behavior of epicardium under isothermal biaxial loading” by Wells PB, Harris JL, Humphrey JD, 2004. ASME J Biomech Engr, vol. 126, pg. 492-497, Copyright 2004 by ASME.

of heating for the 1.03 constraint, then a duration of 900 seconds is reasonable. The alteration in mechanical behavior varies systematically with the level of isometric stretch, and follows closely the trend in mechanical alteration for biaxial isotonic tests (Harris et al., 2003).

METHODS

The mechanical behaviors reported herein are for those biaxial isometric isothermal experiments as described in Chapter IV. Recall, too, (from Chapter II) that because the anisotropy was highly variable from specimen-to-specimen, and following (Harris et al., 2003), comparison of the native and damaged mechanical responses was facilitated by plotting the magnitude of the Cauchy stress resultant tensor $|\mathbf{T}|$ versus the magnitude of the left stretch tensor $|\mathbf{V}|$.

RESULTS

When subjected to the lowest isometric stretch ('1.03') during heating, the damaged equibiaxial response differed from that of the native in two ways (Figure 5.2) - the extensibility was reduced by approximately 11%, and there was a 15-fold increase in initial stiffness (obtained by calculating the slope of a line fitted to the first four data points). The latter difference is more characteristic of native endocardium, which contains greater elastin than native epicardium (Kang et al., 1996). As the isometric stretch during heating was increased, these differences systematically diminished to the point where equibiaxial tests

on native and damaged specimens were nearly indistinguishable for the ‘high’ constraint (Figure 6.1).

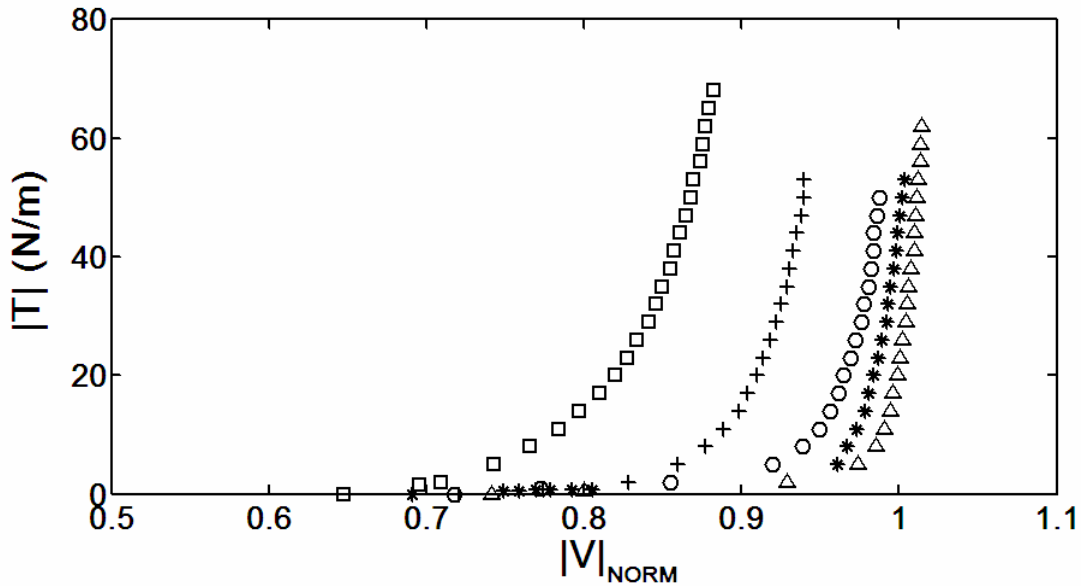


Figure 6.1 Plot of the mean equibiaxial data from the four test groups ($n = 5$ to 7 per group) and a representative mean ‘native’ curve (*). In comparison to Figure 5.2, the magnitude of V is normalized here to the maximum value in the mean native data. The squares (\square), pluses ($+$), circles (o), and triangles (Δ) represent the ‘1.03’, ‘low stretch’, ‘elbow’, and ‘high’ constraints, respectively. As the isometric constraint increased (i.e. greater stretch was imposed) given the same temperature level and duration of exposure, the equibiaxial response of the heated tissue differed less from that of the native tissue, suggesting that stretch delays thermal damage.

To quantify further how the extensibility changed with respect to the imposed constraint, we define the parameters Φ and Ψ as follows:

$$\Phi = \frac{|V|_C}{|V|_N} \quad \text{and} \quad \Psi = \frac{|V|_D}{|V|_N}, \quad (6.1)$$

where $|V|_C$ is the magnitude of the left stretch tensor calculated for a constraint relative to β_N . Similarly, $|V|_N$ and $|V|_D$ are the magnitudes of the left stretch tensors for the native and heated tissues, respectively, corresponding to a

chosen value of $|T|$. Thus, Φ is a relative measure of the isometric stretch imposed during heating and Ψ is a relative extensibility of the heated tissue. Figure 6.2 reveals a generally linear correlation between Φ and Ψ for the heating parameters studied and the constraints imposed.

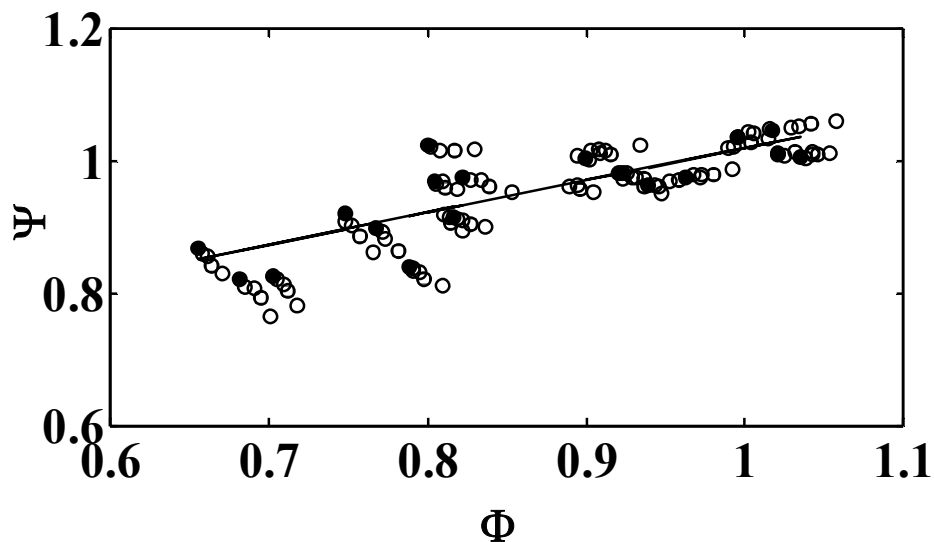


Figure 6.2 Nearly linear correlation between the relative extensibility of the damaged tissue (Ψ) at various levels of $|T|$ (15, 25, 35, 45 and 55 N/m) and the relative amount of isometric stretch imposed during heating (Φ). Because physiologic loads are more likely to be high, we chose the data corresponding to $|T|=55$ N/m ('filled' circles) as the basis for a best-fit linear trend-line, which has an R^2 value of 0.687. 'Open' circles correspond to $|T|=15, 25, 35,$ and 45 N/m, and as can be seen, they too correspond well to the linear trend.

We previously showed that the effect of preconditioning on thermally damaged tissues depended on the amount of equilibrium shrinkage (see Table 1 in Harris et al., 2003). That is, preconditioning had a greater effect on tissues having a greater degree of heating-induced shrinkage. For comparison, we calculated the principal stretches relating β_N to β_C , defined as λ_1 and λ_2 , as well as the principal stretches relating β_R to β_C , defined as δ_1 and δ_2 (recall Figure 4.2

for configurations). We then computed the mean changes in area due to heating ($1-\lambda_1\lambda_2$) and those due to preconditioning ($1-\delta_1\delta_2$) for each test group (Table 6.1). Area changes due to the heating were small – on the order of ten percent or less for all constraints – thus revealing one effect of the isometric constraint during heating and recovery. Interestingly, the ‘1.03’ constraint allowed area shrinkage, whereas the other constraints resulted in a slight area expansion. Regardless, preconditioning had small effects (< 3% change) on all groups.

Table 6.1 Percent area changes for the four isometric test groups. Area changes calculated from β_N to β_C are given by $1-\lambda_1\lambda_2$, and area changes calculated from β_R to β_C are given by $1-\delta_1\delta_2$. Note, the ‘1.03’ specimens were the only ones to shrink upon heating. Furthermore, area changes due to preconditioning were generally small relative to similar data presented in Table 1 of (Harris et al., 2003). The bias error associated with sampling of each configuration (β_x) is approximately 1%, and therefore the total error when calculating the deformation between two of them is on the order of 2%.

Constraint	n	$(1-\lambda_1\lambda_2) * 100$ (mean \pm SD)	$(1-\delta_1\delta_2) * 100$ (mean \pm SD)
1.03	5	12.7 \pm 0.5	0.3 \pm 0.1
Low	6	-10.1 \pm 0.3	2.6 \pm 0.1
Elbow	5	-12.6 \pm 0.8	-2.1 \pm 0.1
High	7	-10.1 \pm 0.4	0.1 \pm 0.0

DISCUSSION

Uniaxial studies have dominated the thermal damage literature and are useful for delineating general characteristic behaviors of soft tissues under many different conditions. Nevertheless, one-dimensional quantitative results cannot, in general, be extended to multi-dimensional problems. This is a severe

shortcoming, for most tissues targeted during thermal therapies cannot be approximated as one-dimensional and are subjected to multiaxial loading (e.g., blood vessels, cornea, prostate, skin, uterus). Moreover, in vivo constraints during heating may be isotonic, isometric, or a complicated combination of the two. For example, catheter-based techniques allow heating of blood vessels to supra-physiologic temperatures while maintaining a near-constant diameter of the balloon (Lee et al., 1989). Although the vessel may shrink in the axial direction (possibly isotonicity), the balloon enforces a radial isometric constraint. Indeed, even tissues normally considered to be one-dimensional may be subjected to combined constraints. For example, consider the ablation of the glenohumeral joint capsule to treat joint laxity (Hayashi et al., 1997; Hayashi et al., 2000; Moran et al., 2000; Levy et al., 2001). The target ligaments are primarily constrained nearly isometrically along two boundaries: that at the humerus and the glenohumeral capsule. All other boundaries are essentially traction-free (isotonic), however. Clearly, multiaxial tests are essential to understand better most in vivo applications. The present study is the first to report on the mechanical changes of a tissue thermally treated under biaxial isometric constraints.

We found that the degree of stretch imposed on the tissue during heating dramatically affected the resulting mechanical behavior (Figure 6.1). Specifically, higher values of stretch yielded mechanical behaviors that were more similar to the native tissue. Furthermore, we found the effect to be nearly

linear in the range of constraints we imposed (Figure 6.2). More work is needed, however, to elucidate the mechanisms responsible for the observed changes; of particular interest is the possible role of the activation entropy for the different constraints. Miles et al. (1995) showed that collagen fibers are more thermally stable in the native state than when swollen in 0.5M acetic acid. They suggested that the stabilization effect of water was due to a decrease in the entropy of activation, not an increase in the energy of activation. Intermolecular distances within a native fiber are small relative to those within a swollen fiber. Thus, the molecules in the former are more constrained by their neighbors, thereby reducing their configurational entropy and increasing their stability. Likewise, as the fibers within our tissue are stretched, they become more limited in the number of configurations they can assume (much like a Gaussian chain whose end-to-end distance is constrained to higher and higher values). Therefore, their configurational entropy is reduced. Based on a model by Doi and Edwards (1986), Miles and Ghelashvili (1999) proposed further that collagen molecules within a fiber may be analogous to a 'polymer-in-a-box'. Briefly, a single collagen molecule (the polymer) is surrounded by many neighboring molecules, which impose geometric constraints in a manner similar to a box. As the box becomes smaller, the molecule is restricted further in the number of configurations it can assume, hence it loses configurational entropy.

Fibers constrained to a 3-D box with two dimensions much greater than the third have a lower configurational entropy than those constrained to a box of

equal volume but three sides of equal length. When the epicardium is stretched in the principal ('x' and 'y') directions, it thins in the third ('z') direction (assuming an isochoric deformation), thereby reducing interfibrillar distances in the 'x-z' and 'y-z' planes (the 3-D box thins). Thus, imposing a biaxial stretch likely reduces the configurational entropy, and thereby stabilizes the collagen fibers. Following this reasoning, with the heating parameters being equal (i.e. $T = 75^{\circ}\text{C}$ and $\tau = 900$ sec), one would expect that the isometric constraint which imposes a negligible stretch (e.g. '1.03' constraint) would result in the most drastic alteration of mechanical properties because of a higher activation entropy (i.e. decreased fibrillar stabilization). Furthermore, as the isometric stretch is increased, one would expect the alteration in mechanical properties to be less pronounced. Indeed, this appears to be the case (Figure 6.1). If the process is indeed entropically-driven, the same trend should be present for isotonic tests wherein different loads are applied to the tissue.

We previously reported thermally altered mechanical behavior of epicardium under multiple multiaxial isotonic (constant load, including zero) constraints (Harris et al., 2003). Briefly, we followed a protocol similar to the present (Figure 4.2) except that tissues were subjected to an elevated temperature ($T = 65, 70, 75, \text{ or } 80^{\circ}\text{C}$) while applying a constant first Piola-Kirchhoff stress resultant ($P_{ii} = 0.0, 6.0, 12.8, \text{ or } 21.3$ N/m) along both axes for a specified period ($\tau = 600, 900, 1200, \text{ or } 7200$ sec). During heating, marker positions were recorded to monitor shrinkage rather than force. We have re-

plotted equibiaxial data for (T, τ, P) combinations of $(75,900,12.8)$ and $(75,900,21.3)$, which were chosen for their consistency with tests herein with respect to temperature and duration of heating, and for $(65,900,0.0)$, that is, free-shrinkage, because it is a probable bound. These data were plotted in Figure 6.3 with respect to their native, undeformed configurations (β_0 , in our previous paper). It is evident that increasing isotonic loads had an effect similar to that of increasing isometric stretches, with respect to the normalized extensibility ($|\mathbf{V}|_{\text{norm}}$). Similar to the '1.03' tests, in which negligible stretch was imposed, isotonic tests wherein zero load was applied resulted in approximately 11% reduction in extensibility. Furthermore, all of the isotonic tests resulted in a 15- to 20-fold increase in initial stiffness for the heated tissues, as evidenced by their non-zero initial slopes (or, more gradual curves). The '1.03' tests herein exhibited a similar behavior, but the other three test groups did not exhibit a marked increase in initial stiffness (Figure 6.1). Interestingly, the '1.03' tests were the only group to shrink upon heating (Table 6.1), and therefore shrinkage may be a prerequisite for the observed change in the initial stiffness.

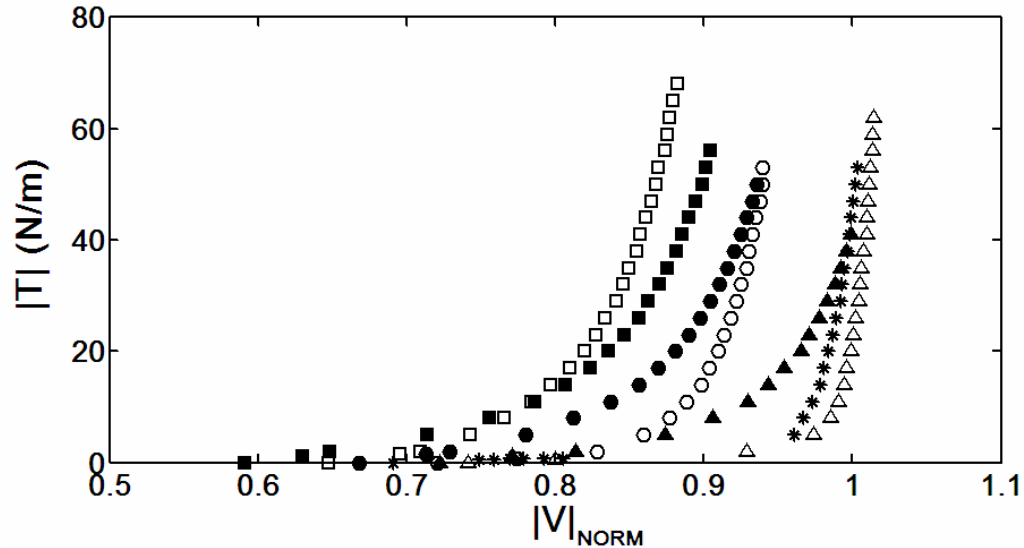


Figure 6.3 Relation between resulting equibiaxial mechanical responses in isometric and isotonic tests. The asterisks (*) represent the mean native response, the open squares (□), circles (○), and triangles (Δ) represent the ‘1.03’, ‘low stretch’, and ‘high’ isometric constraints, respectively. The filled squares (■), circles (●), and triangles (▲) represent the (T, τ, P) combinations of (65, 900, 0.0), (75, 900, 12.8) and (75, 900, 21.3) from (Harris et al., 2003), respectively. The latter two were chosen for consistency with respect to the temperature and duration of heating, while the former represents a bound.

We previously suggested that “...the mechanical response depends on the amount of equilibrium shrinkage..., not the specific thermomechanical protocol that produced the damage” (Harris et al., 2003). Thus, in the case of biaxial, isotonic, isothermal tests on bovine epicardium, zero shrinkage implies no changes in the mechanical properties. These results agree with previous uniaxial isotonic tests on chordae tendinae (Chen and Humphrey, 1998). Our biaxial isometric results did not reveal the same relationship between shrinkage and material behavior, however, for the obvious reason that the constraint inhibited shrinkage. We found significant changes in the mechanical behavior with little or no changes in the dimensions of the epicardium between the native

state and the damaged state (Table 6.1). Hence, equilibrium shrinkage is not a universal metric by which we can measure thermal damage. Rather, there is a need to identify an independent metric by which we can determine the extent of thermal damage that would apply to all types of conditions. Possibilities include, but are not limited to, birefringence, fluorescence, confocal microscopy, and gross histologic examination. This is the subject of the next chapter.

CHAPTER VII

HISTOLOGY

INTRODUCTION

Imposition of biaxial mechanical constraints (i.e. load or stretch) during heating reduces the extent of thermal damage as measured by changes in mechanical properties (see Chapter V and Chapter VI). Gross mechanical data thus reveal a key role of mechanical load on the rate and extent of thermal denaturation of collagen. To understand better the mechanism(s) behind such mechanical changes, we seek to identify a reliable metric of thermal damage. Thermal denaturation results in an irreversible helix-to-coil transition of the collagen molecule. On a macromolecular level, thermal damage is marked by swelling of collagen bands, thickening of collagen-rich layers, hyalinization, and loss of birefringence (Thomsen et al., 1989; Sankaran and Walsh, 1998; Thomsen, 1999). In this chapter, we show that by combining diffuse white light microscopy (LM) and transmission polarizing microscopy (TPM) one can assess the extent of prior thermal damage within tissues heated at a set temperature for various fixed durations (under zero load) and subject to multiple mechanical constraints. Moreover, we demonstrate that biaxial isometric constraints imposed prior to heating inhibit histological aberrations that would otherwise occur due to heating.

METHODS

Three groups of mechanically-controlled heating tests were performed on excised bovine epicardium: free-shrinkage tests, equibiaxial isometric tests, and non-equibiaxial isometric tests. Tissue dissection was identical for all three test groups, and is detailed in Chapter II, but preparation was slightly modified for the free-shrinkage tests.

Free-Shrinkage Tests

Two pieces of tissue were taken from the right ventricle of the same bovine heart. Each tissue was cut in half along the preferred direction, which yielded two rectangular sections that were again cut in half to yield four (eight total) square pieces of tissue approximately 15 mm square. A 200 ml beaker filled with normal saline was placed atop a hotplate (Cole-Parmer model # 4803-00) and heated to equilibrium at 75°C, which took approximately 15 minutes, during which the beaker was covered to prevent evaporation and thus a change in solute concentration. The cover was then removed, and the tissue samples were placed in the beaker for 1, 3, 5, 10, or 60 seconds and then quenched in room temperature saline. A sixth tissue section was not heated, and thus served as a native control (the remaining pieces of tissue were discarded). Note that there were no mechanical tests performed on the free-shrinkage tissue. Finally, the tissues were fixed and processed for light microscopy as detailed in Chapter II.

Equibiaxial-Stretch Isometric Tests

Specimen preparation and mechanical testing was done in the manner described in Chapter II. Following mechanical testing in the native state, specimens were subjected to one of three isometric conditions: (a) '1.03', wherein the in-plane stretches $\lambda_1 \approx \lambda_2 = 1.03$, with $\lambda_1 = F_{11}$, $\lambda_2 = F_{11}$ and \mathbf{F} is the deformation gradient relative to β_N , (b) 'low-stretch', with $\lambda_1 \approx \lambda_2 = 1+0.4(\lambda_{MAX}-1)$, where λ_{MAX} is the maximum stretch ratio attained during the initial equibiaxial loading test to 0.88 N, (c) 'high-stretch', with $\lambda_1 \approx \lambda_2$ chosen such that the load was initially equal to 100 g (0.98 N) in the stiffer direction. Note that tissues satisfying conditions (a) and (b) were previously tested (see Chapter IV), and therefore the only additional testing done specifically for this group was to satisfy condition (c).

Specimens were first taken to the prescribed equibiaxial stretch ratio (e.g., $\lambda_1 \approx \lambda_2 = 1.03$), and the loading carriages were moved inward (toward the specimen) a set distance of 10 mm such that the sutures became slack. The specimen was placed within a polystyrene insulating cell filled with room temperature saline, and the room temperature solution in the chamber was then replaced with a high temperature, normal saline solution maintained at 75°C, following the procedure described in Chapter II. Adequate time was allowed for all chamber components to reach thermal equilibrium; although the load cells are thermally compensated, small heat-induced offsets were observed and recorded. The specimen was then removed from its insulating cell and

suspended above the heated chamber (for no more than 15 seconds to avoid premature thermal damage). Each loading carriage was then rapidly (and simultaneously) moved outward (10 mm) so that the prescribed equibiaxial stretch was regained, and the specimen quickly submerged (it took approximately one second to get the specimen back to this configuration). The specimen was kept in the high temperature bath for 900 seconds, during which the forces required to maintain the tissue at its fixed length were recorded. The high temperature saline was then replaced with room temperature normal saline, using the procedure described in Chapter II, and the specimen was allowed to 'recover' for 60 minutes while maintaining the isometric constraint. Immediately following recovery, the configuration β_p was recorded. The motors were then moved inward once again until the sutures became slack and the unloaded configuration, β_R , was recorded. For consistency, the specimen was again preconditioned from 0.02 to 0.78 N for ten cycles, and the new unloaded configuration, β_C , recorded for use in subsequent stretch-controlled mechanical testing. Mechanical tests were then carried out in the same manner as for the native tissue (see Chapter II). Figure 4.2 is a schema of the overall experimental protocol. Immediately following testing, samples were formalin-fixed, stored, and processed for light microscopy as described in Chapter II.

Equibiaxial-Load Isometric Tests

These tests were performed in the same manner as the equibiaxial-stretch isometric tests, with the exception of the defined constraints. Following native mechanical testing, the tissues were subjected to one of two equibiaxial-load isometric constraints: (a) '50g-50g', with λ_1 and λ_2 chosen such that the load was initially 50g (0.49 N) in each axis, and (e) '100g-100g', with λ_1 and λ_2 chosen such that the load was initially 100g (0.98 N) in each axis.

Histological Analysis

Analysis of all histological slides was done such that the pathologist (Dr. Thomsen, University of Texas at Austin) was only made aware of the group to which each slide belonged (i.e. free-shrinkage, equibiaxial isometric, or non-equibiaxial isometric). For free-shrinkage samples ($n = 6$) and equibiaxial isometric samples ($n = 4$), the letters 'A' through 'J' were randomly drawn and assigned to a randomly selected tissue sample. The slides (H&E and WvG) associated with each tissue were labeled only with the appropriate letter, sorted according to the test group to which they belonged, and given to the pathologist. The challenge was to sort the tissues according to the severity of thermal damage. Each section of every tissue was examined using LM and TPM. The following features were evaluated to determine the severity of thermal damage:

1. Swelling of collagen bands, which are interwoven bundles of collagen fibers forming the major tissue components of epicardium.

2. Thickening of the different anatomic collagen-rich layers of the epicardium (Layers 2 & 4; see Results).
3. Collagen hyalinization.
4. Loss or diminution of the intensity of birefringence in the collagen bands.

A similar methodology was used for the non-equibiaxially constrained samples, with the exception that computer-captured images were given to the pathologist, as opposed to the actual slides. Histological images were captured to jpeg files using an Olympus DP70 12-bit color digital camera coupled to an Olympus BX51 research microscope by way of a 0.5X C-mount adapter. The objectives were a 20X UplanFI (0.5 aperture), a 40X UplanFI (0.75 aperture), and a 60X oil immersion UplanFI (1.25 aperture). For TPM, a linear polarizing filter (Olympus U-POT) and analyzer (Olympus) were placed on opposing sides of the microscope stage with their polarizing axes orthogonal to one another. A large number of images were collected to allow an accurate histological analysis of each tissue sample. The images were grouped according to the constraint to which they belonged, assigned a random number, and given to the pathologist for examination. Again, the challenge was to order the tissues according to severity of thermal damage based on the four features described above.

RESULTS

Native Epicardium

The architecture of the native epicardium was consistent for all groups. There were four distinct layers, most evident in the sections stained with WvG (Figure 7.1). The surface layer was a simple squamous epithelium, albeit was missing in some sections due to handling. The second layer consisted of fine collagen fibers (primarily type I with small amounts of type III) forming a loose feltwork in which fibroblasts were found. This layer was separated from the deeper connective tissues of the epicardium by a third, distinct membranous layer of interlacing, wavy elastin fibers. The fourth layer consisted of thicker collagen fibers (type I predominating) forming interlacing bands. Occasional thin, wavy or straight elastin fibers were intermixed with the collagen bands in layers two and four. Nerves and small blood vessels were also present in these layers. No pathological damage that can be ascribed to heat was seen in any of the native sections.

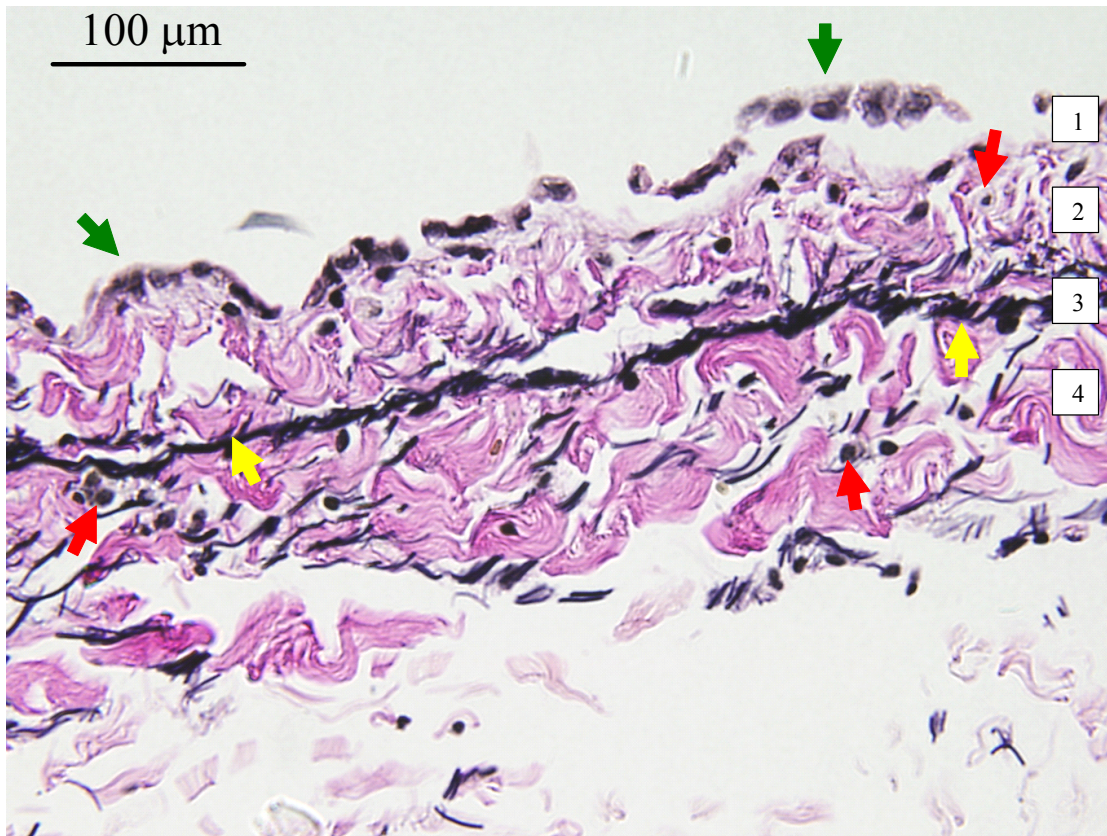


Figure 7.1 Representative cross-section of native epicardium. The various layers are distinct in this image. The simple squamous epithelium (layer 1; green arrows) covers the surface although in some areas it is detached from the subjacent layer 2. The fibrillar collagen of layer 2 forms narrow ribbons or bands. Layer 2 is separated from layer 4 by the distinct, black staining feltwork of elastin fibers forming a membrane (layer 3; yellow arrows). Ribbons of black elastin are present among the collagenous bands of layer 4 and are more prominent there than the finer elastin fibers present in layer 2. The dark nuclei of fibroblasts and an occasional inflammatory cell are present in both layers 2 and 4 (red arrows). (Weigert van Gieson's elastin stain)

Free-Shrinkage Tissues

The pathologist was able to order the samples by degree of thermal damage severity. The order correlated perfectly with the duration of thermal exposure at 75°C. As one would expect, the severity of thermal damage increased with exposure times 1, 3, 5, 10, and 60 seconds (Figure 7.2). The general order of

histological changes reflective of the severity of thermal damage going from the least severe to the most severe was

1. Swelling of collagen bands, soon followed by
2. Thickening of the different collagen-rich layers;
3. Spotty hyalinization of collagen fibers within bands;
4. Increasing regional volumes of diffuse collagen hyalinization;
5. Decreasing regional birefringence due to spotty diminution of image light intensity and/or birefringence loss within random zones of the collagen bands; and
6. General loss of regional birefringence due to loss of birefringence in most of the collagen bands.

Each tissue was scrutinized closely for these changes, and results are provided in Table 7.1. Note that scattered elastin fibers were distorted by swollen collagen bands into spiral profiles in the more severely damaged tissues (for all test groups), but these changes were not consistent across all specimens. Thus, although examined carefully, the WvG-stained images are not shown.

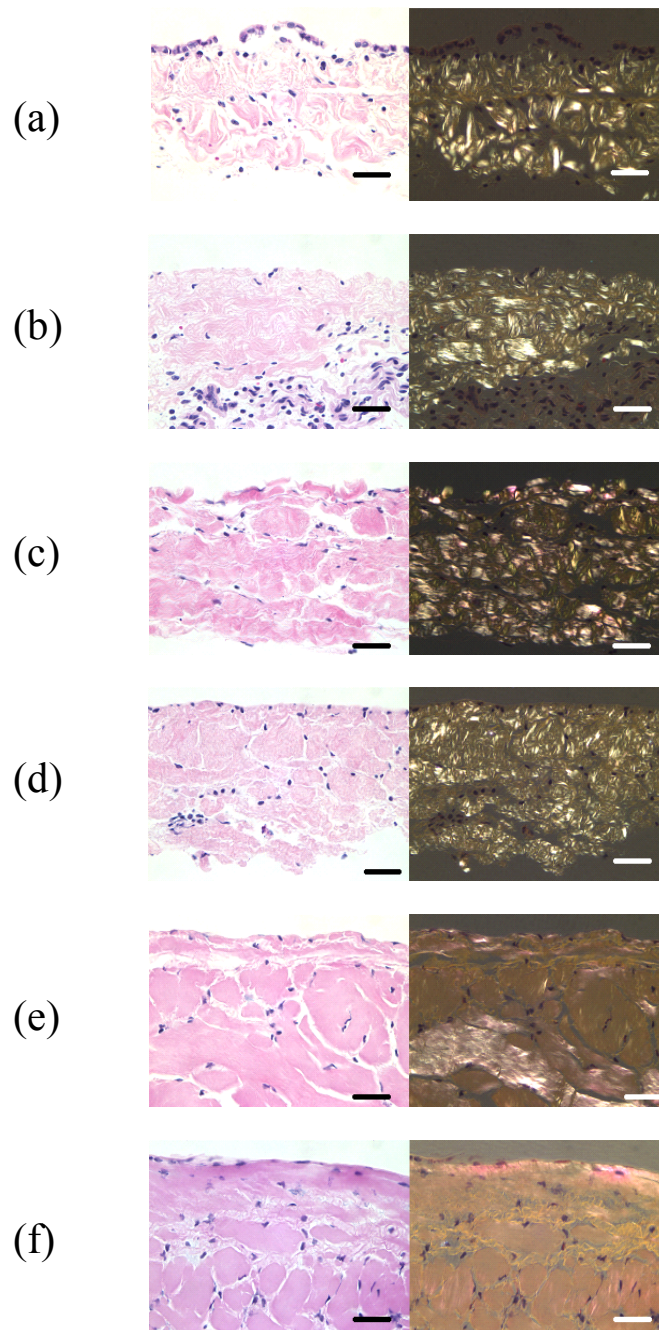


Figure 7.2 Progression of histological changes of bovine epicardium heated for various times at 75°C in the absence of mechanical constraints. Panels (a) to (f) correspond to heating times of 0, 1, 3, 5, 10, and 60 seconds, respectively. (H&E stain, 500X, bars = 25μm)

Table 7.1 Histological results for the free-shrinkage (i.e., mechanically unconstrained) group of tissues. Tissues were ranked according to the combination of six thermal damage indicators. A “0” indicates an absence of that particular marker, and a “+” indicates some change. A greater number of “+” signs means a greater amount of change. All tissues were heated in 75°C normal saline. An ‘NA’ means that specific changes were not apparent or they were obscured by more severe changes.

Ordering Epicardial Specimens	Heating Times at 75° C (seconds)	Collagen Band Swelling	Pericardial Layer Thickening	Focal Collagen Fiber Hyalinization	Diffuse Collagen Hyalinization	“Spotty” Birefringence Image Change	Diffuse Birefringence Image Change
A	0	0	0	0	0	0	0
D	1	+	0/+	++	0	0	0
I	3	++	+	++++	++	0	0
F	5	+++	++	NA	++++	0	0
C	10	++++	++++	NA	++++	++	0
E	60	++++	++++	NA	++++	++++	+++

Isometric Tissues

Recall that the isometric constraints were imposed by the sutures, and that histological sections included the entire cross-section of the tissue. Therefore, a single tissue section consisted of three distinct regions: the central region wherein stress was imposed and two outer edges that were stress-free except around the sutures. The histopathologic ordering of the thermal damage severity was based solely on examination of the constrained central region. The unconstrained edges provided a 900 second free-shrinkage “control” for each constraint condition. The order of severity of thermal damage (least to most) in the equibiaxial-stretch group (1.03, low-stretch, and high-stretch protocols) was inversely proportional to the degree of isometric constraint imposed during heating (Table 7.2). The histologic features of the unheated native epicardium were compared to those of the heated specimens (Figure 7.3). The collagen bands in the native specimen, J, consisted of distinct collagen fibrils with no

hyalinization, and the birefringence intensity patterns were uniform showing the usual waviness of the collagen bands (Figure 7.3a). The histologic features of the center of the “high-stretch” specimen, G, were similar to those of the native specimen however a minimal amount of collagen band swelling, hyalinization, and spotty birefringence intensity changes suggested some thermal damage (Figure 7.3b). The severity of thermal damage increased as the peripheral suture line was approached and became maximally severe along the free edges, similar to all free edges of the specimens in this series. The entirety of the low-stretch tissue, B, demonstrated thermal damage with some regional variations (Figure 7.3c). The collagen bands were stretched, partially hyalinized, hyperchromatic (increased staining intensity) and partially swollen. Over all, the birefringence image intensity was uniformly diminished within the constrained center, yet some scattered bands showed increased birefringence intensity. This intensity increase could be due to closer packing of the collagen fibrils within the stretched bands that would enhance the form birefringence of the macromolecules. Finally, the 1.03 specimen, H, exhibited significant and uniform thermal damage (Figure 7.3d). The collagen fibers in all locations central to the suture line showed nearly equivalent shrinkage, hyperchromasia, hyalinization, and complete loss of birefringence. However, the hyalinized collagen bands of the relatively thin central portion were less swollen than those of the free edges of the same specimen. In all heated specimens, the centers were thinner than the severely damaged free edge

Table 7.2 Histological results for equibiaxial-stretch group of tissues. Tissues were ranked according to the combination of five thermal damage indicators. A “0” indicates an absence of that particular marker, and a “+” indicates some change. A greater number of “+” signs means a greater amount of change. All tissues were heated in 75°C normal saline. An ‘NA’ means that specific changes were not apparent or they were obscured by more severe changes.

Ordering of Epicardial Specimens	Equibiaxial Isometric Stretch Conditions	Collagen Band Swelling	Pericardial Layer Thickness Changes	Diffuse Collagen Hyalinization	“Spotty” Birefringence Image Change	Diffuse Birefringence Image Change
J	<i>Native Control</i>	0	0	0	0	0
G	<i>High-stretch</i>	+	<i>Decreased from native</i>	+	+	0
B	<i>Low-stretch</i>	++	<i>Decreased from native</i>	++	+	0
H	<i>1.03</i>	+++	<i>Same as native</i>	+++	NA	++++
Free Edges	<i>Unconstrained</i>	++++	<i>Approx. twice the native thickness</i>	++++	NA	++++

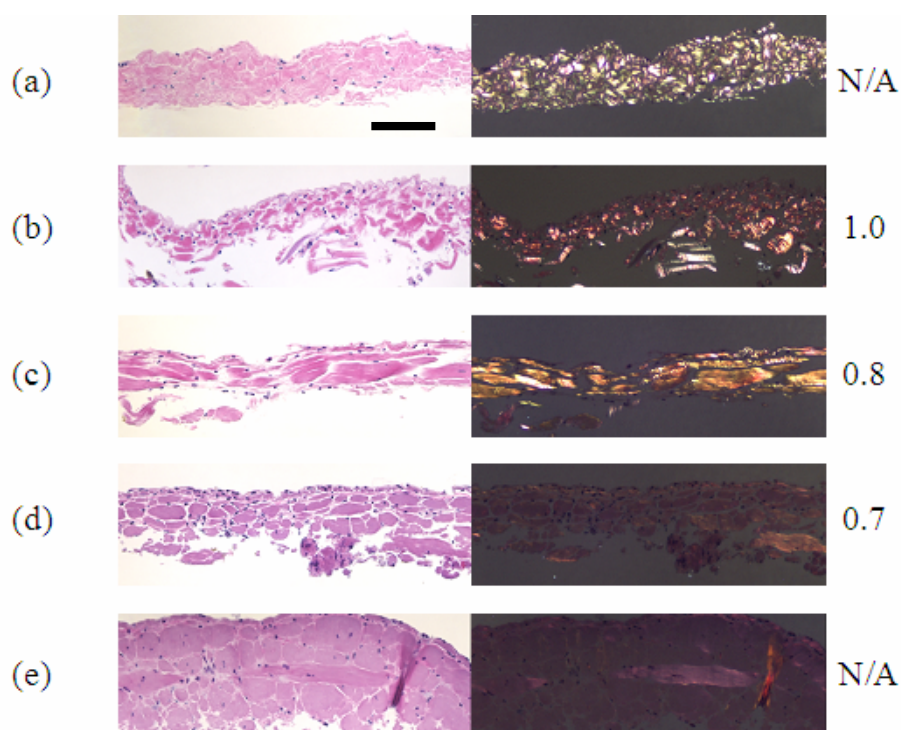


Figure 7.3 Effect of equibiaxial isometric stretch on histological characteristics of thermal damage in epicardium heated *in vitro*. Panels (a) – (d) show representative images from the central region for native (unheated), ‘high stretch’, ‘low stretch’, and ‘1.03’ constraints, respectively. Panel (e) is representative of the end (unconstrained) regions for all isometric tissues. The values to the right of the images indicate the isometric stretch relative to the maximum native stretch attained during an equibiaxial test (λ_{max}). Tissues were immersed in 75°C saline for 15 minutes and fixed in an unloaded configuration. (H&E stain, 125X, Bar = 100 μ m)

Differences in the histomorphologic thermal damage were more subtle in the equibiaxial-load group (50g-50g and 100g-100g protocols), but were sufficient to allow the correct ordering, corresponding with the degree of constraint (Figure 7.4, Table 7.3). The 100g-100g specimen, 028 (Figure 7.4b), most resembled the native specimen, 011 (Figure 7.4a). The 50g-50g specimen, 026 (Figure 7.4c), showed more changes that could be attributed to heating but none of the changes were as severe as the heated edge controls (Figure 7.4d). In the 100g-100g specimen the thermal damage changes were most prominent in the collagen bands of layer four. They were slightly swollen and minimally hyalinized, yet retained birefringence image intensity similar to the native specimen. Some collagen bands that hung unconstrained from the deep surface of layer four were hyalinized and showed considerable loss of birefringence intensity comparable to the thermal damage changes of the free edges. The central region was slightly thinner than the native control due to the stretching and spreading apart of the elastin fibers and the spreading apart of the collagen bands. The collagen fibers of layer 2 did not demonstrate any definite thermal damage at the light microscopic level. Within the 50g-50g specimen (Figure 7.4c), collagen bands two and four exhibited thermal damage. The more swollen bands showed a wavy conformation with individual fibers arranged in coherent waves. Sometimes these wavy band segments segued into more amorphous segments where the fibrillar features were lost and the bands became hyalinized, thicker, and hyperchromatic. The birefringent image

intensity of these bands was greater than that of the native control and 100g-100g specimens, and it emphasized well the wavy patterns. Because of the collagen band swelling, the 50g-50g specimen center was nearly as thick as the native specimen.

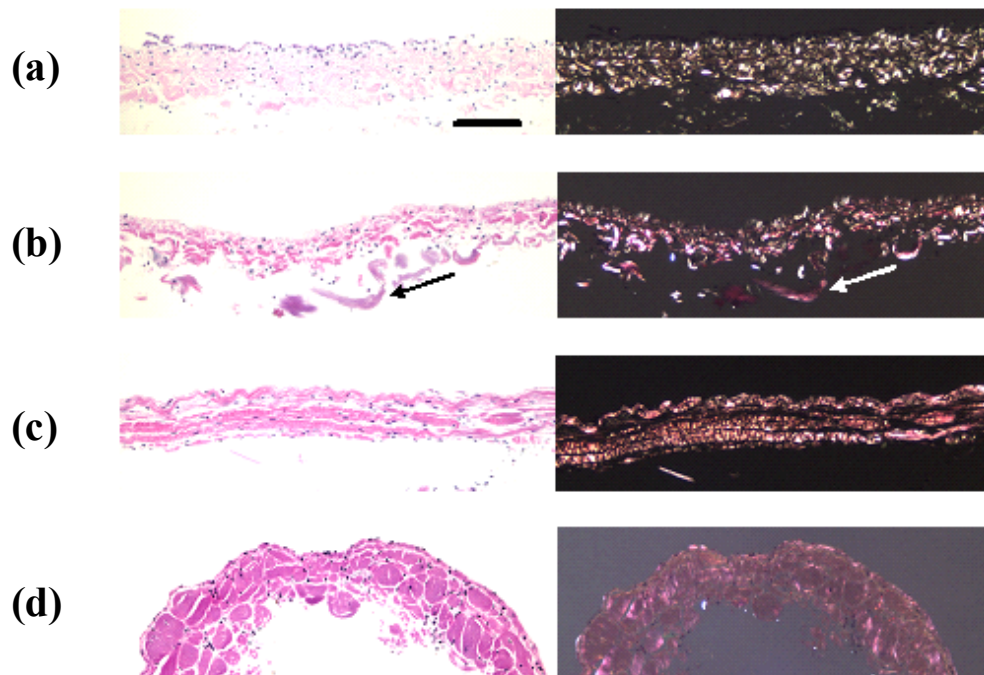


Figure 7.4 Effect of equibiaxial isometric load (at onset of heating) on histological characteristics of thermal damage in epicardium heated *in vitro*. Panels (a)-(c) show representative images of the central regions for (a) unheated native epicardium, and heated epicardium subjected to (b) 100g-100g and (c) 50g-50g constraints. Panel (d) is representative of the unconstrained free edges found in all heated isometric specimens. Loose, non-constrained collagen bands in the deep surface of the 100g-100g specimen are hyperchromatic, hyalinized (black arrow) and show decreased birefringence intensity (white arrow) reflecting more severe thermal damage compared to the constrained bands in layer four. (H&E stains. 125X Bar = 100 μ m)

Table 7.3 Histological results for equibiaxial-load group of tissues. Tissues were ranked according to the combination of five thermal damage indicators. A “0” indicates an absence of that particular marker, and a “+” indicates some change. A greater number of “+” signs means a greater amount of change. All tissues were heated in 75°C normal saline. An ‘NA’ means that specific changes were not apparent or they were obscured by more severe changes.

Ordering of Epicardial Specimens	Equibiaxial Isometric Load Conditions	Collagen Band Swelling	Pericardial Layer Thickness Changes	“Spotty” Collagen Hyalinization	Diffuse Collagen Hyalinization	Diffuse Birefringence Intensity Decrease
011	<i>Native Control</i>	0	0	0	0	0
028	100g-100g	+	<i>Slightly decreased from native</i>	++	0	0
026	50g-50g	++	<i>Same as native</i>	+++	++	+*
Free Edges	<i>Unconstrained</i>	++++	<i>Approx. twice thickness of native</i>	NA	++++	++++

*This tissue actually had an increase in birefringence, relative to native.

DISCUSSION

Recent advances in medical technology, accompanied by increased use of heat in clinical therapies, necessitate a deeper understanding of the role of mechanical constraints on the thermal damage processes. We have long known that heating an isotonicity constrained (i.e., constant load, including zero) collagenous tissue results in an evolving shrinkage process (Lennox, 1949). Not surprisingly then, we found that increasing durations of heating caused the morphology and birefringence of thermally treated traction-free tissues to evolve to the point of severe thermal coagulation and total loss of birefringence (see Figure 7.2). The gradual increase in the volume of thermal damage about a finite number of ‘nucleation’ points in these tissues reflects the complex influence of the local environment on the molecular response to heat in intact tissues. For instance, collagen hyalinization and loss of birefringence image intensity seemed to be spotty at shorter durations of heating, but more

extensively diffuse as durations increased. Thermal damage of collagenous tissue is a rate process (Miles et al., 1995; Wright and Humphrey, 2002) wherein the rate likely depends on a host of factors, including temperature, loading, and prior thermal damage, but also local constituent to constituent interactions (Danielsen, 1981). A consequence of this is that not all collagen molecules denature simultaneously. One can envision a process whereby all molecules have the same initial probability of denaturing. Upon heating, however, a sparse distribution of localized helical unfolding may occur (hence, spotty birefringence). Once a molecule is 'unzipped', it will shorten (or attempt to) and therefore influence its nearest neighbors. Note that molecules are hooked in both series and parallel, and when a single molecule denatures (and thus shortens to a random coil), those parallel to it may be placed more in compression and therefore could have a higher tendency to shorten. Conversely, those in series may be stretch further by the denatured molecule, and thus may have a decreased tendency to shorten. Thus, if the parallel relationship dominates, denaturation of a single molecule could create a cascade effect (the first unzipped molecule could be analogous to a nucleation point).

Free-shrinkage tests are useful in that they represent the lower bound of mechanical constraints. That is, the tissues are free of external constraints, which appears to allow the maximum amount of thermal damage given a particular thermal application. In vivo, however, tissues are rarely unconstrained and therefore the role of mechanical constraints on modulating thermal damage

must be addressed. The effects of mechanical constraints on the thermal damage of soft tissue are manifold: they may alter the apparent shrinkage temperature (Lennox, 1949), delay the onset of shrinkage at a set temperature (Chen et al., 1998a; Harris and Humphrey, 2004), reduce biaxial equilibrium shrinkage (Harris and Humphrey, 2004), and modulate biaxial mechanical properties (Harris et al., 2003). There has been little attempt to correlate gross changes in metrics of damage with histological evidence. Recently, Bass et al. (2004) identified histological differences between an unconstrained (free-shrinkage) and a constrained tissue subjected to the same thermal histories. Briefly, they immersed both an intact and an excised (free) porcine annulus fibrosus in 85°C saline for 15 minutes *in vitro*. TPM revealed that collagen birefringence was partially preserved for the intact annulus, but completely lost for the excised annular tissue. They suggest that the *in situ* constraints on the intact tissue somehow retard denaturation, consistent with previous studies on thermal shrinkage (Chen et al., 1998a; Harris and Humphrey, 2004) and thermally-induced changes in mechanical behavior (Chapter VI; Harris et al., 2003). Indeed, we report similar histological effects for the isometric tests herein. Birefringence was generally preserved in the constrained central region, but completely lost in the unconstrained outer regions (see Figure 7.3). TPM alone, however, is not generally sufficient for quantifying thermal damage under experimental conditions in which a single or flat heat volume heat source is not involved (Thomsen 1999). However, careful analysis of the constellation of all

histologic markers strongly characteristic of thermal damage can be used to determine semi-quantitatively the severity of thermal damage in soft tissues (Thomsen, 1991; 2000; Whittaker et al., 2000).

Our results demonstrate clear histological differences for the same temperature and duration of heating (75°C, 900 seconds), but different levels of mechanical constraint (both equibiaxial-stretch and equibiaxial-load). Note that it can be shown that in-plane fiber orientations are maintained during equibiaxial stretching (Harris and Humphrey, 2004), thus the equibiaxial-stretch isometric tests enabled us to isolate the effects of stretch from the effects of fiber re-alignment. Our results correlate well with our previous study (Wells et al., 2004), which showed that a larger equibiaxial isometric stretch during heating resulted in a mechanical behavior more similar to native tissue. Likewise, the histology of the 'high-stretch' tissue (Figure 7.3b) herein is most similar to native. As the level of isometric constraint decreased, thermal damage became more severe because the specimen was less hindered. Epicardium is comprised of randomly oriented collagen fibers (type I, primarily). Each fiber is a collection of fibrils, which are composed of collagen molecules arranged in a quarter-stagger array and attached to one another via covalent crosslinks in the non-helical terminal ends (Gross, 1973; Hulmes, 2002). Excised tissues contain fibers that are undulated in their native, unloaded state (i.e. stretch ratio equal to unity). For illustrative purposes, one may think of a fiber as a simple collection of collagen molecules connected in series. When the fiber is slack, the individual molecules

may be relatively free to transition from a helix to a random coil, and therefore shrink. If enough molecules shrink, so as to cause the length of the fiber to equal the fixed end-to-end distance (defined by the isometric constraint), the molecules no longer shrink independent of one another. In essence, they then 'feel' the effect of the constrained length. Larger isometric stretches imposed prior to heating may thereby reduce the number of molecules that are able to denature independently. For the 'high stretch' case, most undulations are likely removed prior to heating, and therefore molecules would be highly constrained and essentially not 'allowed' to denature. Because hyalinization and loss of birefringence are markers of structural change, it makes sense that they would be absent for the highly constrained tissue wherein the molecules do not denature as easily. It is important to note that the effect of such constraints is entropic in nature, not energetic. In other words, the ability, not the tendency, of the molecules to denature is altered.

Recall that the outer regions of all isometric tissues were unconstrained, and therefore provided information for the lower bound of mechanical constraints (see Figure 7.3e and Figure 7.4d). It is beneficial to know what happens nearer the upper bound of mechanical constraints (i.e. when the tissue is near maximum extension in both directions, but not damaged mechanically). Because epicardium is anisotropic, it is often impossible to impose an extreme value of force ($f \geq 100g$) along the non-preferred axis in an equibiaxial-stretch test without damaging (mechanically) the tissue along the preferred axis. Thus,

we employed the equibiaxial-load experiments, in which we defined the initial value of force along each axis irrespective of the stretch. Similar to the equibiaxial-stretch tests, the tissue was more resistant to thermal damage with increased equibiaxial-load. Though the two types of equibiaxial tests (load and stretch) differed in nature, qualitative comparisons of results from the two groups may be beneficial. For example, the 50g-50g tissue was clearly more constrained than the low-stretch tissue, which had a negligible pre-load in both directions. Consequently, one would expect thermal damage to the 50g-50g tissue to be less than for the low-stretch tissue. Though the differences are mild, it appears to be true. This suggests that the effects of fiber alignment may be negligible when compared to the effects of stretch. Interestingly, the low-stretch and the 50g-50g tissues had “spotty” and diffuse increases in the intensity of birefringence, respectively. This phenomenon has been seen at the edges of thermal coagulation lesions produced in cornea by laser irradiation and radiofrequency current (Vogel and Thomsen, unpublished observations). It is thought to be due to a closer packing of the collagen molecules and fibrils that enhances the form birefringence of type I collagen. The cause of the tighter packing is not understood.

Native structure was largely retained within the 100g-100g tissue following heating, much like the high-stretch tissue. There were, however, more “spots” with a loss of birefringence. Recall, the high-stretch protocol initially imposed a load of 100g in the preferred direction, yet the non-preferred direction

had an initial load typically between 60g and 80g. Qualitatively then, it is reasonable to say that the 100g-100g tissues were more constrained than the high-stretch tissues. Therefore, it is possible that the spotty hyalinization in the 100g-100g tissues occurred secondary to thermomechanical damage induced by the high degree of stretch. The mechanical stress combined with thermally-induced contraction forces may have been great enough to rupture covalent crosslinks, therefore reducing the stability of many molecules. The mechanical damage was especially evidenced by full-thickness rupture seen only in the 100g-100g tissue (Figure 7.5). This result reminds us that although high values of stretch may tend to thermally 'protect' the native structure, there is an upper limit on the stretch that can be imposed before thermo-mechanical damage occurs, which in turn may render the tissue more thermally labile. That is, there may be a relatively narrow range of mechanical constraints wherein damage to the tissue is minimized during thermal treatment. The constraints imposed during a clinical procedure, however, should be dictated by the desired outcome.

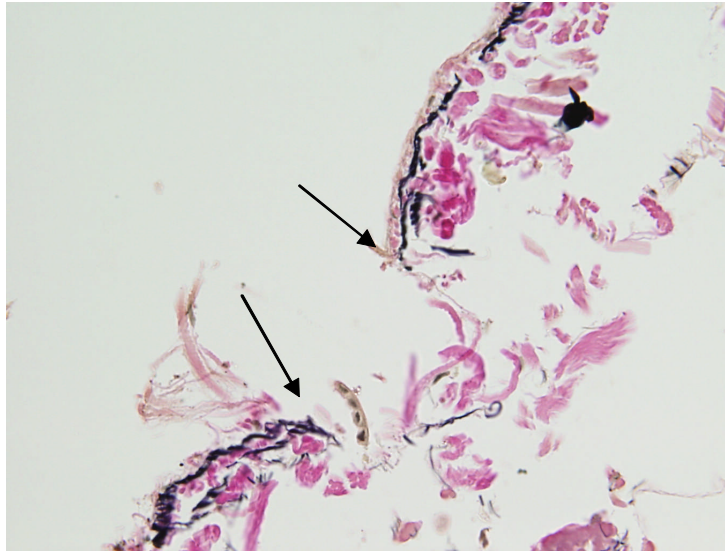


Figure 7.5 Rupture (arrows) in the central region of heated epicardium subjected to the 100g-100g constraint prior to heating. The elastin membrane of layer 3 is stained black. (Weigert van Gieson's elastin stain)

We have demonstrated the efficacy of histological evaluation for grading relative effects of heating durations and levels of stretch imposed during heating for bovine epicardium. Histology reveals a progressive deviation from native as heating time is increased (in free-shrinkage experiments) or as isometric constraint is decreased. These findings, consistent with our prior studies that showed similar deviations in mechanical properties (Harris et al., 2003; Wells et al., 2004), confirm that combining TPM and LM provides a reliable measure of graded thermal damage. It may, therefore, be possible to use histological data to predict changes in mechanical behavior. It remains to be seen, however, if the histological markers can be quantified in such a manner that allows for comparison of tissues subjected to fundamentally different thermomechanical

protocols (i.e., isometric versus isotonic, or isothermal versus non-isothermal). Future studies may include tissues subjected to combined constraints (e.g., isotonic on one axis, isometric on the other), or tissues heated at different temperatures.

CHAPTER VIII

EFFECTS OF GLYCEROL

INTRODUCTION

We are far from understanding fully the effects of heat on collagenous tissues. That should not preclude us, however, from applying our knowledge to clinical applications that could have significant and immediate impact on the medical field. Efficient delivery of optical energy to deep layers of tissue is central to effective treatment of various pathologies, including port wine stains and varicose veins. Yet, optical scattering within healthy tissue superficial to the target compromises treatment outcome, and therefore it is advantageous to optically "clear" (i.e. increase the transparency of) the superficial tissue. A proven method for doing so is by application of hyperosmotic agents (Vargas et al., 1999; Yeh et al., 2003; Khan et al., 2004). Though the mechanisms of optical clearing with hyperosmotic agents are not completely understood, refractive-index matching of agents with collagen ($n \sim 1.43$; Wang et al., 1996) has been used empirically for selection and use. Glycerol is one such agent, with a refractive index $n = 1.47$ (Gregory, 1991). Glycerol is inexpensive, biologically inert (i.e. non-toxic; Segur, 1953), and approved for topical medications and cosmetics, thus lending itself well to similar clinical applications. Indeed, it has proven effective for reversibly reducing turbidity in skin (Vargas et al., 1999; Yeh et al., 2003). Reversibility in skin is key, as skin turbidity normally

plays a protective role for underlying tissue. Tissues often play important mechanical roles as well. van Noort et al. (1981) showed that the uniaxial mechanics of a collagenous membrane (human dura mater) are unchanged after sustained immersion in glycerol and subsequent rehydration. Their study did not fully demonstrate reversibility, however, as they did not report mechanical properties of the tissue while in glycerol. Furthermore, results from uniaxial studies cannot be applied directly to multiaxial settings, such as the native state of stress in skin *in vivo*. It is also known that glycerol alters the mechanical properties of skin (Olsen and Jemec, 1993; Gardner and Briggs, 2001). Finally, it is important to examine the effect of glycerol on thermal stability, for local heating will occur in the optically cleared tissue as thermal energy is applied (e.g. via laser).

In this chapter, we demonstrate complete reversibility of the biaxial mechanical behavior of the epicardium when immersed in 10M glycerol and then rehydrated in normal saline. Furthermore, we demonstrate that glycerol increases the resistance to thermal damage for epicardium constrained isometrically during heating at a near-physiologic length.

METHODS

Mechanical Reversibility Tests

Tissues samples were prepared and mechanically tested as detailed in Chapter II. Following mechanical testing in the native state, the motors were

moved inward such that the tissue was unconstrained. The normal saline in the chamber was then evacuated to the room temperature reserve by placing pump 'PA' in reverse flow (cf. Figure 2.7). Then, glycerol (10M) was slowly poured into the chamber until the load carriages were immersed, and the tissue was allowed to "clear" for 45 min. The tissue became much more buoyant in the glycerol, and therefore wire frames were placed over the sutures to hold the tissue down (Figure 8.1). Next, the unconstrained configuration, β_G , was recorded and the tissue was preconditioned as before. The unconstrained configuration, β_{GP} , was recorded and mechanical tests repeated as performed on the native tissue. The tissue was again placed in an unconstrained state and the glycerol was evacuated from the chamber using a hand-held siphon pump. Then, the chamber was rinsed by pouring approximately one liter of normal saline into the chamber and quickly removing it via the siphon pump. Next, the chamber was re-filled with room temperature normal saline by placing pump 'PA' in forward flow at a moderate speed. Following a 60 minute rehydration period, the unconstrained configuration β_S was recorded. Finally, the tissue was again preconditioned, the configuration β_{SP} recorded, and mechanical testing was repeated.

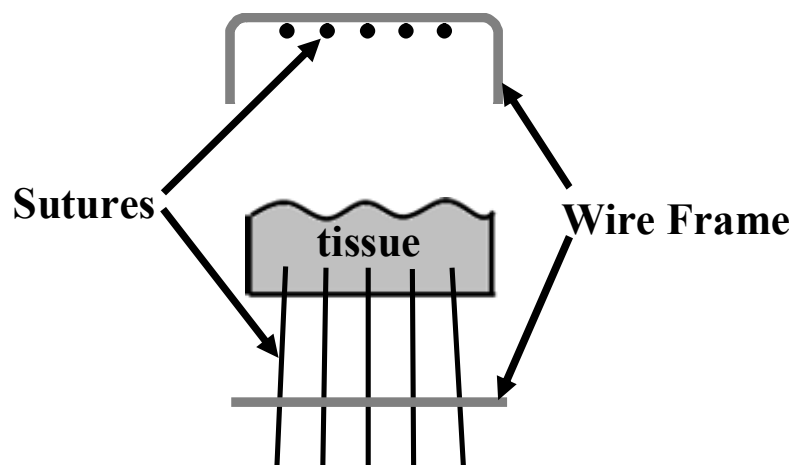


Figure 8.1 Profile and top views of the wire-frame (~15g) that was used to counter the increased buoyancy of the tissue when immersed in glycerol. A single wire frame was placed on each of the four sets of sutures.

Thermal Damage Tests

Thermal damage tests were carried out in much the same manner as those in Chapter IV. Specimens were prepared and mechanically tested following the procedure in Chapter II. Following mechanical testing, the specimens were subjected to the elbow constraint (recall from Chapter IV, $\lambda_1 \approx \lambda_2 = 1 + 0.7(\lambda_{MAX} - 1)$). This value of stretch placed the tissue at a physiologically relevant length. The loading carriages were then moved inward 10 mm such that the sutures became slack, and the specimen was placed within a polystyrene insulating cell filled with room temperature glycerol (10M). The tissue was then allowed to “clear” for 45 minutes, during which the tissue become visibly more transparent. Next, the room temperature saline in the chamber was replaced with circulating glycerol (10M) maintained at 75°C, using the procedure detailed in Chapter II, and adequate time was allowed for all

chamber components to reach thermal equilibrium (~15 minutes). The specimen was then removed from its insulating cell and suspended above the heated chamber (for no more than 15 seconds to avoid premature thermal damage). Each loading carriage was then rapidly (and simultaneously) moved outward (10 mm) so that the prescribed equibiaxial stretch was regained, and the specimen quickly immersed (approximately one second elapsed to return the specimen to this configuration). The specimen was kept in the high temperature bath for 900, 1800 or 3000 seconds, during which time the forces required to maintain the tissue at its fixed length were recorded at 30Hz. The heated glycerol was then replaced with room temperature normal saline, using the procedure outlined in Chapter II, and the specimen was allowed to 'recover' and rehydrate for 60 minutes while maintaining the isometric constraint. Immediately following recovery, the configuration, β_P , was recorded and then the motors were moved inward until the sutures became slack and the unloaded configuration, β_R , was recorded. The specimen was preconditioned from 0.02 to 0.78 N for ten cycles, and the new unloaded configuration, β_C , was recorded for use in subsequent stretch-controlled mechanical testing. Mechanical tests were then carried out in the same manner as for native tissue (see Chapter II).

RESULTS

Recall the raw stress-stretch response for a representative equibiaxial test on native epicardium (cf. Figure 5.1). The tissue is easily stretched to a

certain point (i.e. when all undulations have been removed), then it goes through a short transition (elbow) region wherein the slope begins to increase slowly, and finally becomes very stiff and anisotropic. Recalling the procedure for the reversibility experiments (cf. Figure 8.2), representative mechanical data for a sample in native, cleared, and rehydrated states (stretch ratios calculated relative to β_N , β_{GP} , and β_{SP} , respectively) are shown in Figure 8.3A. Note that the stress and stretch for the two axes of pull were not combined into single scalar measures, as in the previous chapters. This is so that we could appreciate any changes to the material symmetry, which is important for demonstrating reversibility. Following 45 minutes of clearing in 10M glycerol, the characteristics of the stress-stretch curves were similar to those of native, but the length of the initial compliant region was drastically reduced. After rehydration in normal saline for 60 minutes, however, the tissue mechanics were practically indistinguishable from those of the native tissue. Figure 8.3A thus illustrates well the change in mechanical properties relative to the new, potentially altered reference configuration.

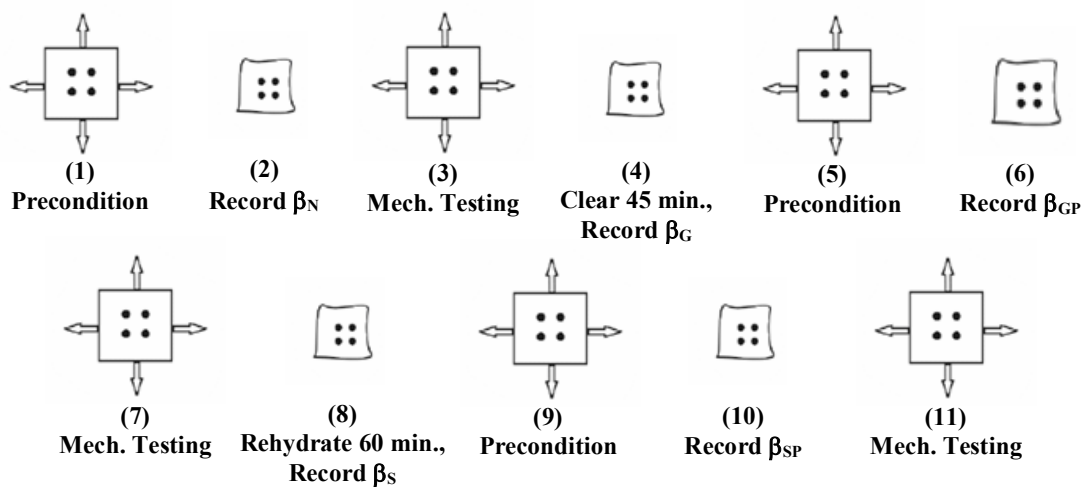


Figure 8.2 Schema of the testing protocol for investigating the mechanical reversibility of glycerol. Images with arrows represent dynamic, cyclic loading of the tissue. Images without arrows represent static, unconstrained tissue. Note the increased dimensions of the tissue from step (4) to (6).

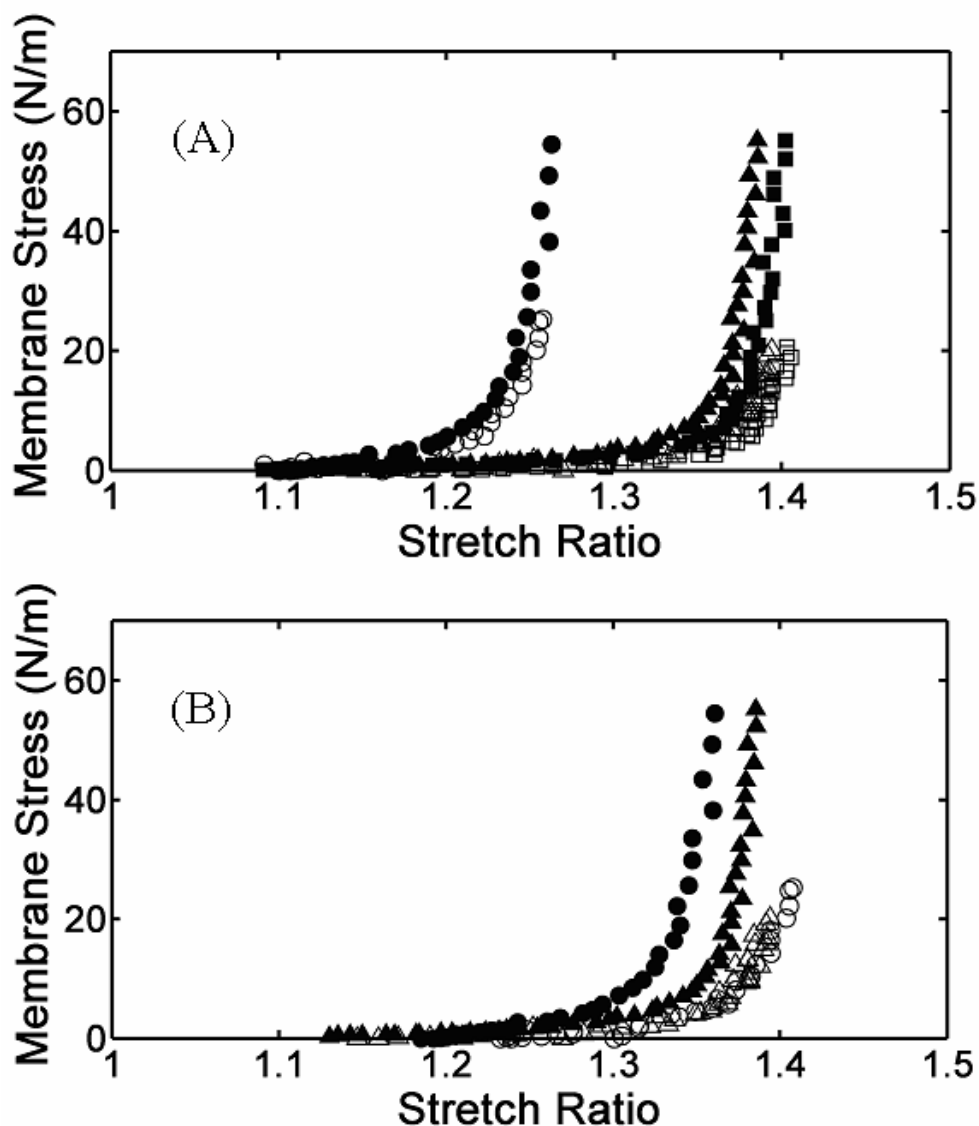


Figure 8.3 Reversibility of glycerol-induced changes in the mechanical behavior of a representative sample. The triangles, circles, and squares represent the native, glycerol-treated, and rehydrated tissues, respectively. The open and closed symbols represent the primary stretching axes for each case. In panel (A), stretches are calculated relative to the current reference configurations, which illustrates well that mechanical changes were reversed with rehydration. Note that the extensibility and the material symmetry were both restored upon rehydration. In panel (B), all stretches are calculated relative to β_N , which reveals that the glycerinated tissue achieved nearly the same maximum dimensions as the native tissue. Both figures taken together reveal that glycerol primarily affects the unconstrained length of the tissue.

In Figure 8.3B, we compare the native tissue response to the glycerol tissue response, with all stretch ratios calculated relative to β_N . In this case, the maximum stretch ratio of the glycerol tissue is similar to the native tissue, which suggests that the glycerol-induced changes in Figure 8.3A are due primarily to a shift in the reference configuration. To verify this, we performed an analysis on the various reference configurations. Table 8.1 shows average values of the percent area change from one configuration to the next (see also Figure 8.2) as well as the overall area change from the native to rehydrated state. Area change induced by glycerol was negligible ($\sim 2\%$) prior to preconditioning, but it increased by 17% following preconditioning. Upon rehydration, tissue area reduced by 18%, thereby recovering the original dimensions. Preconditioning of the rehydrated sample had a negligible effect on tissue dimensions. Overall, area change was less than one percent and glycerol-induced geometrical alterations were fully reversed upon rehydration.

Table 8.1 Average change in planar tissue area in the central region for the various configurations recorded in the experiment. Area changes were calculated with the formula $((\Lambda_1 * \Lambda_2) - 1)$ where Λ_1 and Λ_2 are the stretch ratios, in the primary directions, which relate the two configurations. See Figure 8.2 for a schema of the configurations.

Deformation	Experimental Step	Area Change (%) (mean \pm SD)
$\beta_N \rightarrow \beta_G$	Optical Clearing	1.9 \pm 2.6
$\beta_G \rightarrow \beta_{GP}$	Preconditioning Cleared Tissue	17.4 \pm 4.5
$\beta_{GP} \rightarrow \beta_S$	Rehydration	-18.1 \pm 4.2
$\beta_S \rightarrow \beta_{SP}$	Preconditioning Rehydrated Tissue	1.6 \pm 1.1
$\beta_N \rightarrow \beta_{SP}$	Initial to Final	-0.7 \pm 0.9

Recall the procedure used for the thermal damage study (cf. Figure 8.4). Mean “contraction stresses” for the 3000-second duration of heating were compared to those for tissue heated under the same conditions in saline (see Chapter IV) Figure 8.5. Like the tissues heated in saline, the stress curves exhibit three distinct regimes. First a slow regime, followed by an abrupt and rapid increase in force, and finally by a second slow regime wherein the rise in force is only detectable if time is plotted logarithmically. Of note is that the characteristic times (τ_1 , $\tau_{1/2}$, and τ_2 ; cf. Figure 4.4) were three to five times greater for the tissues heated in glycerol (Table 8.2), which shows that glycerol delayed the onset of thermal damage. Only part of the delay may be accounted for by the greater viscosity and lower thermal diffusivity of glycerol (relative to saline), which leads to an increased time for the tissue to achieve thermal equilibrium (~4.5 seconds, versus 1.8 seconds for saline). Also, the ultimate values of stress during the glycerol heating were less than those for the saline

heating, which suggests that the tendency for thermal damage to occur is reduced when heated in glycerol.

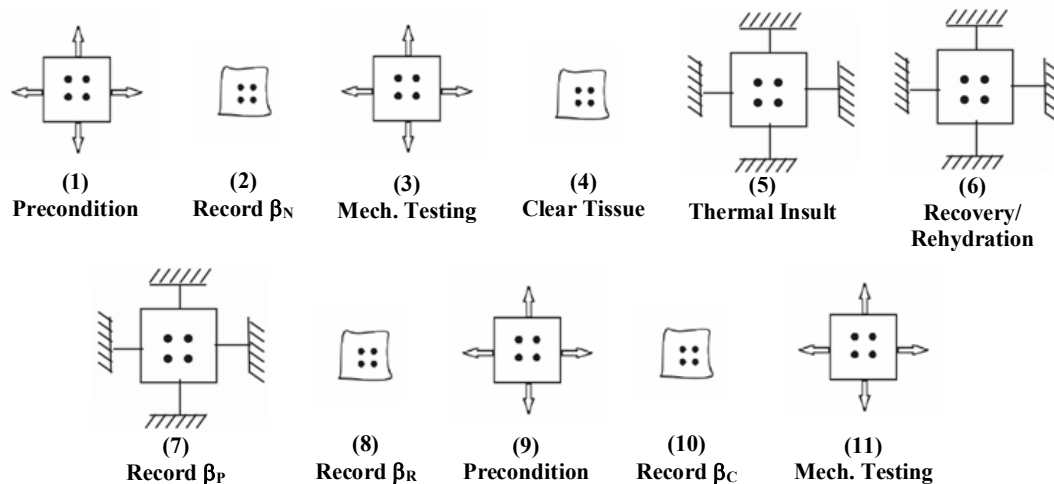


Figure 8.4 Testing schema for investigating the effect of heated glycerol on the mechanical behavior. Images with arrows represent dynamic, cyclic loading of the tissue. Images without arrows represent static, unconstrained tissue. Images in steps (5) - (7) represent an imposed isometric constraint.

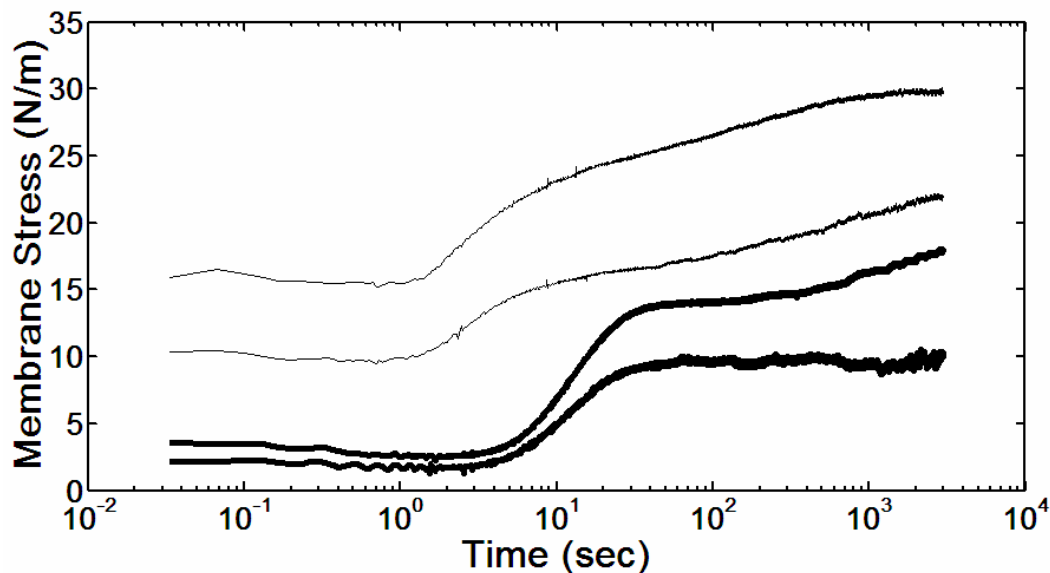


Figure 8.5 Data on the force (per length) generated by the tissue during heating as it tried to shrink against the fixed isometric constraint. The thinner lines are for the tissue heated in saline, and the thicker lines are for tissue heated in glycerol. Note the delay in the onset of force increase in the glycerol.

Table 8.2 Comparison of the characteristics times for the elbow-type isometric tests heated in glycerol and saline.

	Saline			Glycerol		
	τ_1	$\tau_{1/2}$	τ_2	τ_1	$\tau_{1/2}$	τ_2
Preferred	0.72	1.80	5.55	4.18	8.50	20.18
Non-preferred	0.87	2.10	5.67	3.71	8.50	19.72
Average	0.79	1.95	5.61	3.95	8.50	19.95

Mean mechanical responses (calculated as described in Chapter II) are shown in Figure 8.6 for tissues heated in saline (panel A) and 10M glycerol (panel B) for different durations of time. Tissues heated in saline display a progressive deviation from the native mechanical response as heating time increased (in the range of time tested in this chapter). For a 50 minute heating, extensibility was reduced by 32%. The mechanical response for tissues heated in glycerol differed little with heating duration over the range tested. Furthermore, the maximum reduction in extensibility (~11%) was much less than that of tissues heated in saline.

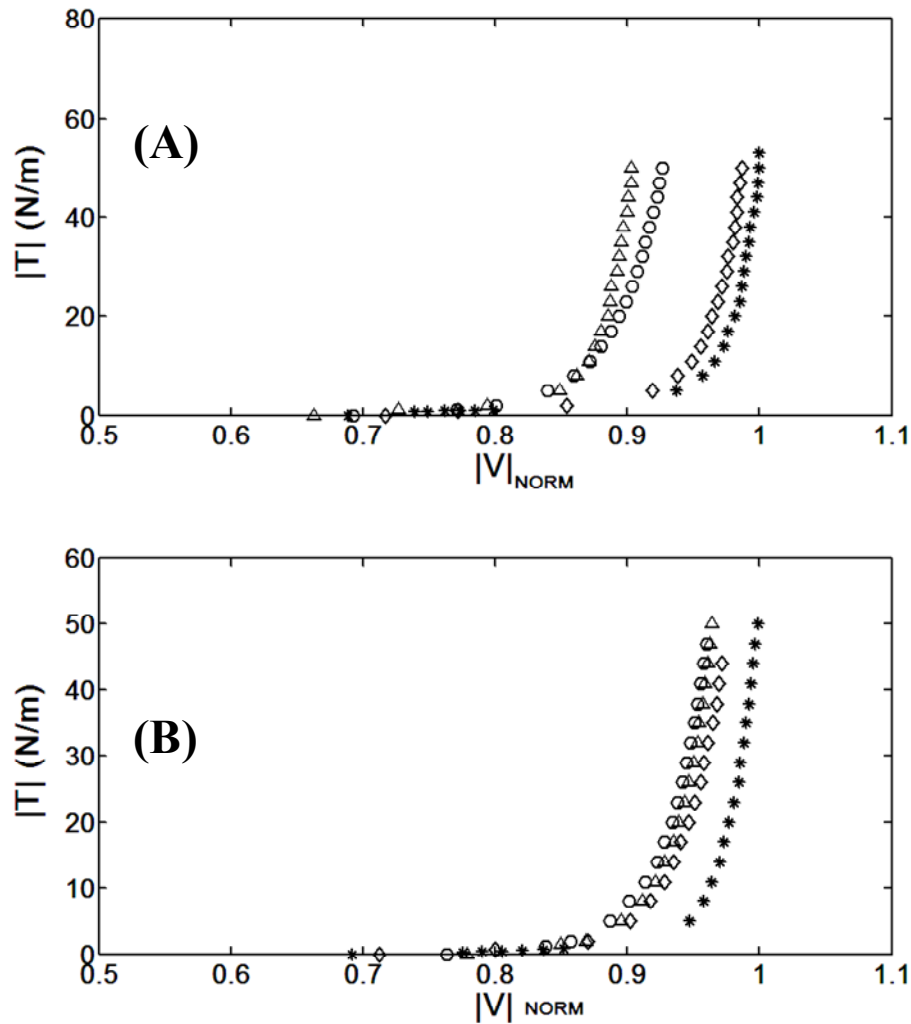


Figure 8.6 Magnitude of the biaxial stress resultants versus normalized biaxial stretches. Asterisks denote native tissue responses, whereas open diamonds, circles, and triangles denote 15, 30, and 50 minutes of heating, respectively. Tissues heated in saline deviated progressively from native behavior as heating time increased (Panel A), whereas tissues heated in glycerol differed little as a function of the duration of heating (in the range of times tested). Stretch is calculated relative to β_N for all tests here.

DISCUSSION

Optical clearing is intended to improve the efficacy of light-based clinical procedures, thus it should not irreversibly alter (damage) healthy tissue.

Furthermore, because optical clearing would typically be followed by a thermal assault (e.g. laser treatment), clearing should not exacerbate thermal damage of the healthy tissue. A few clearing techniques have been explored. For example, reducing inter-scatter distances within tissue has proven effective (Cilesiz and Welch, 1993; Chan et al., 1997), yet the methods used (namely, dehydration and compression) are difficult to control, and may irreversibly alter the conformation of healthy collagen molecules (Mogilner et al., 2002). Tissue immersion in glycerol is also an effective means for optical clearing, and affords more control than dehydration or compression. The mechanism(s) behind this approach and its net effects on tissue properties and thermal damage characteristics are not fully understood, however. Yeh et al. (2003) demonstrated reversibility of glycerol-induced structural and optical changes in various rat tissues. Polarized light and nonlinear optical microscopy using second harmonic generation were used to visualize reversible perturbations to, and dissociation of, collagen structure in rat tail dermis and cell-seeded collagen constructs during tissue optical clearing using glycerol. These results suggested a molecular mechanism for reducing tissue turbidity: the reversible dissociation of collagen fibers. The present data support this finding and are the first to show complete reversibility of glycerol-induced changes in the biaxial mechanical behavior of a mature collagenous tissue, the epicardium, and to demonstrate its inhibitory effects on the thermal damage process of collagenous tissue constrained near its physiologic length.

Water comprises over 70% of the mass of epicardium (unpublished data). Much of this water is non-covalently bound to hydroxyproline residues within the collagen molecules and forms inter- and intra-molecular water bridges that stabilize the triple helix (Ramachandran et al., 1973; Bella et al., 1995). Polar interactions among bound water molecules may be responsible, in part, for inducing characteristic collagen fiber undulations via non-covalent mechanical restoring (or contraction) forces. These forces would be relatively weak, thus explaining the compliant region of the stress-stretch response, which is widely believed to coincide with removal of the undulation. Water may therefore play a direct role in the tensile mechanical properties. When epicardium is immersed in glycerol, water is osmotically driven from the tissue at a rate dependent on the fiber density, glycerol concentration, and temperature (Tuchin et al., 1997). Glycerol simultaneously diffuses into the tissue, but at a slower rate than the exit of water, due to its larger molecular size. The net effect of this fluid exchange on the biaxial mechanical behavior of epicardium is a reduced extensibility (Figure 8.3A), which is fully attributable to an increase in unloaded tissue dimensions (recall β_{GP} was 17% larger than β_N ; cf Table 8.1). We suggest that the removal of water molecules from the tissue reduces the restoring force, and thus the degree of undulation that is recovered after preconditioning, thereby increasing the unconstrained tissue size (i.e. $\beta_{GP} > \beta_N$). The covalent crosslinks that dictate ultimate extensibility of the tissue remain intact however (Figure 1b in Yeh et al., 2003), thus the maximum extension relative to β_{GP} is reduced (Figure 8.3A)

while that relative to β_N is unchanged (Figure 8.3B). When immersed in normal saline, the tissue rehydrated and was restored to its original length, further supporting the idea that non-covalent interactions among water molecules are responsible for fiber undulation. Finally, we have shown that the rehydrated tissue, having regained its water bridges, behaves like native tissue. This is further proof that glycerol is non-reactive and a mechanically safe chemical agent for reducing tissue turbidity.

In a clinical setting, clearing would be used in conjunction with optical-based therapeutics. Understanding the effects of clearing agents on thermomechanical properties would thus be important for the clinical management of patients. Furthermore, it is important to recognize roles of mechanical constraints in a thermal damage process, as most tissues are loaded multiaxially *in vivo*. Thermal stability is increased by decreasing the activation entropy (Miles and Burjanadze, 2001). In Chapter VI we have discussed the possibility that a biaxial isometric constraint confers thermal stability on the epicardium by reducing the activation entropy. Vargas et al. (1999) also point out that a rapid release of water combined with the slow uptake of glycerol may lead to closer packing of the collagen fibers, which would also decrease activation entropy. Thus there are two mechanisms by which the activation entropy may have been reduced in the present study, which should have increased the thermal stability. Thermal stability of collagen is also significantly affected by water bridges that anchor to hydroxyproline residues

(Berg and Prockop, 1973; Ramachandran et al., 1973; Miles and Bailey, 2001). There is some debate over the exact location of these water bridges (see Miles and Bailey, 2001), but it is generally agreed that the majority of stabilization is conferred through intermolecular bridges. Replacement of water by glycerol, therefore, could have profound effects.

It is well-established that glycerol stabilizes collagen monomers (Hart et al., 1971; Russell, 1973; Na, 1986; Penkova et al., 1999) but destabilizes precipitated collagen fibrils (Na et al., 1986; Kuznetsova et al., 1998). Its thermomechanical effects on mature, covalently crosslinked collagenous tissues is poorly understood, however. Because mature epicardium is covalently crosslinked, and because of the aforementioned constraints on the activation entropy, the role of fibril destabilization is likely negligible in the present case. The increased stability of collagen molecules, however, is significant. In essence, we not only constrained the extent to which a helix-to-coil transition could occur (i.e. decreased activation entropy), we also reduced the likelihood of a helix-to-coil transition occurring in the first place. That is what we see in Figure 8.5. The decreased “contraction” stress is a result of the decreased activation entropy, and the increased stability of the collagen molecules is shown by a delay in the onset of thermal contraction. The net result of the increased thermal stability is illustrated well in comparing the two panels of Figure 8.6, where we see more modest changes in the mechanical behavior following significant thermal insult (up to 50 minutes at 75°C) in glycerol. Thus, while

seeking to show that glycerol does not exacerbate the thermal damage process, we have fortuitously found that it may protect healthy tissue.

In summary, we have demonstrated that glycerol does not permanently alter the biaxial mechanical properties of bovine epicardium, a model collagenous tissue. Furthermore, we have shown that glycerol slows the thermal damage process, and thus makes damage to healthy tissue less likely. These results, combined with those of Yeh et al. (2003), suggest that the use of glycerol as a clearing agent for optical diagnostics and thermo-optical therapies is thermomechanically safe as well as effective. This study focused on a primarily collagenous tissue, thus it is not clear how other, nontrivial tissue constituents such as fat, muscle, and hemoglobin would affect comparable tests. Furthermore, laser-based treatments will likely result in more varied heating due to differences in absorption amongst tissue constituents, whereas we have forced thermal equilibrium between tissue constituents in the present study. Future work should thus include studies on full-thickness tissue specimens with implementation of thermo-optical delivery devices.

CHAPTER IX

SUMMARY AND CONCLUSIONS

The manifold effects of supraphysiologic temperatures continue to be exploited for the treatment of various pathologies, often motivated by the availability of new technology (see Humphrey, 2003). Yet, our understanding of the thermal damage process still falls well short of what is needed to fully predict treatment outcomes. A significant complicating factor is the diverse constituency of tissue, and the body's ability to grow and remodel. It is not clear, therefore, if an appropriate thermal damage model can be based on the precepts of classical thermomechanics (Humphrey, 2003). Indeed, a more successful approach may be to use a mixture theory wherein the local effects of thermal damage on each constituent are accounted for separately. Thus, the challenge becomes one of delineating characteristics for the individual tissue constituents, which is impractical due to their quantity and coupled nature. There is, therefore, tremendous value in performing tests on a simple, model tissue such as the epicardium. As evidenced by our results and those of previous research (Chen et al., 1997; 1998a; 1998b; Harris et al., 2003; Harris and Humphrey, 2004), however, even a tissue with relatively few constituents is difficult to characterize fully.

Isotonic studies reveal that the end result of thermal intervention (i.e. equilibrium shrinkage) is the sole determinant of resultant mechanical behavior

in collagenous tissues (Chen and Humphrey, 1998; Harris et al., 2003). The relation clearly does not hold for the isometric tests herein, as there were changes in the mechanical behaviors of tissues that experienced no shrinkage (cf. Table 6.1 and Figure 6.1). Furthermore, when we examined the mechanical behaviors after different durations of isometric heating, a biphasic trend was apparent. No such trend appears in the literature for isotonic tests. The results imply that there is some dependence of the altered mechanical behavior on the type of mechanical constraint applied during heating. Because tissues *in vivo* are likely subjected to both types of constraints (perhaps dynamically), we must seek ways in which to compare the two. One such way is to perform experiments that are both isotonic and isometric. A pilot study in our lab has shown the feasibility of applying such a constraint. Based on the data from Harris and Humphrey (2004), we reasoned that there should be some value of stress that would prevent the epicardium from shrinking. Recall that the preferred direction herein exerted a larger isometric contraction force during heating than did the non-preferred direction (cf. Figure 4.3). Therefore, a prudent starting point was to perform an isotonic test wherein we applied a greater Piola-Kirchhoff stress to the preferred direction of the tissue. Specifically, we chose to apply first Piola-Kirchhoff stresses of 51.2 N/m (60g) and 31.4 N/m (40g) to the preferred and non-preferred directions, respectively.

Execution of the isotonic heating tests was similar to that of the isometric tests, however the device required a slight reconfiguration. Following

mechanical testing in the native state, load carriages were removed from the motors that did not contain load cells. Then, a system of low-friction pulleys was installed to facilitate the hanging of the weights (see Figure 9.1). One end of a string was attached to the tissue mounting rod, the string was routed around the pulleys, and a weight was hung on the other end. The loaded tissue was then placed inside an insulating capsule filled with room temperature saline. Next, the room temperature saline in the chamber was replaced with circulating, high temperature saline ($T = 75^{\circ}\text{C}$), as described in Chapter II. Adequate time was given for all chamber components to reach thermal equilibrium (~ 15 min), and then the tissue was removed from its insulating capsule and rapidly (and gently) immersed in the heated saline. The tissue was heated for 900 seconds, after which the heated saline was exchanged for room temperature saline in the manner described in Chapter II. The tissue was allowed to 'recover' for 60 minutes without removing the loads. Immediately following recovery, the configuration β_p was recorded. The loads were then removed from the tissue, and the device returned to its original configuration. After placing the tissue mounting rods back into the load carriages, the motors were moved inward once again until the sutures became slack and the unloaded configuration, β_R , was recorded. For consistency, the specimen was again preconditioned from 0.02 to 0.78 N for ten cycles, and the new unloaded configuration, β_C , was recorded for use in subsequent stretch-controlled mechanical testing. Mechanical tests were then carried out in the same manner as for the native tissue (see Chapter II).

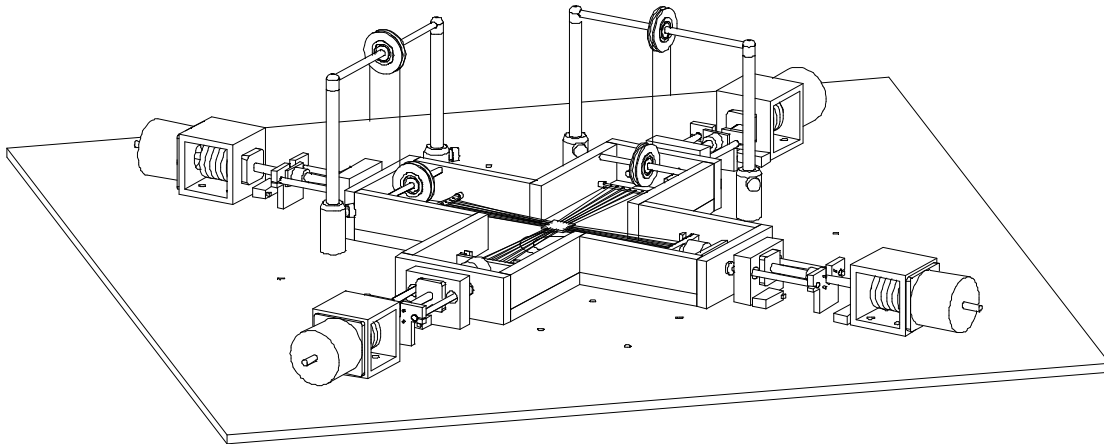


Figure 9.1 Biaxial device as configured for isotonic tests. Compare to Figure 2.4. (Figure taken from Harris, 2002)

When we applied the loads of 0.59 N ($P_{11} = 51.2$ N/m) and 0.39 N ($P_{22} = 34.1$ N/m) in the stiff and less-stiff directions, respectively, the tissue experienced both zero shrinkage and zero creep during heating at 75°C for 900 seconds (Figure 9.2). Thus we have demonstrated the efficacy of applying an isotonic/isometric constraint. We expected the high stretches (or loads) applied during these tests to limit any alterations in the post-heated tissue mechanics. The resultant mechanical behavior is not markedly different from the native mechanical behavior, indeed it falls in line with the high-stretch isometric and high-load isotonic tests (Figure 9.3, solid line). These findings are a significant first step toward bridging the gap between isotonic and isometric studies. In particular, although it may be more convenient to quantify results from isometric and isotonic tests using different thermodynamic functions (e.g., Helmholtz potential; see Humphrey, 2003), there will be a need for a single constitutive function for damage evolution in terms of applied loads, temperatures, and

kinematic constraints. Such a formulation must be founded on an expanded data base.

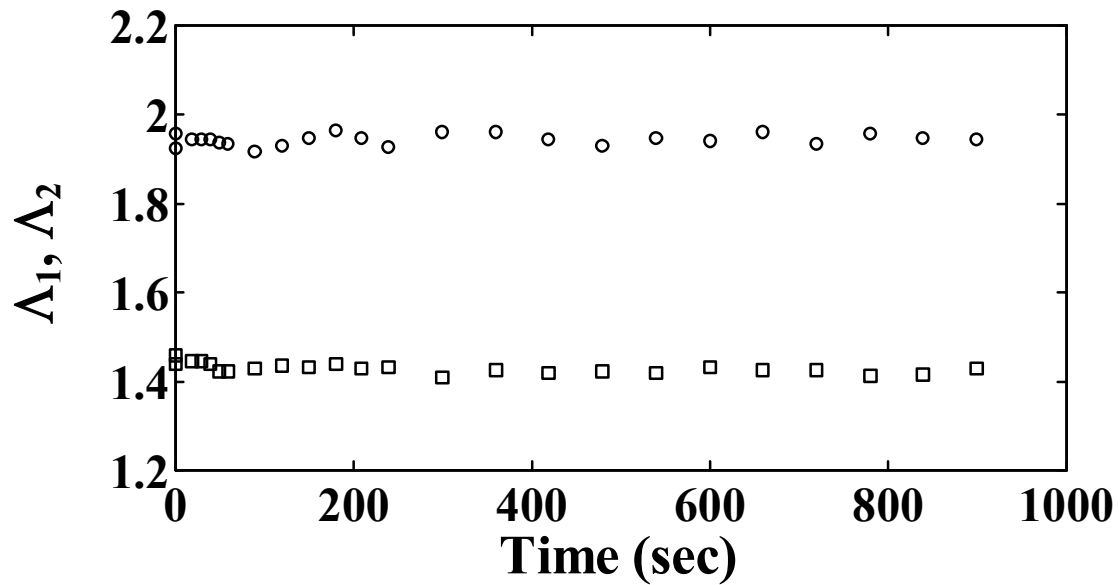


Figure 9.2 Representative data showing a lack of shrinkage during a single test in which high isotonic loads are applied to the tissue during heating. This illustrates that the stretches in both directions remain constant during heating, and therefore an isotonic/isometric constraint is enforced.

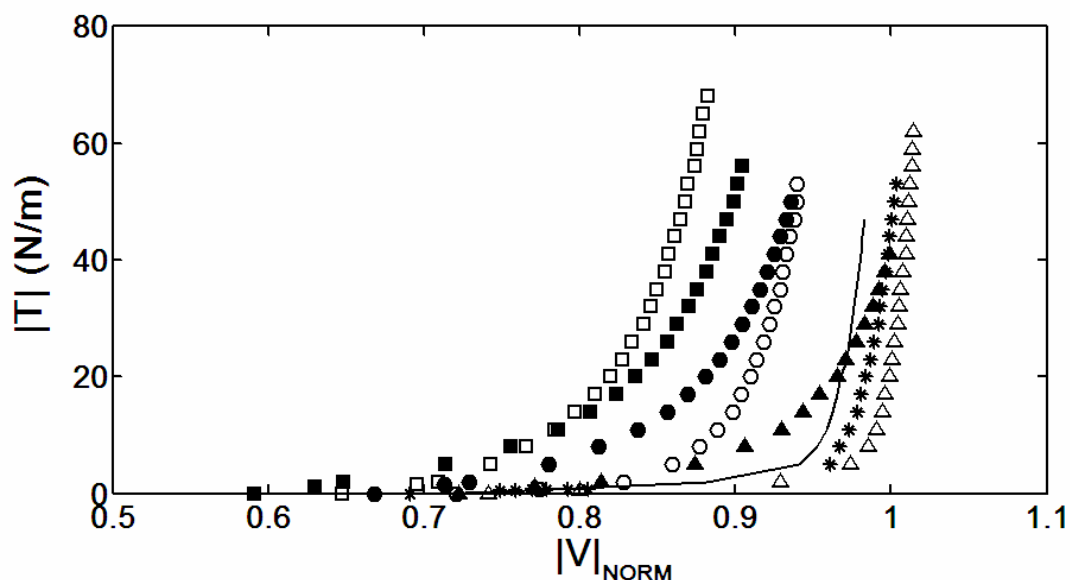


Figure 9.3 Relation between resulting equibiaxial mechanical responses in isometric and isotonic tests. The asterisks (*) represent the mean native response, the open squares (□), circles (○), and triangles (Δ) represent the '1.03', 'low stretch', and 'high' isometric constraints, respectively. The filled squares (■), circles (●), and triangles (▲) represent the (T, τ, P) combinations of (65, 900, 0.0), (75, 900, 12.8) and (75, 900, 21.3) from (Harris et al., 2003), respectively. The latter two were chosen for consistency with respect to the temperature and duration of heating, while the former represents a bound. The solid line shows the combined isotonic/isometric constraint.

Altered mechanical behavior need not be the sole indication of prior thermal damage to collagenous tissue. Thermal damage can be seen on electron micrographs (cf. Figure 3 in Humphrey, 2003), by comparing sequential DSC thermograms on the same piece of tissue (Miles et al., 1995), by monitoring changes in dimensions of tissue (Ramachandran, 1982; Chen et al., 1997; Harris and Humphrey, 2004), and through histology (Henriques, 1947; Thomsen et al., 1989; Whittaker et al., 2000). It is reasonable to ask, then, if the changes seen through these various techniques occur in concert. Indeed, tissue shrinkage and mechanical behavior are shown to be coupled in specific cases

(Chen and Humphrey, 1998; Harris et al., 2003). We have shown that collagen hyalinization and birefringence evolve with thermal damage in our isometric experiments and in free-shrinkage experiments (Chapter VII), which agrees well with changes to the mechanical behaviors (Chapter VI and Harris et al., 2003). Yet, as mentioned previously, the isometric tests herein exhibit differences in mechanical behavior with very little difference in changes to the dimensions of the tissue. Clearly, certain measures of thermal damage lend themselves better to specific classes of experiments (e.g. shrinkage), whereas other measures may be more universal (e.g. histology). Future work should focus partly on identifying, and quantifying such measures.

Finally, it is important to recognize that, while caution should be exercised, we need not wait for a comprehensive understanding of the thermal damage process before applying our knowledge in a practical way. For example, we have known for over 50 years that mechanically-loaded collagenous tissues take longer (or require more heat) to thermally damage (Lennox, 1949; Weir, 1949). Yet we know of no procedural specifications for the amount a tissue should be stretched prior to heating. In fact, the stretch applied to a tissue during heating seems to be dictated more by convenience (i.e. certain physiologic positions lend themselves better to the procedure). Indeed, a lack of appreciation for the little we do know, in particular with regard to the role of mechanical constraints, may be a contributing factor to the large variance of clinical outcomes.

Clearly, a comprehensive understanding of the thermal damage process remains elusive. The general characteristics of thermal damage to collagenous tissues heated under various biaxial thermomechanical protocols have been delineated well. However, a good kinetic model that accounts for the effects of mechanical load, and constitutive formulations to describe the biaxial mechanical behavior remain wanting. Though the collagenous tissues used for thermal damage studies are simpler than most other tissue, they remain less understood than the most complicated non-biological materials. We do not understand fully the role of the secondary constituents such as proteoglycans, fibroblasts, and elastin. Indeed, all thermal damage studies that utilize native biological tissues yield the composite result of thermal damage to each constituent. When manufacturing new materials, it is often the practice to start with a single constituent (e.g. polystyrene) for which we can easily characterize the behavior, and then add more constituents to alter the behavior for a specific application (e.g. the application of rubber to polystyrene to make it more impact-resistant). Similarly, we can 'construct' collagen matrices with varying amounts and diversity of constituents, and potentially elucidate better the role of each constituent. It may be that the bulk tissue response to thermal intervention can be modeled as a mixture of the responses for each constituent. Therefore, investigations similar to those herein, but on engineered tissues, is a prudent next step to sorting out the biothermomechanics of thermal damage.

REFERENCES

- Aksan A, McGrath JJ (2003) Thermomechanical analysis of soft-tissue thermotherapy. *J Biomech Eng* 125(5):700-708
- Allain JC, Le Lous M, Bazin S, Bailey AJ, DeLaunay A (1978) Isometric tension developed during heating of collagenous tissues: Relationship with collagen cross-linking. *Biochimica et Biophysica Acta* 533: 147-155
- Andreassan TT, Seyer-Hansen K, Bailey AJ (1981) Thermal stability, mechanical properties and reducible cross-links of rat tail tendon in experimental diabetes. *Biochimica et Biophysica Acta* 677: 313-317
- Baek S, Wells PB, Rajagopal KR, Humphrey JD (2005) Heat-induced changes in the finite strain viscoelastic behavior of a collagenous tissue. *ASME J Biomech Engr* (in press)
- Bass EC, Wistrom EV, Diederich CJ, Nau WH, Pelligrino R, Ruberti J, Lotz JC (2004) Heat-induced changes in porcine annulus fibrosus biomechanics. *J Biomech* 37:233-240
- Bella J, Brodsky B, Berman HM (1995) Hydration structure of a collagen peptide. *Structure* 3(9):893-906
- Berg RA, Prockop DJ (1973) The thermal transition of a non-hydroxylated form of collagen. Evidence for a role for hydroxyproline in stabilizing the triple-helix of collagen. *Biochem Biophys Res Commun* 52:115-120
- Brinkmann R, Radt B, Flamm C, Kampmeier J, Koop N, Birngruber R (2000) Influence of temperature and time on thermally induced forces in corneal collagen and the effect on laser thermokeratoplasty. *J Cataract Refract Surg* 26: 744-754
- Burjanadze TV (2000) New analysis of the phylogenetic change of collagen thermostability. *Biopolymers* 53:523-528
- Chan E, Sorg B, Protsenko D, O'Neil M, Motamedi M, Welch AJ (1997) Effects of compression on soft tissue optical properties. *IEEE J Select Topics Quant Electr* 2:943-950
- Chen SS, Humphrey JD (1998) Heat-induced changes in the mechanics of a collagenous tissue: Pseudoelastic behavior at 37°C. *J Biomech*, 31: 211-216

Chen SS, Wright NT, Humphrey JD (1997) Heat-induced changes in the mechanics of a collagenous tissue: Isothermal free-shrinkage. *ASME J Biomech Engr* 119:372-378

Chen SS, Wright NT, Humphrey JD (1998a) Heat-induced changes in the mechanics of a collagenous tissue: Isothermal isotonic-shrinkage. *ASME J Biomech Engr*, 120: 382-388

Chen SS, Wright NT, Humphrey JD (1998b) Phenomenological evolution equations for heat-induced shrinkage of a collagenous tissue. *IEEE Trans Biomed Engr*, 45: 1234-1240

Cilesiz IF, Welch AJ (1993) Light dosimetry: Effects of dehydration and thermal damage on the optical properties of the human aorta. *Appl Opt* 32:477-487

Consigny PM, Teitelbaum GP, Gardiner GG, Kerns WD (1989) Effects of laser thermal angioplasty on arterial contractions and mechanics. *Cardiovas Interven Radiol* 12: 83-87

Danielsen CC (1981) Thermal stability of reconstituted collagen fibrils: shrinkage characteristics upon in vitro maturation. *Mechanisms of Aging and Devel* 15:269-278

Doi M, Edwards SF (1986) *The Theory of Polymer Dynamics*, Clarendon Press, Oxford, UK

Flory PJ, Garrett RR (1958) Phase transformations in collagen and gelatin systems. *J Am Chem Soc* 80: 4836-4845

Gardner TN, Briggs GAD (2001) Biomechanical measurements in microscopically thin stratum corneum using acoustics. *Skin Res Technol* 7:254-261

Gregory SR (1991) Physical properties of glycerine. In: Jungermann E (ed), Sonntag NOV (ed) *Glycerine: A Key Cosmetic Ingredient*. Marcel Dekker, New York

Gross J (1973) Collagen biology: Structure, degradation and disease. *The Harvey Lectures* 68:351-432

Harris JL (2002) Thermal modification of collagen under biaxial isotonic loads. Ph.D. dissertation, Department of Biomedical Engineering, Texas A&M University, College Station

Harris JL, Humphrey JD (2004) Kinetics of thermal damage of a collagenous membrane under biaxial isotonic loading. *IEEE Trans Biomed Eng* 51:371-379

Harris JL, Wells PB, Humphrey JD (2003) Altered mechanical behavior of epicardium due to isothermal heating under biaxial isotonic loads. *ASME J Biomech Engr* 125:381-388

Hart GJ, Russell AE, Cooper DR (1971) The effects of certain glycols, substituted glycols and related organic solvents on the thermal stability of soluble collagen. *Biochem J* 125:599-604

Haut TL, Haut RC (1997) The state of tissue hydration determines the strain-rate sensitive stiffness of human patellar tendon. *J Biomech* 30: 79-81

Hayashi K, Peters DM, Thabit III G, Hecht P, Vanderby Jr R, Fanton GS, Markel MD (2000) The mechanism of joint capsule thermal modification in an in vitro sheep model. *Clinical Ortho and Related Res* 370: 236-249

Hayashi K, Thabit III G, Massa KL, Bogdanske JJ, Cooley AJ, Orwin JF, Markel MD (1997) The effect of thermal heating on the length and histologic properties of the glenohumeral joint capsule. *Am J Sports Med* 25(1):107-112

He X, Bischof JC (2003) Quantification of temperature and injury response in thermal therapy and cryosurgery. *Crit Rev Biomed Eng* 31:355-421

Henriques FC (1947) Studies in thermal injury. V. The predictability and the significance of thermally induced rate processes leading to irreversible epidermal injury. *Arch Path* 43: 489-502

Horgan DJ, King NL, Kurth LB, Kuypers R (1990) Collagen crosslinks and their relationship to the thermal properties of calf tendons. *Archives of Biochem Biophys* 281:21-26

Hulmes DJS (2002) Building collagen molecules, fibrils, and suprafibrillar structures. *J Struct Biol* 137:2-10

Humphrey JD (2003) Continuum thermomechanics and the clinical treatment of disease and injury. *Appl Mech Rev* 56(2):231-260

Humphrey JD, Strumpf RK, Yin FCP (1990) Biaxial mechanical behavior of excised ventricular epicardium. *Amer J Physiol* 259:H101-H108

Humphrey JD, Strumpf RK, Yin FCP (1992) A constitutive theory for biomembranes: Applications to epicardium. *ASME J Biomech Engr* 114:461-466

Humphrey JD, Vawter DL, Vito RP (1987) Quantification of strains in biaxially tested soft tissues. *J Biomechanics* 20(1):59-65

Kang T, Humphrey JD, Yin FCP (1996) Comparison of biaxial mechanical properties of excised endocardium and epicardium. *Am J Physiol* 270:H2169-H2176

Khan MH, Choi B, Chess S, Kelly KM, McCullough J, Nelson JT (2004) Optical clearing of in vivo human skin: Implications for light-based diagnostic imaging and therapeutics. *Las Surg Med* 34:83-85

Kuznetsova N, Chi SL, Leikin S (1998) Sugars and polyols inhibit fibrillogenesis of type I collagen by disrupting hydrogen-bonded water bridges between helices. *Biochem* 37:11888-11895

Lanir Y (1979) Biaxial stress-strain relationship in the skin. *Isr J Technol* 17:78-85

Le Lous M, Allain JC, Cohen-Solal L, Maroteaux P (1983) Hydrothermal isometric tension curves from different connective tissues. Role of collagen genetic types and noncollagenous components. *Connect Tissue Res* 11(2-3):199-206

Lee BI, Becker GJ, Waller BF, Barry KJ, Connolly RJ, Kaplan J, Shapiro AR, Nardella PC (1989) Thermal compression and molding of atherosclerotic vascular tissue with use of radiofrequency energy: Implications for radiofrequency balloon angioplasty. *JACC* 13:1167-1175

Lee JM, Pereira CA, Abdulla D, Naimark WA, Crawford I (1995) A multi-sample denaturation temperature tester for collagenous biomaterials. *Med Engr Phys* 17: 115-121

Lennox FG (1949) Shrinkage of collagen. *Biochimica et Biophysica Acta* 3:170-187

Levy O, Wilson H, Williams H, Bruguera JA, Dodenhoff R, Sforza G, Copeland S (2001) Thermal capsular shrinkage for shoulder instability. Midterm longitudinal outcome study. *J Bone Joint Surg Br* 83(5):640-645

Miles CA, Bailey AJ (2001) Thermally labile domains in the collagen molecule. *Micron* 32: 325-332

Miles CA, Burjanadze TV (2001) Thermal stability of collagen fibers in ethylene glycol. *Biophys J* 80:1480-1486

Miles CA, Ghelashvili M (1999) Polymer-in-a-box mechanism for the thermal stabilization of collagen molecules in fibers. *Biophysical J* 76: 3243-3252

Miles CA, Burjanadze TV, Bailey AJ (1995) The kinetics of the thermal denaturation of collagen in unrestrained rat tail tendon determined by differential scanning calorimetry. *J Mol Biol* 245: 437-446

Mixer G, DeLhery GP, Derksen WL, Monahan TI (1963) The influence of time on the death of hela cells at elevated temperatures. In: Herzfeld CM (ed) *Temperature: Its Measurement and Control in Science and Industry*, Vol. 3. Reinhold Publishing, New York

Mogilner IG, Ruderman G, Grigera JR (2002) Collagen stability, hydration and native state. *J Mol Graphics Modell* 21:209-213

Moran K, Anderson P, Hutcheson J, Flock S (2000) Thermally induced shrinkage of joint capsule. *Clin Orthop* 381:248-255

Morgan JE, Ellingham RB, Young RD, Trmal GJ, (1996) The mechanical properties of the human lens capsule following capsulorhexis or radiofrequency diathermy capsulotomy. *Arch Ophthalmol* 114:1110-1115

Na GC (1986) Interaction of calf skin collagen with glycerol: Linked function analysis. *Biochemistry* 25:967-973

Na GC, Butz LJ, Bailey DG, Carroll RJ (1986) In vitro collagen fibril assembly in glycerol solution: Evidence for a helical cooperative mechanism involving microfibrils. *Biochemistry* 25:958-966

Na GC (1989) Monomer and oligomer of type I collagen: Molecular properties and fibril assembly. *Biochemistry* 28:7161-7167

Olsen OL, Jemec GBE (1993) The influence of water, glycerine, paraffin oil and ethanol on skin mechanics. *Acta Derm Venereol (Stockh)* 73:404-406

Pearce J, Thomsen S, Vijverberg H, McMurray T (1993) Kinetics for birefringence changes in thermally coagulated rat skin collagen. *SPIE* 1876:180-186

Penkova R, Goshev I, Gorinstein S, Nedkov P (1999) Stability of collagen during denaturation. *J Protein Chem* 18(4):397-401

- Privalov PL (1982) Stability of proteins: Proteins which do not present a single cooperative system. In: *Advances in Protein Chemistry*, Vol. 35, Academic Press, New York, pp. 55-104
- Prockop DJ, Kivirikko KI (1995) Collagens: Molecular biology, diseases, and potentials for therapy. *Annu Rev Biochem* 64:403-434
- Ramachandran GN, Bansal M, Bhatnagar RS (1973) A hypothesis on the role of hydroxyproline in stabilizing collagen structure. *Biochim Biophys Acta* 322(1):166-171
- Rasmussen DM, Wakim KG, Winkelmann RK (1964) Isotonic and isometric thermal contraction of human dermis. I. Technic and controlled study. *J Invest Derm* 43:333-339
- Russell AE (1973) Effect of alcohols and neutral salt on the thermal stability of soluble and precipitated acid-soluble collagen. *Biochem J* 131:335-342
- Sacks MS, Chuong CJ (1992) Biaxial Mechanical Properties of passive right ventricular free wall myocardium. *J Biomech Eng* 115:202-205
- Sacks MS, Chuong CJ, More R (1994) Collagen fiber architecture of bovine pericardium. *ASAIO J* 40:M632-637
- Sacks MS, Gloeckner DC (1999) Quantification of fiber architecture and biaxial mechanical behavior of porcine intestinal submucosa. *J Biomed Mater Res* 46:1-10
- Sacks MS, Smith DB, Hiester ED (1997) A small angle light scattering device for planar connective tissue microstructural analysis. *Ann Biomed Eng* 25(4):678-689
- Sankaran V, Walsh JT Jr (1998) Birefringence measurement of rapid structural changes during collagen denaturation. *Photochem Photobiol* 68:846-851
- Segur JB (1953) Uses of glycerine. In: Miner CS (ed), Dalton NN (ed) *Glycerol*. Reinhold Publishing, New York
- Thomsen S (1991) Pathologic analysis of photothermal and photomechanical effects of laser-tissue interactions. *Photochem Photobiol* 53:825-835
- Thomsen S (1999) Mapping of thermal injury in biologic tissues using quantitative pathologic techniques. *Proc SPIE* 3594: 82-95

Thomsen S (2000) Qualitative and quantitative pathology of clinically relevant thermal lesions. *Crit Rev Optical Sci Tech* 75:425–459

Thomsen S, Pearce JA, Cheong W (1989) Changes in birefringence as markers of thermal damage in tissues. *IEEE Trans Biomed Eng* 36:1174-1179

Tuchin VV, Maksimova IL, Zimnyakov DA, Kon IL, Mavlutov AH, Mishin AA (1997) Light propagation in tissues with controlled optical properties. *J Biomed Opt* 2(4):401-417

van Noort R, Black MM, Martin TRP, Meanley S (1981) A study of the uniaxial mechanical properties of human dura mater preserved in glycerol. *Biomaterials* 2(1):41-45

Vargas G, Chan EK, Barton JK, Rylander III HG, Welch AJ (1999) Use of an agent to reduce scattering in skin. *Las Surg Med* 24:133-141

Wall MS, Deng XH, Torzilli PA, Doly SB, O'Brien SJ, Warren RF (1999) Thermal modification of collagen. *J Shoulder Elbow Surg* 8: 339-344

Wallace AL, Hollinshead RM, Frank CB, (2001) Electrothermal shrinkage reduces laxity but alters creep behavior in a lapine ligament model. *J Shoulder Elbow Surg* 10(1):1-6

Wang X, Milner TE, Change MC, Nelson JS (1996) Group refractive index measurement of dry and hydrated type I collagen films using optical low-coherence reflectometry. *J Biomed Opt* 1:212-216

Weir CE (1949) Rate of shrinkage of tendon collagen-Heat, entropy and free energy of activation of the shrinkage of untreated tendon. Effect of acid salt, pickle, and tannage on the activation of tendon collagen. *J Am Leather Chem Assoc* 44: 108-140

Wells PB, Harris JL, Humphrey JD (2004) Altered mechanical behavior of epicardium under isothermal biaxial loading. *ASME J Biomech Engr* 126:492-497

Whittaker P, Zheng S, Patterson MJ, Kloner RA, Daly KE, Hartman RA (2000) Histologic signatures of thermal injury: Applications in transmural laser revascularization and radiofrequency ablation. *Lasers Surg Med* 27:305-318

Wiederhorn NH, Reardon GV (1953) Studies concerned with the structure of collagen. II Stress-strain behavior of thermally contracted collagen. *J Appl Poly Sci* 9: 315-325

Wright NT, Humphrey JD (2002) Denaturation of collagen via heating: An irreversible rate process. *Ann Rev Biomed Engr* 4:109-128

Yeh AT, Choi B, Nelson JT, Tromberg BJ (2003) Reversible dissociation of collagen in tissues. *J Invest Dermatol* 121:1332-1335

APPENDIX A

EQUIBIAXIAL STRETCH

For a purely equibiaxial stretch, it can be shown that the angle between any two line segments is unchanged upon deformation, and therefore fiber orientations are unchanged relative to one another (note that rigid body rotation may change the global orientations, but not the relative ones). Consider two fibers in the referential configuration represented by line segments that have orientations \mathbf{M}_1 and \mathbf{M}_2 , with magnitudes dS_1 and dS_2 , respectively. Upon deformation, the line segments (i.e. fibers) will have new orientations \mathbf{m}_1 and \mathbf{m}_2 , with magnitudes ds_1 and ds_2 , respectively. The line segments are related through the deformation gradient by

$$\begin{aligned} ds_1 \mathbf{m}_1 &= \mathbf{F} \cdot dS_1 \mathbf{M}_1, \\ ds_2 \mathbf{m}_2 &= \mathbf{F} \cdot dS_2 \mathbf{M}_2. \end{aligned} \tag{A.1}$$

The inner product between the line segments in the deformed configuration is given by

$$ds_1 \mathbf{m}_1 \cdot ds_2 \mathbf{m}_2 = ds_1 ds_2 \cos \theta, \tag{A.2}$$

where θ is the angle between the fibers in the deformed configuration.

Substituting the relations (A.1) into equation (A.2) yields

$$\mathbf{F} \cdot dS_1 \mathbf{M}_1 \cdot \mathbf{F} \cdot dS_2 \mathbf{M}_2 = ds_1 ds_2 \cos \theta$$

$$\Rightarrow \mathbf{M}_1 \cdot \mathbf{C} \cdot \mathbf{M}_2 = \frac{ds_1}{dS_1} \frac{ds_2}{dS_2} \cos \theta. \quad (\text{A.3})$$

Now, using the definition of the stretch ratio (cf. equation (2.11)), and for simplicity taking M_1 and M_2 to lay along the primary stretching axes (cf. equation (2.16)) we get,

$$\frac{C_{12}}{\sqrt{F_{11}^2 + F_{21}^2} \sqrt{F_{22}^2 + F_{12}^2}} = \cos \theta. \quad (\text{A.4})$$

Recall that \mathbf{C} is free of rigid body motion (cf. equation (2.15)), and therefore for a pure equibiaxial stretch, the off-diagonal components ($C_{12} = C_{21}$) should equal zero. Thus, $\theta = \pi/2$, and \mathbf{m}_1 and \mathbf{m}_2 are orthogonal, just as \mathbf{M}_1 and \mathbf{M}_2 were.

VITA

Name: Paul Brian Wells

Permanent Address: 2208 Western Avenue
Fort Worth, TX 76107

Date of Birth: October 13, 1976

Collegiate Education:

Institution	Major	Degree	Date of Graduation
Texas A&M University	Biomedical Engineering	Ph. D.	May 2005
Texas A&M University	Mechanical Engineering	B.S.	May 2000

Professional Publications:

Wells PB, Harris JL, and Humphrey JD (2004) Altered mechanical behavior of epicardium under isothermal biaxial loading. ASME Journal of Biomechanical Engineering 126(4):492-497

Harris JL, **Wells PB**, and Humphrey JD (2003) Altered mechanical behavior of epicardium due to isothermal heating under biaxial isotonic loads. ASME Journal of Biomechanical Engineering 125(3):381-388

Baek S, **Wells PB**, Rajagopal KR, and Humphrey JD (2005) Heat-induced changes in the finite strain viscoelastic behavior of a collagenous tissue. ASME Journal of Biomechanical Engineering (in press)

Wells PB, Yeh AT, and Humphrey JD. Influence of glycerol on the mechanical reversibility and thermal damage susceptibility of collagenous tissues. IEEE Transactions on Biomedical Engineering (submitted)